Invited Paper

Precision measurement of $\hbar/m_{Cs}$ based on photon recoil using laser-cooled atoms and atomic interferometry

D. S. Weiss*, B. C. Young, S. Chu

Physics Department, Stanford University, Stanford, CA 94305, USA
(Fax: + 1-415/723-9173, E-mail: BCYOUNG@leland.stanford.edu)

Abstract. The recoil of an atom due to the absorption of up to 64 photons is measured, using laser-cooled cesium atoms which are made to interfere in an atomic fountain. Measurement of the photon recoil allows a determination of $\hbar/m_{Cs}$, and hence the fine-structure constant. The measurement is described and a detailed theoretical and experimental study of potential systematic errors is presented. A relative precision in the photon recoil measurement of 0.1 ppm is obtained in two hours of data collection. The measurement is currently 0.85 ppm below the accepted value of $\hbar/m_{Cs}$. We cannot now formally ascribe a systematic error, but suspect that the bulk of the discrepancy is due to imperfections of the interferometer beams used to induce the Raman transitions.

PACS: 32.00, 35.00, 42.50

1 Introductory remarks

The recoil of an atom when it absorbs a photon was first observed spectroscopically in the doubling of certain spectral peaks in saturation spectroscopy[1]. The authors pointed out at the time that the splitting of these peaks lets one measure $\hbar/m$ in frequency units, which could be accomplished with high precision. In recent years, intense research in laser cooling and atom interferometry has led to a proliferation of new, powerful techniques. These advances have allowed us to precisely measure the recoil shift [2], in an experiment that is the first precision measurement of a fundamental constant using atomic interferometry.

The quantity $\hbar/m$ can be determined from the measurement of a recoil splitting when it is combined with

accurate knowledge of the photon wavelength. Mass ratios of atoms to the proton and the proton to the electron can be measured to high precision, so that the particular mass in the ratio $\hbar/m$ is of secondary importance. Recently, $\hbar/m_{neutron}$ has been measured to an accuracy of 8×10^{-7} by diffracting neutrons from a silicon crystal [3]. In this paper we describe in detail a measurement of $\hbar/m_{Cs}$ that obtains a precision of 1×10^{-7} in a few hours, and appears to have the potential to yield precisions near 1×10^{-9} in a comparable time.

The ratio $\hbar/m$ is significant in quantum mechanics because both the particle mass and $\hbar$ appear in the basic quantum mechanical equations of motions only in that ratio. Alternately, mass appears in the de Broglie wave function in that ratio, and a particle's wavefunction contains the complete description of its position and momentum. Thus for the purposes of comparing quantum theories to experiments one often need only know this ratio, and not m independently. The most important example of this is that $\hbar/m_e$ can be combined with R_∞, the Rydberg constant, to obtain α, the fine-structure constant,

$$\alpha^2 = \frac{2R_\infty}{c} \frac{h}{m_e}. \tag{1}$$

There are currently five distinct kinds of experiments that can measure the fine-structure to an accuracy of 0.4 ppm or better [4]. These measurements are: the electron g-2; the muon hyperfine splitting; the quantum Hall resistance (R_H); the proton gyromagnetic ratio (γ_p); and $\hbar/m$ measurements. The current accuracies of the α measurements and their constituent components are shown in Table 1. The first two depend on the correctness of QED to yield α, which means that they alone are not sufficient to test QED. The next two may be approaching the final limits of their accuracy, at a relative precision of 1 to 2×10^{-8} [5]. They appear to have almost reached their limit because each requires a highly accurate characterization of a macroscopic object, either the calculable capacitor that enables R_H to be expressed in SI units or the giant solenoid used to create the NMR bias

* *Present address:* Ecole Normale Supérieure, 24 rue Lhomond, F-75231 Paris Cedex 05, France (Fax: + 33-1/45 35 00 76, E-mail: DSWEISS@physique.ens.fr)

Table 1. Some of the current best methods for determining the fine-structure constant, α. The table items are separated into groups of physical quantities that can be combined to yield α. The relative accuracy of each quantity is given in the first column of numbers. The sensitivity of the determinations of α to the uncertainties in each quantity are indicated by the dependences on α in the second column. The resulting relative accuracy of each determination of α is given in the third column. The relative accuracy of the Cs photon recoil measurement has not yet been assigned

Physical quantities measured	Relative accuracy [ppb]	Dependence on α	Relative accuracy of α [ppb]	Ref.
g-2 of the electron (exp.)	3.7	–	8.1	[6]
g-2 of the electron (QED theory)	7.2	–		[4]
Muon hyperfine structure (exp.)		–	190	[7]
Muon hyperfine structure (theory)		–		[8]
Quantum Hall effect	2.9	α^{-1}	24	[9]
Calculable capacitor	22.0			[10]
Proton gyromagnetic ratio	110	α^3	37	[9, 11]
Rydberg constant	0.029	α^3		[12]
ac Josephson effect	8.9	α^{-3}		
Quantum Hall effect	2.9	α^{-3}		
Neutron de Broglie wavelength	800	α^2	400	[3]
Rydberg constant	0.029	α^2		
Proton/electron mass ratio	20	α^2		[6]
Neutron proton mass ratio	9.0	α^2		
Cs photon recoil		α^2		This work
Rydberg constant	0.029	α^2		
Proton/electron mass ratio	20	α^2		
Cs/proton mass ratio	27	α^2		[13]

field in the γ_p experiment. Measurements of $\hbar/m$ do not require accurate knowledge of macroscopic objects, and therefore have the potential to significantly improve the measured accuracy of α.

1.1 Simplified version of the experiment

The basic physical principle of the measurement of the recoil shift is straightforward, and does not depend on atomic interference or any detailed atomic physics. We can ignore the subtleties of the atom-photon interaction and reduce it to its basic nature, that of a two body collision. The initial and final atom + photon states in this process are shown in Fig. 1. Conservation of momentum dictates that when an atom absorbs a photon it
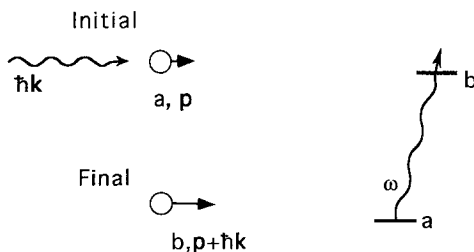

Fig. 1. An atom absorbs a photon and receives a recoil momentum kick. The *diagram on the left* illustrates conservation of momentum in the process. The *diagram on the right* illustrates conservation of energy; the photon energy must be higher than the energy separation in the atom to account for the change in atomic energy due to the photon recoil
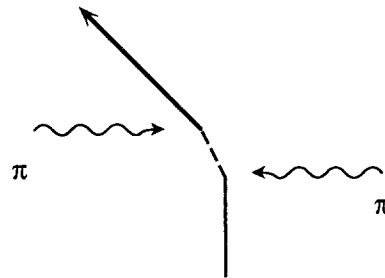

Fig. 2. Simplified measurement of the photon recoil. The *solid* and *dashed lines* indicate the atom is in states $|a\rangle$ and $|b\rangle$, respectively

receives a momentum recoil kick, $\hbar k$, where $k = \omega/c$ and ω is the frequency of the light. Conservation of energy implies the resonance condition

$$\omega - \omega_{ab} = \mathbf{k} \cdot \mathbf{v} \pm \frac{\hbar k^2}{2m}, \tag{2}$$

where $\hbar\omega_{ab}$ is the energy difference between the atomic levels, and the sign of the last term depends on whether the initial energy level is higher or lower than the final one.

In Fig. 2 we illustrate a simple experiment to measure the quantity $\hbar k^2/m$, which is proportional to the recoil shift term in (2) and to the Doppler shift due to the recoil kick. An atom in state $|a\rangle$ with zero velocity in the laboratory frame is made to absorb a photon from a leftward propagating laser beam with frequency ω. The atom recoils by $\hbar k/m$ and the process has the resonance

condition

$$\omega - \omega_{ab} = \frac{\hbar k^2}{2m}.$$

(3)

The atom can then be de-excited from state $|b\rangle$ by a photon from a rightward propagating beam with frequency ω'. It receives another velocity kick $\hbar k'/m$ in the same direction, and the new resonance condition is

$$\omega' - \omega_{ab} = -\frac{\hbar k k'}{m} - \frac{\hbar k'^2}{2m}.$$

(4)

The two resonances are shifted relative to each other by $\Delta\omega = \omega - \omega' = \hbar(k+k')^2/2m$. The simple experiment would be to measure this frequency difference, for instance by fixing ω at the resonance peak and scanning ω' to find the maximum number of atoms that come back to state $|a\rangle$.

Half of $\Delta\omega$ comes from the addition of a Doppler shift due to the recoil velocity, $kv = \hbar k^2/m$, and half comes from the recoil energy shift, $\hbar k^2/2m$, which has a different sign for emission and absorption. Note that if the second beam is made to propagate in the same direction as the first there is no shift in the resonance relative to the first excitation, because the change in the recoil energy shift cancels the additional Doppler shift.

1.2 Important features of this experiment

Our experiment is the separated oscillatory field version (Ramsey spectroscopy) [14] of the experiment described in the previous section. The Ramsey spectroscopy version yields increased resolution, allows more atoms to contribute to the signal, and reduces systematic errors. As shown in Fig. 3, each π pulse in Fig. 2 is replaced with two $\pi/2$ pulses. This is the same pulse sequence used in optical Ramsey spectroscopy [15], and has previously

been studied using Ca and Mg atoms in thermal atomic beams in order to test the feasibility of optical frequency standards and as early demonstrations of atomic interferometry [16, 17].

To appreciate the improved accuracy in the recoil measurement obtained using a four-pulse sequence one need only study Fig. 3. As opposed to the π pulses of the simple measurement, the $\pi/2$ pulses can be made so brief that atoms in a broad inhomogeneous velocity distribution can contribute to the signal without sacrificing resolution. Each of these pulses divides the trajectory of an atom in two, like a 50–50 beamsplitter, so that after the third pulse each atom is in a superposition of eight different trajectories. When the spacing between the first two $\pi/2$ pulses is equal to the spacing between the last two, two pairs out of the eight paths overlap and hence interfere at the final $\pi/2$ pulse. In this double interferometer, the only essential difference between the two interfering pairs is that their velocities are shifted with respect to each other by two photon recoils, so that the sets of Ramsey fringes they produce are displaced by $2\hbar k^2/m$. Because of the differential nature of the measurement, the measured recoil shift is unaffected by the atom's initial velocity, the acceleration due to gravity, and all frequency shifts that are position independent.

We have improved the optical Ramsey experiment for the purpose of measuring $\hbar/m$ in three basic ways. First, we excite from one hyperfine ground state to another via a velocity-selective stimulated Raman transition [18]. The recoils from the two photons that excite this transition are in the same direction, so the effective wavenumber is $k_{\mathrm{eff}} = k_1 + k_2$, but the effective frequency of the transition is the hyperfine splitting. We therefore obtain the large momentum kicks one would get with single violet photons, at the same time as we have the convenience and accuracy of working with microwave frequencies. Second, since both atomic levels are ground states, the linewidth of the stimulated Raman transition is limited only by the measurement time, and unperturbed measurement times can be quite long in an atomic fountain
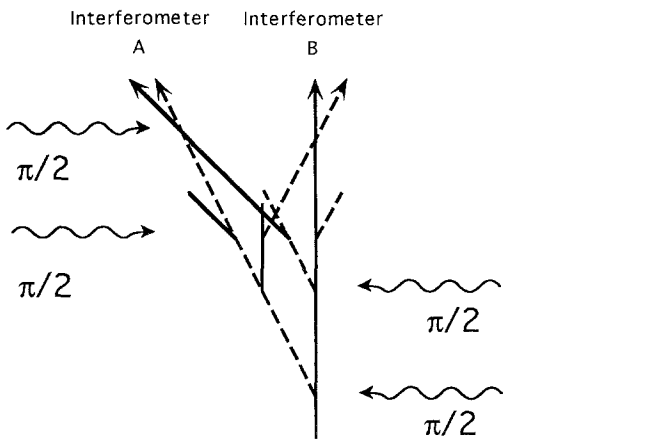

Fig. 3. The double atomic interferometer. The *solid* and *dashed lines* denote the atom is in $|a\rangle$ and $|b\rangle$, respectively. The four paths that do not interfere at the final light pulse are prematurely truncated, in order to highlight the two pairs which do interfere
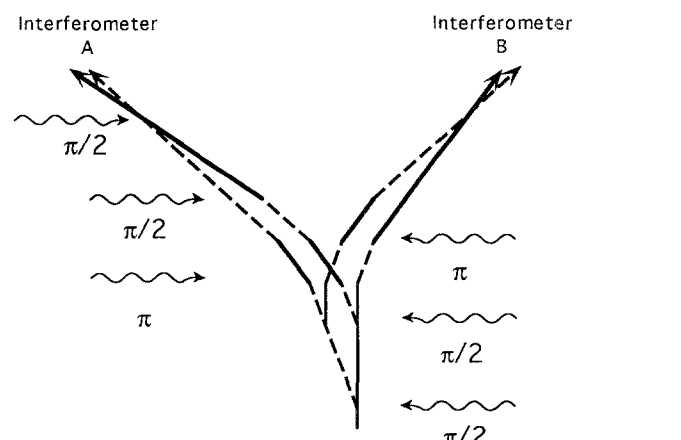

Fig. 4. Double atomic interferometer with two intermediate π pulses. All paths are shown except the four which are truncated in Fig. 3. Many more π pulses can be added in the same way

[19]. Third, we add up to 15 π pulses to our interferometer, sandwiched in between the middle two $\pi/2$ pulses, with alternating propagation directions (see Fig. 4). Each additional pulse adds one effective photon recoil to the center of mass velocity of each path. For N π pulses the separation between the two sets of interference fringes is multiplied by $N + 1$. All these improvements together lead to a current resolution which is several orders of magnitude higher than any previous form of optical Ramsey spectroscopy would be for measuring the photon recoil.

Light-pulse interferometry has previously been combined with velocity-selective stimulated Raman transitions and laser cooled atoms in order to measure changes in the local acceleration of gravity with a relative precision of 3×10^{-8} [20]. Atomic interferometry has been touted as a potentially potent tool for such diverse applications as testing the weak equivalence principle, testing the charge neutrality of atoms [21], oil exploration, navigation [22], testing quantum mechanics, and precision frequency measurements [23].

This experiment also provides a quantitative handle on the systematic errors in a light-pulse atomic interferometer in general. Using literature values for the various constants involved, we can obtain an accepted value for the photon recoil of a cesium atom with a relative accuracy of 8×10^{-8}, which allows us to characterize and reduce systematic errors in the light pulse interferometer to this level. Even if there were no accepted value at or beyond that level of accuracy, since this experiment contains myriad reversals and switches for diagnosing the existence of systematic errors, still higher accuracy should be possible.

1.3 A new mass standard?

It has been suggested that mass be redefined in terms of the de Broglie frequency of a fundamental particle, mc^2/h [24]. Wignall suggested that were a new mass standard to be adopted with units of frequency, measurements of $\hbar/m$ would be particularly well placed to be the basis for such standards. The basic aesthetic argument in favor of a redefinition of mass as frequency is that $\hbar$ would drop out of the equations of quantum mechanics. Many of the observables in quantum mechanics are frequencies, so the energy-frequency conversion is only really necessary when an observable involves mass. However, such a redefinition of mass as frequency is unlikely to offer a practical advantage. In addition, $\hbar/m$ measurements are not uniquely placed to help in the adoption of new mass standards, although they are among the relevant measurements. To understand the place of $\hbar/m$ in considerations of a new mass standard, we will review the current direction of the precision measurement community in this regard.

The current SI mass standard is based upon an artifact, a 1 kg Pt-Ir bar located in Paris. No other current basic SI unit relies on such a unique, impermanent object. Therefore there has been much discussion about replacing the current definition of mass with an inherently more fundamental one, like for instance, the mass of the electron [25, 26]. The mass of the electron can be related to other base units by a simple inversion of (1),

$$m_e = \frac{2R_\infty h}{c\alpha^2}, \tag{5}$$

and the equation [26]

$$h = 4(W_{90}/W)/K_{J-90}^2 R_{K-90}, \tag{6}$$

which shows how Planck's constant can be determined based on the SI voltage and resistance standards (K_{J-90} and R_{K-90}, which are realized from the Josephson constant, K_J, and the von Klitzing constant, R_K, of the quantum Hall effect), and the ratio of the mechanical watt (W), which depends on a standard kilogram mass, to the electrical watt (W_{90}), which depends on the electrical standards. The physics underlying (6) lies in the relation, $K_J^2 R_K = (2e/h)^2(h/e^2) = 4/h$. Since the measurement of h gives m_e in kg, and because particle mass ratios are relatively well known, the determination of h can be viewed as a measurement of Avogadro's number, N_A. Once m_e is taken as the mass standard, the watt measurement that is now used to determine m_e would serve the purpose of calibrating secondary 1 kg standards. Other approaches to realizing a new definition of mass along similar lines include the direct determination of N_A, for instance, by precisely measuring the volume and density of a perfect crystal [27, 28].

These practical approaches to changing the mass standard would be unaffected by a change in the definition of mass in terms of a frequency. For fundamental physics experiments where only the ratio $m/\hbar$ is necessary, this ratio will probably continue to be known to better accuracy than either m or $\hbar$, either by combining R_∞ and α or by direct measurement of $\hbar/m$. For other experiments or measurements which require m or $\hbar$ separately, the only issue with regard to a new definition of mass is whether a conversion like the watt balance is performed before or after the mass standard is invoked.

1.4 Testing QED

One of the goals of this work is to contribute to a measurement of α using a theory-insensitive technique in order to test QED. This goal raises the obvious questions – in what sense is this measurement theory insensitive and how does this measurement relate to other α measurements?

The raw quantity which is measured, the photon recoil, is about as theory independent as experimental physics can be. First, the photon momentum must be assumed to be $\hbar\omega/c$. This assumption relies on three elementary things: a basic precept of quantum mechanics, that frequency is related to energy, the energy-momentum transformations of special relativity, $E^2 = (pc)^2 + (mc^2)^2$, and the empirical fact that the photon is massless to high precision. The frequency difference between the resonances of the two inter-

ferometers depends only on conservation of energy and conservation of momentum. As long as the two interferometers are treated identically, any complicated atomic physics that shifts energy levels drops out of the measurement. The ratio $m/\hbar$ is the only intrinsic atomic property that is measured, and it is an external quantity, independent of what goes on in the atom[1]. The step where an energy separation of two peaks becomes the separation of two sets of interference fringes uses only general quantum mechanics, and not any particular field theory.

To determine α from $\hbar/m$ requires the use of the Rydberg constant, R_∞, which is defined according to (1). The Rydberg constant is determined by measuring the separation of energy levels in hydrogen or deuterium and making several corrections to this value. Thus R_∞ is not so manifestly theory insensitive. The relative importance of the various corrections differs with the transition that is measured. When the hyperfine structure is resolved in a Rydberg measurement, the largest correction is due to the hyperfine splitting of the levels and these have been independently measured for low lying levels. The second order Doppler shift must be corrected for, but this correction is based only on special relativity. The reduced mass must also be known, but m_e/m_p is known to high precision from a separate measurement [6]. The only correction which depends on the details of QED is the correction for the Lamb shift. For hydrogen this quantity has been precisely measured, while for deuterium the adjustment is based on a Lamb shift calculation. The Rydberg constant has been measured using many different transitions. These measurements are in generally good agreement to 3 parts in 10^{11}. The theory that underlies R_∞ is thus on solid experimental ground, especially at the level required for helping to determine α [12, 29].

If we forego the details, the procedure for testing QED using this type of determination of α is straightforward. The anomalous magnetic moments of electrons and muons are calculated using QED, by performing an expansion in orders of α/π. Measurements of these quantities are used to solve for α. The two values for α are then compared.

Currently the two most accurate methods of determining α without a long QED calculation, using the quantum Hall effect and the proton gyromagnetic ratio, disagree at about the two standard deviation level, which underscores the need for further independent measurements. There is in particular some concern because there is no microscopic theory of the quantum Hall effect, so it is not clear to what level of precision the remarkable relation $R_H = h/e^2$ holds [30]. It is encouraging that the value for R_H has been shown to be the same for different materials to ≈ 0.1 ppb [31]. Although it is certainly not surprising, it is notable that the determinations of α which use the quantum Hall effect, the proton gyromagnetic ratio and $\hbar/m_n$ are all limited by systematic errors.

To check the consistency of theory and guard against systematic error, it is desirable to determine α in as many

ways as possible. Even measurements with inherently less precision are helpful for assessing systematic errors in other measurements, even if they do not ultimately figure into the ultimate value of a constant [32]. The fine structure constant can be obtained with accuracies near 1 ppm from measurements of the hyperfine structure of elementary particles, the Lamb shift in hydrogen, the decay rate of orthopositronium, and high energy collisions of electrons and positrons [33]. It is difficult to predict what new measurement techniques may arise, but there are a couple of possibilities which deserve mention. An $\hbar/m$ measurement has been proposed which combines the measurement of the mass ratio of two ions related by nuclear beta decay with knowledge of the associated gamma ray energy [34]. Single electron tunneling devices could be used to count the number of electrons deposited on a calculable capacitor. This could yield an α determination with the same precision as the quantum Hall α measurement, but without relying on R_H [35].

1.5 Overview

Section 2 presents a detailed analysis of stimulated Raman transitions and of atomic interferometry based on these transitions. Section 3 is devoted to describing the details of the experiment. Section 4 contains the results of the recoil measurement, including discussion of potential systematic errors. Finally, in Sect. 5 we discuss the future prospects for this experiment.

2 Theory

The underlying theory behind the recoil measurement is presented in this section. In subsection 2.1 we derive the full quantum mechanical equations governing velocity-selective stimulated Raman transitions. Then in subsection 2.2 we discuss atomic interference in general and consider in detail the semi-classical spatial picture in which the double atomic interferometer is easiest to understand. Subsection 2.3 considers the double atomic interferometer in particular.

2.1 Stimulated Raman transitions

Velocity-selective stimulated Raman transitions give a four times larger recoil shift than single photon transitions using comparable wavelengths. They allow both internal states in our state-labeled interferometer to be ground states, so that we can take advantage of the long measurement times afforded by the atomic fountain. Also, because the frequency difference between those levels is in the microwave region, it is only necessary to precisely control microwave and not optical frequencies.

2.1.1 Classical analysis. In this subsection, as in the 'simplified experiment' in the introduction, we will look only at the states of the system before and after the excitation, so that we do not need to know anything about the

---
[1] The mass of the atom is different in the two ground states by 3×10^{-16}
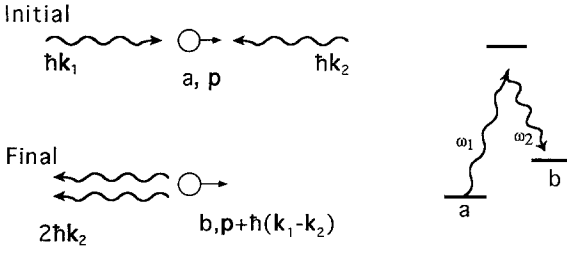
Fig. 5. An atom undergoes a stimulated Raman transition and receives a momentum kick due to both photons. This is directly analogous to Fig. 1

intermediate level or the atomic physics of the excitation. The black box picture of a stimulated Raman transition is shown in Fig. 5. The atom is initially in the state $|a\rangle$ and is excited by a rightward traveling photon with frequency ω_1 to a virtual level many linewidths away from the excited state $|i\rangle$, so that the probability of spontaneous emission from the excited state is small. It is then stimulated down to the state $|b\rangle$ by a leftward traveling photon with frequency ω_2. If we require energy and momentum to be conserved in this process, we find the resonance condition,

$$(\omega_1 - \omega_2) - \omega_{ab} = \mathbf{v}_0 \cdot (\mathbf{k}_1 - \mathbf{k}_2) \pm \frac{\hbar}{2m}(\mathbf{k}_1 - \mathbf{k}_2)^2, \qquad (7)$$

where a positive sign for the last term corresponds to the initial energy level being lower than the final one and vice versa. Comparison to (2) shows that the stimulated Raman transition behaves like a one-photon transition between states $|a\rangle$ and $|b\rangle$ when the following two correspondences are made. First, the effective photon has the frequency ω_{12}, which is the frequency difference between the two photons. Second, the effective photon has an effective $\mathbf{k}$-vector, $\mathbf{k}_{eff} = \mathbf{k}_1 - \mathbf{k}_2$, which for counter-propagating comparable frequency beams is double the single photon recoil. Thus, interference diagrams like those in Figs. 3 and 4 can still be used when stimulated Raman transitions are applied, as long as the illustrated photon is understood to be this effective photon.

2.1.2 Quantum mechanical analysis.

The quantum mechanical analysis is somewhat more involved and has been done elsewhere [20, 36]. It will be necessary in the analysis of systematic errors to refer to some of the details of this derivation, so we will present much of it here. In the limit where spontaneous emission can be neglected the equations governing a three-level system take the same form as equations for a two-level system. In order to aid our analysis we will also explicitly include additional excited states and allow both laser beams to interact with any excited state level. In this analysis we include the effect of both Raman beams on both ground state levels.

The Hamiltonian for the two ground state-many excited state system, in the absence of spontaneous emission, is

$$\hat{H} = \frac{\hat{p}^2}{2m} + \hbar\omega_a |a\rangle \langle a| + \hbar\omega_b |b\rangle \langle b|$$
$$+ \sum_{\substack{excited \\ states}} [\hbar\omega_i |i\rangle \langle i| + (\hat{\mathbf{d}}_{ia} + \hat{\mathbf{d}}_{ib} + \hat{\mathbf{d}}_{ai} + \hat{\mathbf{d}}_{bi}) \cdot \mathbf{E}(\mathbf{r}, t)], \qquad (8)$$

where $\hbar\omega_\alpha$ is the energy of level α, $\mathbf{E}$ is the electric field of the light, and $\hat{\mathbf{d}}_{ij}$ is the electric dipole operator associated with state j and the i-th excited state, $\hat{\mathbf{d}}_{ij} = |i\rangle \mathbf{d}_{ij} \langle j|$. The electric field for two incident beams is given by

$$\mathbf{E}(\mathbf{r}, t) = \mathbf{E}_1 \cos (\mathbf{k}_1 \cdot \mathbf{r} - \omega_1 t + \varphi_1)$$
$$+ \mathbf{E}_2 \cos (\mathbf{k}_2 \cdot \mathbf{r} - \omega_2 t + \varphi_2). \qquad (9)$$

It is useful to define Rabi frequencies to characterize the level couplings,

$$\Omega_{kji} = \frac{\langle i|\hat{\mathbf{d}}_{ij} \cdot \mathbf{E}_k |j\rangle}{\hbar}, \qquad (10)$$

where $k = 1, 2$ specifies the light beam, and $j = a, b$ specifies the ground state.

Solutions of the Schrödinger equation can be found using a basis of states of the form

$$a_{\alpha, p'} \exp \left[-i \left(\omega_\alpha + \frac{p'^2}{2m\hbar} \right) t \right] |\alpha, \mathbf{p}'\rangle. \qquad (11)$$

We now explicitly start with an atom in state

$$|a, \mathbf{p}\rangle,$$

so the states that are coupled by the light are

$$|a, \mathbf{p}\rangle, \ |b, \mathbf{p} + \hbar\mathbf{k}_{eff}\rangle, \ |i, \mathbf{p} + \hbar\mathbf{k}_1\rangle, \ |i, \mathbf{p} + \hbar\mathbf{k}_2\rangle,$$

and

$$|i, \mathbf{p} + \hbar\mathbf{k}_{eff} + \hbar\mathbf{k}_1\rangle.$$

The equations that govern the time evolution of the coefficients of this closed family of states are

$$\dot{a}_{a,\mathbf{p}} = \frac{i}{2} \sum_{k,i} \Omega^*_{kai} e^{i\Delta_{kai}t} e^{-i\varphi_k} a_{i,\mathbf{p}+\hbar\mathbf{k}_k},$$

$$\dot{a}_{b,\mathbf{p}+\hbar\mathbf{k}_{eff}} = \frac{i}{2} \sum_{k,i} \Omega^*_{kbi} e^{i\Delta_{kbi}t} e^{-i\varphi_k} a_{i,\mathbf{p}+\hbar\mathbf{k}_{eff}+\hbar\mathbf{k}_k},$$

$$\dot{a}_{i,\mathbf{p}+\hbar\mathbf{k}_1} = \frac{i}{2} \left(\Omega_{1ai} e^{-i\Delta_{1ai}t} e^{i\varphi_1} a_{a,\mathbf{p}} + \Omega_{2bi} e^{-i\Delta_{2bi}t} e^{i\varphi_2} a_{b,\mathbf{p}+\hbar\mathbf{k}_{eff}} \right),$$

$$\dot{a}_{i,\mathbf{p}+\hbar\mathbf{k}_2} = \frac{i}{2} \Omega_{2ai} e^{-i\Delta_{2ai}t} e^{i\varphi_2} a_{a,\mathbf{p}},$$

$$\dot{a}_{i,\mathbf{p}+\hbar\mathbf{k}_{eff}+\hbar\mathbf{k}_1} = \frac{i}{2} \Omega_{1bi} e^{-i\Delta_{1bi}t} e^{i\varphi_1} a_{b,\mathbf{p}+\hbar\mathbf{k}_{eff}}, \qquad (12)$$

where the detunings of the two beams from the various levels are given by

$$\Delta_{kji} = \omega_k - (\omega_i - \omega_j) + \frac{p_j^2}{2m\hbar} - \frac{|\mathbf{p}_j + \hbar\mathbf{k}_k|^2}{2m\hbar}, \qquad (13)$$
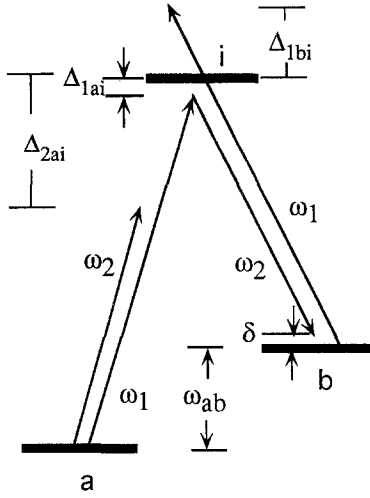
Fig. 6. Energy level diagram for a stimulated Raman transition. One intermediate level is shown, but the formalism allows for many levels which are not necessarily coupled by the light to both ground states

with $\mathbf{p}_a = \mathbf{p}$ and $\mathbf{p}_b = \mathbf{p} + \hbar\mathbf{k}_{\mathrm{eff}}$. These detunings from a single intermediate state $|i\rangle$ are illustrated in Fig. 6. Equations (12) are exact to within the rotating wave approximation.

In the limit where the detunings from the excited states are much larger than the Rabi frequencies, $\Delta \gg \Omega$, the coefficients a vary slowly compared to the explicitly time dependent terms. We can thus adiabatically eliminate all the coefficients $a_{i,\mathbf{p}_j + \hbar\mathbf{k}_k}$ from (12). We next dismiss all terms in the remaining two equations that oscillate at $\omega_1 - \omega_2$, which corresponds to the limit that the detuning from the Raman resonance condition is much smaller than ω_{ab}, the splitting between the ground state levels. We are left with the following pair of equations,

$$\dot{a}_{a,\mathbf{p}} = -i\Omega_a^{AC} a_{a,\mathbf{p}} - i e^{i\delta t} e^{i\varphi_{\mathrm{eff}}} \Omega_{\mathrm{eff}} a_{b,\mathbf{p}+\hbar\mathbf{k}_{\mathrm{eff}}},$$

$$\dot{a}_{b,\mathbf{p}+\hbar\mathbf{k}_{\mathrm{eff}}} = -i\Omega_b^{AC} a_{b,\mathbf{p}+\hbar\mathbf{k}_{\mathrm{eff}}} - i e^{-i\delta t} e^{-i\varphi_{\mathrm{eff}}} \Omega_{\mathrm{eff}}^* a_{a,\mathbf{p}}, \quad (14)$$

which are analogous to the equations of motion for a two-level atom in a single frequency driving field. In these equations,

$$\Omega_{\mathrm{eff}} = \sum_i \frac{\Omega_{1ai}^* \Omega_{2bi}}{4\Delta_{1ai}}, \quad \Omega_j^{AC} = \sum_{k,i} \frac{|\Omega_{kji}|^2}{4\Delta_{kji}}, \quad \varphi_{\mathrm{eff}} = \varphi_2 - \varphi_1,$$

$$\delta = (\omega_1 - \omega_2) - \left(\omega_{ab} + \frac{\mathbf{p}\cdot\mathbf{k}_{\mathrm{eff}}}{m} + \frac{\hbar k_{\mathrm{eff}}^2}{2m}\right). \quad (15)$$

For the purposes of these identifications the distinction between Δ_{1ai} and Δ_{2bi} is negligible in this limit. Also, in the expression for Ω_{eff} there is no sum over the beam index, k, because all such terms which contain Δ_{2ai} or Δ_{1bi} dropped out for oscillating too fast. For each excited state, only the one combination of states and beams that roughly satisfies the Raman resonance condition appears in the Rabi frequency. There are some excited states that, for reason of angular selection rules, couple to one of the ground states and not to the other. These states appear

in the ac Stark shift sum but not in the Rabi frequency sum.

Ω_j^{AC} are the total ac Stark shifts of levels a and b, Ω_{eff} is the Rabi frequency in this effective two-level system and δ is the detuning from the Raman resonance in the absence of the ac Stark shift. In the analogy with the two-level system, the ac Stark shifts correspond to the energies of the two levels, and δ is the frequency of the coupling radiation. Only the Rabi frequency is described unchanged in the analogy.

The solution of (14) for a pulse of duration τ beginning at time t_0 is well known from the early days of NMR [37], and is given by

$$a_{a,\mathbf{p}}(t_0 + \tau) = \exp\left\{\frac{i}{2}[\delta - (\Omega_a^{AC} + \Omega_b^{AC})]\tau\right\}$$

$$\times \left\{\left[i\cos\Theta\sin\left(\frac{\omega\tau}{2}\right) + \cos\left(\frac{\omega\tau}{2}\right)\right]a_{a,\mathbf{p}}(t_0)\right.$$

$$\left. + \left[i\sin\Theta\sin\left(\frac{\omega\tau}{2}\right)e^{i(\delta t_0 + \varphi_{\mathrm{eff}})}\right]a_{b,\mathbf{p}+\hbar\mathbf{k}_{\mathrm{eff}}}(t_0)\right\},$$

$$a_{b,\mathbf{p}+\hbar\mathbf{k}_{\mathrm{eff}}}(t_0 + \tau) = \exp\left\{\frac{i}{2}\left[-\delta - \left(\Omega_a^{AC} + \Omega_b^{AC}\right)\right]\tau\right\}$$

$$\times \left\{\left[-i\cos\Theta\sin\left(\frac{\omega\tau}{2}\right) + \cos\left(\frac{\omega\tau}{2}\right)\right]a_{b,\mathbf{p}+\hbar\mathbf{k}_{\mathrm{eff}}}(t_0)\right.$$

$$\left. + \left[i\sin\Theta\sin\left(\frac{\omega\tau}{2}\right)e^{-i(\delta t_0 + \varphi_{\mathrm{eff}})}\right]a_{a,\mathbf{p}}(t_0)\right\}, \quad (16)$$

where

$$\omega^2 = (\delta^{AC} - \delta)^2 + 4\Omega_{\mathrm{eff}}^2, \quad \delta^{AC} = \Omega_b^{AC} - \Omega_a^{AC},$$

$$\cos\Theta = \frac{\delta^{AC} - \delta}{\omega}, \quad \sin\Theta = -\frac{2\Omega_{\mathrm{eff}}}{\omega}. \quad (17)$$

As a check to see that the equations behave properly in a situation where the expected result is unambiguous, we can make the effective Rabi frequency be zero, but still allow light to be present which causes ac Stark shifts. Then (16) reduces to

$$a_{a,\mathbf{p}}(t_0 + \tau) = e^{-i\Omega_a^{AC}\tau} a_{a,\mathbf{p}}(t_0),$$

$$a_{b,\mathbf{p}+\hbar\mathbf{k}_{\mathrm{eff}}}(t_0 + \tau) = e^{-i\Omega_b^{AC}\tau} a_{b,\mathbf{p}+\hbar\mathbf{k}_{\mathrm{eff}}}(t_0), \quad (18)$$

as expected.

When we consider atomic interference we will be interested in the phase shifts which accrue along distinct atomic trajectories. Equations (16) can be reexpressed so that the phases and amplitudes are kept distinct. In general, we will care mostly about the phase shifts accrued during $\pi/2$ or π pulses. When $\omega\tau/2 = \pi/4 + \varepsilon$, (with ε small so that we have approximately a $\pi/2$ pulse), and $\cos\Theta$ is small (that is, the detuning from the ac Stark shifted Raman resonance is small compared to the Rabi

frequency) we find

$$a_{a,\mathrm{p}}(t_0+\tau) = \exp\left[\mathrm{i}(\delta\tau/2 - \varphi_{\mathrm{acs}})\right]$$

$$\times \frac{1}{\sqrt{2}}\left((1-\varepsilon)\exp\left(-\mathrm{i}\varphi_{\mathrm{off}}\right)a_{a,\mathrm{p}}(t_0)\right.$$

$$\left. + \left\{(1+\varepsilon)\exp\left[\mathrm{i}\left(\delta t_0 + \varphi_{\mathrm{eff}} + \frac{\pi}{2}\right)\right]\right\}a_{b,\mathrm{p}+\hbar\mathbf{k}_{\mathrm{eff}}}\right),$$

$$a_{b,\mathrm{p}+\hbar\mathbf{k}_{\mathrm{eff}}}(t_0+\tau) = \exp\left[\mathrm{i}(-\delta\tau/2 - \varphi_{\mathrm{acs}})\right]$$

$$\times \frac{1}{\sqrt{2}}\left((1-\varepsilon)\exp\left(\mathrm{i}\varphi_{\mathrm{off}}\right)a_{b,\mathrm{p}+\hbar\mathbf{k}_{\mathrm{eff}}}(t_0)\right.$$

$$\left. + \left\{(1+\varepsilon)\exp\left[-\mathrm{i}\left(\delta t_0 + \varphi_{\mathrm{eff}} - \frac{\pi}{2}\right)\right]\right\}a_{a,\mathrm{p}}\right), \quad (19)$$

where

$$\varphi_{\mathrm{acs}} = \frac{(\Omega_a^{\mathrm{AC}} + \Omega_b^{\mathrm{AC}})\,\tau}{2}, \quad \varphi_{\mathrm{off}} = \left(\Theta - \frac{\pi}{2}\right)(1+2\varepsilon). \quad (20)$$

The phase subscripts acs and off denote, respectively, the ac Stark shift and any detuning offset from the ac Stark-shifted resonance. For historical reasons [37], Θ has been defined so that $\eta \equiv \pi/2 - \Theta$ is a small number near resonance[2]. Terms up to second order in small quantities have been kept in the phase parts of the above equations, although only first order terms have been kept in the amplitude parts. For $\omega\tau/2 = \pi/2 + \varepsilon$, an approximate π pulse,

$$a_{a,\mathrm{p}}(t_0+\tau) = \exp\left[\mathrm{i}(\delta\tau/2 - \varphi_{\mathrm{acs}})\right]$$

$$\times \left\{\sqrt{\eta^2+\varepsilon^2}\exp\left[-\mathrm{i}\tan^{-1}\left(\frac{\eta}{\varepsilon}\right)\right]a_{a,\mathrm{p}}(t_0)\right.$$

$$\left. + \exp\left[\mathrm{i}\left(\delta t_0 + \varphi_{\mathrm{eff}} + \frac{\pi}{2}\right)\right]a_{b,\mathrm{p}+\hbar\mathbf{k}_{\mathrm{eff}}}(t_0)\right\},$$

$$a_{b,\mathrm{p}+\hbar\mathbf{k}_{\mathrm{eff}}}(t_0+\tau) = \exp\left[\mathrm{i}(-\delta\tau/2 - \varphi_{\mathrm{acs}})\right]$$

$$\times \left\{\exp\left[\mathrm{i}\left(-\delta t_0 - \varphi_{\mathrm{eff}} + \frac{\pi}{2}\right)\right]a_{a,\mathrm{p}}(t_0)\right.$$

$$\left. + \sqrt{\eta^2+\varepsilon^2}\exp\left[\mathrm{i}\tan^{-1}\left(\frac{\eta}{\varepsilon}\right)\right]a_{b,\mathrm{p}+\hbar\mathbf{k}_{\mathrm{eff}}}(t_0)\right\}. \quad (21)$$

When all the population originates in a single state, the amplitude and phase associated with the transfer of amplitude to the other state are first order independent of ε and Θ.

___

[2] φ_{off} is the small detuning limit of the terms which prevent complete population transfer to the excited state when the radiation is tuned off resonance. In the optical Bloch picture, it would be the angle of the torque vector with respect to the x-y (or u-v) plane [38]

2.2 Atomic interference and the semi-classical picture

When an atom is put into a coherent superposition of two energy states, the centers of its two state-labeled spatial wavepackets will start to move away from each other at the photon recoil velocity, separating from each other by $\delta x_{\mathrm{r}} = \hbar k_{\mathrm{eff}} T/m$ in a time T. These two wavepackets will have distinct space-time trajectories which must overlap in space at a later point in time if they are to interfere. In rf and microwave Ramsey spectroscopy the spatial coherence length of the atomic ensemble, $\delta x_{\mathrm{c}} = \hbar/\Delta p$, where Δp is the momentum spread of the atoms, is typically much larger than δx_{r}. Therefore, sufficient overlap for interference occurs without the need to explicitly redirect the atomic trajectories between the establishment of the coherence and the detection of the interference. When Ramsey spectroscopy is performed using optical wavelengths it is usually the case that $\delta x_{\mathrm{r}} \gg \delta x_{\mathrm{c}}$, so it is generally necessary to redirect the parts of the atom separated by a recoil. A scheme to do this using three standing waves was proposed by Baklanov et al. [39] and demonstrated by Bergquist et al. [40]. The latter group identified the traveling wave components that lead to the signal, two oppositely directed pairs of $\pi/2$ pulses, which is essentially the same sequence employed in our experiment. The interpretation of their experiment as an atomic interferometer came a dozen years later [41]. The simplest light-pulse atomic interferometer pulse sequence, using a total of three pulses, has since been demonstrated by Kasevich and Chu [42].

Rigorous calculation of atomic interference is relatively simple in the momentum picture, in which the calculations of the preceding section were performed, because the effect on each atomic plane wave component due to any number of light pulses can be computed independently. Integrals can then be taken over each atom's momentum wave function and over the ensemble of atoms. In contrast, the calculation is difficult in the position picture because there is no closed family of position states that allows the problem to be Fourier-decomposed. Nonetheless, the position picture is heuristically helpful. Furthermore, in calculations which involve spatial gradients of fields the plane wave picture alone is insufficient.

The calculational merit of the plane wave picture can be retained in the spatial picture if we take the classical limit of the quantum mechanical free propagator, which allows us to associate a single momentum with the atomic wavepacket [43]. This is the limit where the classical action, defined as [44]

$$S = \int_{t_i}^{t_f} \frac{1}{2}m\dot{x}^2\,dt = \frac{m}{2}v^2(t_f - t_i), \quad (22)$$

is much larger than $\hbar$. The semi-classical condition $S \gg \hbar$ is well satisfied during the free propagation times in our experiments. However, during the Rabi pulse times this condition is less well satisfied. For instance, we must follow a Cs atom moving at its Raman transition recoil velocity for 25 μs for the action to be equal to $\hbar$. In our

experiments we are typically in the semi-classical limit for the length of a $\pi/2$ pulse by only about a factor of 20.

As long as we can use this approximation, a well-localized atomic wavepacket can be followed in space and its momentum-dependent interactions with external fields can be calculated using the classical momentum, without the need to sum over plane waves. If an atom is split into two coherent parts by a light pulse, the phase accumulated by each separate path can be calculated in this semi-classical limit. Bordé and Riehle et al. have expounded a list of phase shift rules that apply at light-pulse vertices and during free space propagation [43, 45]. We will generalize that exposition by including ac Stark shift terms, which are absent for a single photon transition, and considering the effect of pulse lengths that deviate slightly from $\pi/2$ or π.

Along the freely propagating segments of a path the accumulated atomic phase is equal to the action along that path, $\exp(iL\Delta t/\hbar)$, where L is the atomic Lagrangian. Using the Lagrangian for an unperturbed free atom, this phase term is

$$e^{i\varphi_{free}} = \exp[i(k_a\Delta x - \omega_a\Delta t)], \qquad (23)$$

where $\hbar\omega_a$ is the total energy of the atom and k_a is the atomic wavenumber, $k_a = p_a/\hbar$. If all the forces on the atom are conservative, then the only part of the atom's energy that changes is the energy of the atom's internal state. Other energies remain constant, so the associated global phase factors can be ignored.

Gravity causes an additional phase shift along a freely evolving path,

$$\varphi_g = -\frac{m}{\hbar}\left(v_0\Delta z - \int \sqrt{v_0^2 - 2gz}\,dz\right), \qquad (24)$$

which we obtain using (23) and allowing p_a to evolve in a uniform gravitational field. This phase shift is the same for two paths which intersect at their beginning and end, so free evolution in a gravitational field does not in itself cause an interferometer phase shift [42]. However, gravity does change the point at which the atom interacts with the light field, which we shall soon see does cause an interferometer phase shift.

If the laser beams rotate in the plane of interference, the Sagnac effect contributes a phase shift to each straight path of

$$\varphi_S = (\mathbf{\Omega}\cdot\mathbf{r}\times\mathbf{p})\frac{\Delta t}{\hbar}, \qquad (25)$$

where $\mathbf{r}$ is the position at the end of the path, $\mathbf{p}$ is the atomic momentum for that path in the freely falling reference frame, Δt is the time interval of the path and $\mathbf{\Omega}$ is the angular velocity of the rotating frame [43]. The net effect of these shifts in an atomic interferometer is that the phase shift is proportional to the area swept out in the interferometer. The Sagnac effect has been previously observed in an atomic interferometer, where the entire apparatus was rotated at 0.1 Hz [45]. The earth's rotation should be observable in an apparatus

similar to ours [42]. We show in subsection 4.6 that the Sagnac effect does not cause a systematic error in our experiment.

An external field will also modify the action during the free propagation segments. Phase shifts that are caused by forces on the atom are relatively difficult to model, because they change the atom's path in space and time. In the limit when the perturbing field changes the velocity of the atom by much less than its mean velocity, these shifts can be approximated by phase shifts due to time dependent, spatially independent potential energy changes. These do not change the path, which makes the calculation of their effect more straightforward. This approximation will be most useful in the context of magnetic field gradients.

To determine the effect of the light pulses on the phase accumulated on different semi-classical paths we will rely on (19) and (21). At each successive interaction with a laser beam we apply anew these solutions of the equations of motion for the effective two-level system to each distinct path separately. The phase shifts can basically just be read from (19) and (21), but we will discuss them all briefly here. The phase terms $\pm i\delta t_0$, which keep track of the relative phase evolution between different momentum states when the solution is done with plane waves, are now zero because $t_0 = 0$ in this fragmentary solution to the problem. The laser phase terms $\pm i\varphi_{eff}$, take on an added significance because they now correspond to the phase where the path intersects the laser beam. This is in contrast to the plane wave calculation, where as long as the laser beams are parallel and stable, the laser phase can simply be set equal to zero.

From both (19) and (21) we can see that when a path makes a transition between two states it accrues an additional phase of $\pm\varphi_{eff} = \pm[(\omega_1 - \omega_2)t - \mathbf{k}_{eff}\cdot\mathbf{r}]$. The position and the time are referenced to some fixed point. The constant phase shift $\pi/2$, which appears along with φ_{eff}, will not contribute a phase shift difference between two paths which start and finish in the same state, so it can in general be ignored. Anything that affects this phase must be included in this term, like phase noise on the laser frequency difference or acceleration due to gravity, which changes $\mathbf{r}$ from what it would otherwise be. A phase shift due to a change in $\mathbf{r}$ in the semi-classical picture corresponds to a Doppler shift in the momentum space picture.

Equations (19) and (21) also show that every path that sees a $\pi/2$ pulse gets a phase shift of φ_{acs}. Thus if the ac Stark shift does not depend on the position along the exciting beam this term drops out in any interferometric comparison between paths. Because the ac Stark shift scales in the same way as the Rabi frequency, the size of φ_{acs} is essentially independent of the pulse length. However, in the short pulse limit ($\tau \ll T$), φ_{acs} becomes a vanishingly small fraction of the total phase accumulated along any given path.

From (19), when a path sees a $\pi/2$ pulse and does not make a transition it accrues an additional phase of $\pm\varphi_{off} = (\Theta - \pi/2)(1 + 2\varepsilon)$. If the laser is on the ac Stark shifted resonance, $\varphi_{off} = 0$.
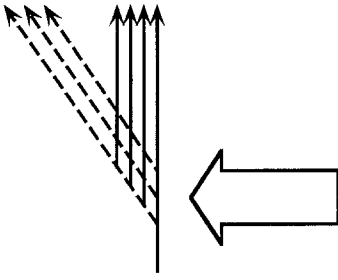
Fig. 7. Qualitative spreading of a wavepacket at a pulse. Amplitude is continually being exchanged between the two coupled states during the light pulse
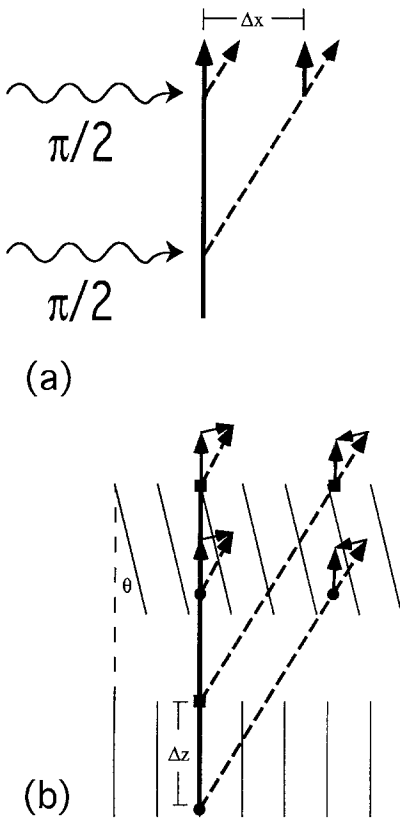

Fig. 8a, b. The atomic paths resulting from a $\pi/2 - \pi/2$ pulse sequence. **a** Δx is the separation of the two pairs of paths immediately after the second $\pi/2$ pulse. **b** Illustration of phase washout due to misaligned beams and a longitudinal spatial spread in the atomic ensemble. The parallel lines represent either parts of a single, curved set of wavefronts or two beams with different **k**-vectors. The boxes correspond to the location of one atom during the pulse, and the circles correspond to the location of another atom with the same initial velocity. The phase difference between the light at the first pulse compared to the last pulse is different for the two atoms, so that they will contribute to velocity fringes with different phases

When a transition between internal states takes place in a finite time, there is an inherent delocalization of the wavefunction. Consider a well localized wavepacket that receives a light pulse. Early in the pulse, the amplitude in the excited state, which has a different momentum from the initial state, begins to grow and separate from the initial state (see Fig. 7). The excited state becomes a source for amplitude in the initial state, even as it gains

amplitude from the initial state. The wavepackets of the atom can be substantially delocalized in this way after a single Rabi pulse. Therefore, two wavepackets need only be overlapped in time to within the pulse width and in space to within the product of the interaction time and the mean atomic velocity in order to have interference. Because various experimental imperfections may lead to imperfect overlap of interfering wavepackets, it is important to keep their inherent fuzziness in mind.

As an application of this semi-classical picture, consider a $\pi/2-\pi/2$ pulse sequence in the usual limit of optical Ramsey spectroscopy, $\delta x_r \gg \delta x_c$. After the second $\pi/2$ pulse the atomic path is coherently divided into four paths, with two paths in each state spatially separated by $\Delta x = (\hbar k_{\text{eff}}/m) T$ (see Fig. 8a). If we take the Fourier transform of this spatial distribution for each internal state, we find fringes in the velocity distribution with a period of λ_{eff}/T [36].

Now suppose the second beam in the $\pi/2-\pi/2$ pulse sequence is misaligned by an angle θ with respect to the first, or equivalently, that wavefront curvature results in a different **k**-vector at the second pulse (see Fig. 8). The spatial separation of the two halves along the second beam will be $\cos \theta \hbar k_{\text{eff}} T/m$ and the periodicity of the velocity fringes is reduced by a factor of $\cos \theta$. If the atoms that contribute to the signal have a spread Δz along their direction of motion, then two atoms that have the same momentum and position along the first beam, but a different position perpendicular to the beam, Δx, will interact at different phase fronts of the second beam. These two atoms will thus contribute to velocity fringes which are phase shifted with respect to each other. If $\Delta z = \lambda_{\text{eff}}/2 \tan \theta$, the two sets of fringes will be π out of phase and wash each other out.

2.3 Double atomic interferometer

2.3.1 General description.
A picture of the four $\pi/2$ pulse sequence is shown in Fig. 3. After the first $\pi/2$ pulse pair the direction of k_{eff} is reversed. This change breaks up the existing closed families of momentum states, $|a, \mathbf{p}\rangle$ and $|b, \mathbf{p}+\hbar\mathbf{k}_{\text{eff}}\rangle$, and matches them each with states whose momenta point away from the first family's mean, $|b, \mathbf{p}-\hbar\mathbf{k}_{\text{eff}}\rangle$ and $|a, \mathbf{p}+2\hbar\mathbf{k}_{\text{eff}}\rangle$, respectively. Four of the eight coherent paths after the third $\pi/2$ pulse do not intersect with other paths at the final $\pi/2$ pulse. The other four coherent paths form two distinct interferometer loops. The differences between the two are minimal and easily enumerated. They are different with regard to: their mean velocities, which are separated by $2\hbar k_{\text{eff}}/m$; their spatial paths; and the internal state they occupy in the time between the middle $\pi/2$ pulses.

The first difference is precisely what we measure, because the velocity difference is proportional to two effective photon recoils. Since it is the difference between two sets of interferometer fringes that is measured, absolute frequency is unimportant. Any homogeneous field, gravity, or Doppler offsets are the same for the two interferometers, and do not affect the measured photon recoil.

The second difference between the interferometers, their spatial paths, is our primary source of systematic error. Inhomogeneous fields will cause different phase shifts in the two interferometers, which will tend to change the separation of their fringe patterns. These inhomogeneous shifts will be considered in detail in the section on systematic errors.

The difference in the internal states between the middle $\pi/2$ pulses is somewhat less significant. Again homogeneous fields cause no error, this time because the phase shifts are equal for the two arms of each interferometer. Inhomogeneous fields remain a potential source of error which must be considered. This difference in the intermediate internal states can be useful, in that it allows us to selectively remove atoms from each of the interferometers.

2.3.2 Numerical calculations. The first detailed calculations on the double atom interferometer were performed by Bordé et al. [15], when they demonstrated single photon optical Ramsey spectroscopy with traveling waves. They used a matrix formalism to keep track of the evolution of the amplitudes and phases associated with two plane wave momentum components for each state. The expressions they find contain the essential physics and analytically demonstrate interference clearly. However, that work considered only single photon transitions and atomic plane waves, and their numerical calculations are in the limit of a negligible photon recoil shift. These differences limit the direct application of those results to this work.

We consider the double interferometer in a reference frame that is accelerating with gravity, so that we can ignore the effect of gravity. As a practical matter, one must take gravity into account either by making the Raman beams horizontal so that there is no acceleration in the velocity selection direction, or by adjusting the detuning to keep the atoms in resonance with the light from pulse to pulse. The required precision of the adjustment is on the order of the Rabi frequency and not the Ramsey fringe width.

Our numerical calculations use the complete solution of the effective two-level equations, (14), assuming square pulses. The beam direction is changed in the calculation by taking the amplitudes in the original closed family of states and evolving them each separately in their new closed family of states. The equations for the new families are identical to each other, except that the momentum, **p**, is shifted either up or down by one recoil. We obtain the probabilities of ending up in each of the four possible momentum-labeled states as a function of the detuning of the second pair of $\pi/2$ pulses. We also find the total probability of finishing the pulse sequence in each of the two internal states, since this is the quantity we actually measure. The calculation is performed for many different initial atomic momenta. The results are weighted according to an initial Gaussian momentum distribution and summed together to yield the expected signal.

For a measurement of the photon recoil, the double interferometer can be excited in two limits: the Rabi
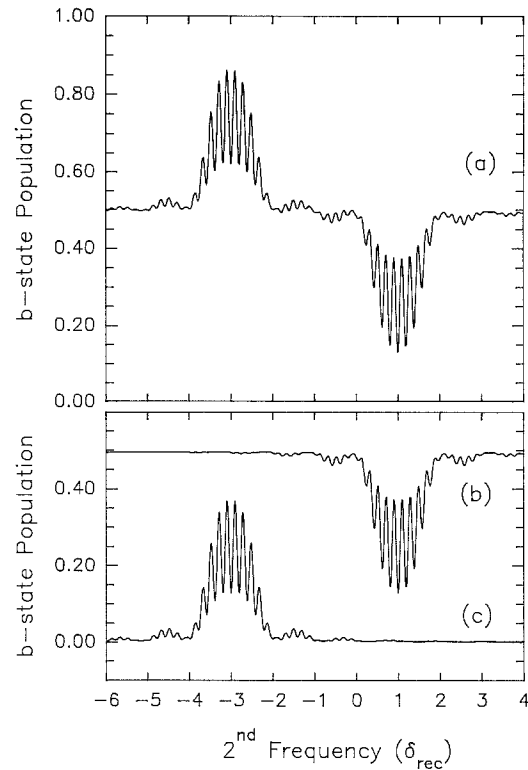

Fig. 9. Numerically calculated double atom interferometer signal for a Raman transition. (*a*) The total fraction of atoms that end up in the excited state after four $\pi/2$ pulses. (*b*) The final fraction in the excited state that are in the excited state between the $\pi/2$ pairs. (*c*) The final fraction in the excited state that are in the ground state between the $\pi/2$ pairs. The parameters correspond to Cs, the Raman Rabi frequencies are 2π (1.1 kHz), $T = 500$ μs, and the initial momentum spread is $0.3 \, \delta_{rec}$, although the momentum integration is carried out over δ_{rec}.

frequency, Ω_{eff}, can be either much larger or much smaller than the recoil splitting, $\omega_{rs} = 2\hbar k_{eff}^2/m$. When $\Omega_{eff} \ll \omega_{rs}$, the two interferometers are not in resonance at the same detuning of the final pulse pair. This is the limit in which our experiment is performed. An illustrative numerically obtained signal is shown in Fig. 9. The ac Stark shifts for the two states are set equal to each other, the four pulses are exactly $\pi/2$ at resonance, and the first $\pi/2$ pulse pair is detuned exactly on resonance. For an initial ensemble of atoms in state $|a, \mathbf{p} = 0\rangle$, we plot the fraction that end the sequence in the $|b, \mathbf{p} - \hbar\mathbf{k}_{eff}\rangle$ state, the $|b, \mathbf{p} + \hbar\mathbf{k}_{eff}\rangle$ state and the sum of those two.

The signals can be understood with reference to the interferometer diagram, Fig. 3. When the final two $\pi/2$ pulses are far from any resonance, the atoms remain as they are after the second $\pi/2$ pulse, evenly divided between the two states. When the interferometer that contains $|b, \mathbf{p} + \hbar\mathbf{k}_{eff}\rangle$ is in resonance, atoms that end the second $\pi/2$ pulse in $|b\rangle$ have a chance to make a transition to $|a\rangle$, so the $|b\rangle$ population dips down. This dip is the sum of two parts: one with oscillations, due to the two paths that interfere, and the other a broad feature, due to the two paths that do not interfere, whose amplitude ends up split between the two states. Conversely, when the interferometer that contains the $|a, \mathbf{p}\rangle$ atoms is in resonance, the $|b\rangle$ population can gain atoms and
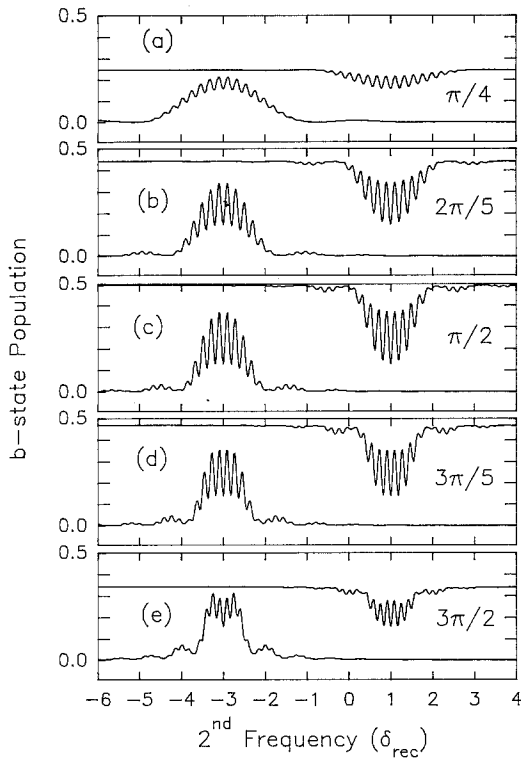
Fig. 10a–e. Incorrect length 'π/2' pulses. The numerically generated fringes in a double atomic interferometer are shown for pulses that differ from π/2. The ac Stark shifts of the two levels have been canceled. Notice that the locations of the central fringes do not shift
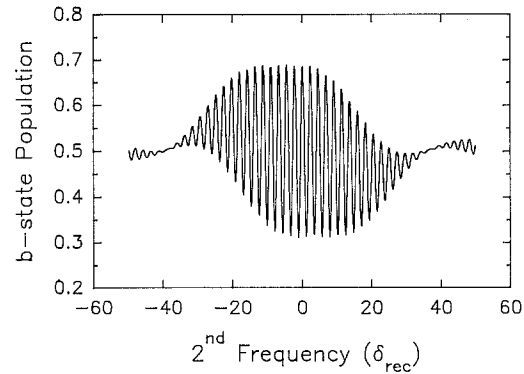

Fig. 11. Interference fringes in the short pulse limit. This is the numerical double atom interferometer signal when the Rabi frequency is 5 times larger than the recoil splitting. The contrast of the fringes depends on the fringe frequency

the signal peaks up. It is important to note that although the parts of the two signals that correspond to the non-interfering paths are inverted with respect to each other, the oscillations are not. This reflects the similarity of the two interferometers after the third π/2 pulse, which is crucial to the recoil measurement.

Analytical solutions are sufficient to demonstrate the insensitivity of the recoil measurement to non-zero ac Stark shifts and deviations from perfect π/2 pulses. To graphically illustrate the latter insensitivity, Fig. 10 shows the calculated signal when the size of the nominal π/2 pulses is varied from π/4 to 3π/2. The central fringes do not change location.

When $\Omega_{\rm eff} \gg \omega_{\rm rs}$, the two interferometers are in resonance at the same frequencies. Although this is not the limit of our experiment, we will consider it here. In this case there is no net contribution to the signal from the non-interfering paths, since they result in equal amplitudes in the two states regardless of the detuning. The signal consists of two identical sets of Ramsey fringes with overlapping Rabi envelopes. The fringes are separated by $\omega_{\rm rs}$, but their amplitude is undiminished at that distance from their central fringes. A numerical calculation of the total signal in this limit is shown in Fig. 11. If n is an integer and T the time between π/2 pulses, then the two fringes will constructively interfere when $2\pi n = \omega_{\rm rs}T$, which is when an integer number of fringes fit between the central peaks. When $2\pi n = \omega_{\rm rs}T + \pi$, the two sets of fringes will destructively interfere in the frequency range between and near the central peaks. If data

were to be taken under these conditions, one would scan T in order to determine $\omega_{\rm rs}$. Alternately, one could use the state separation in the time between the middle π/2 pulses to alternately clear away atoms in the two interferometers, and measure each of their central fringes independently. Similarly, the two sets of fringes could be measured independently if the spatial separation of the two interferometer endpoints was larger than the spatial spread in the atomic ensemble.

2.3.3 Semi-classical picture for homogeneous fields.

Bordé has calculated the relative phase shifts between the two arms of each interferometer for single photon transitions [43]. This shift is

$$\delta\varphi = [(\omega_1 - \omega_2) - \omega_{ab} \pm \delta_{\rm rec}] 2T, \tag{26}$$

where T is the time between π/2 pulses and $\delta_{\rm rec} = \hbar k_{\rm eff}^2/2m$. This follows from repeated applications of (19) at the vertices of the double interferometer and calculation of the action during the free propagation times. As expected, the phase shift difference between the interferometers $\Delta(\delta\varphi) = 4\delta_{\rm rec}T$, so that the frequency shift between the two sets of Ramsey fringes is $2\hbar k_{\rm eff}^2/m$. When inhomogeneous laser beams, imperfect detuning, and imperfect pulse sizes are allowed, some extra spatially dependent phase shifts can occur. We will show here how these shifts cancel exactly when the laser beams do not have these imperfections. In the section on systematic errors we will estimate the size of these errors in realistic experimental situations.

If the ac Stark shift is the same at all vertices its contribution to the phase, $\varphi_{\rm acs}$, is also the same at every vertex and the recoil result is unchanged. When we next keep track of $\varphi_{\rm off}$ to see the effect of being detuned with respect to the Stark shifted resonance (see Fig. 12) we find that

$$\delta\varphi_{\rm off} = -4\left(\Theta - \frac{\pi}{2}\right)(1 + 2\varepsilon) = 2\frac{(\delta^{\rm AC} - \delta)}{\Omega_{\rm eff}}(1 + 2\varepsilon) \tag{27}$$

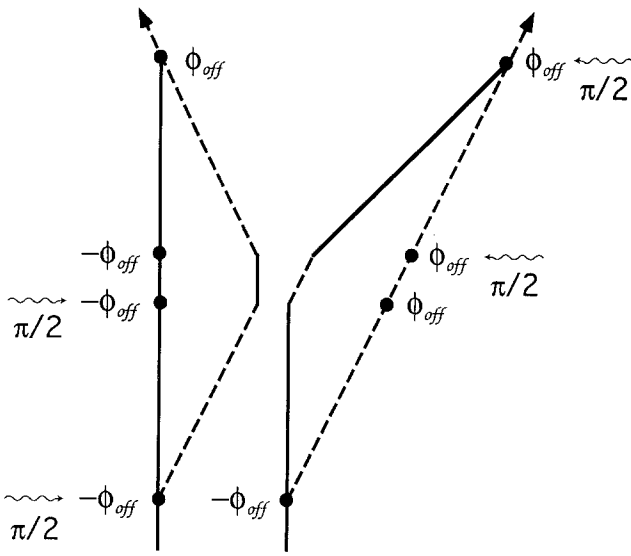for both interferometers. As long as the difference between the Stark shifts of the two levels has no gradient

Fig. 12. Phase shifts due to φ_{off}. The atom enters from below in state $|a\rangle$. These phase shifts, which occur only off resonance, only accrue to paths that do not make transitions. The *arrows* denote the direction of the effective **k** vector

Fig. 13. Schematic of the experiment. Most of the laser beams contain two component beams

along the laser beams, $\Delta(\delta\varphi_{\text{off}}) = 0$ and there is no error from these terms. Because the cancellation occurs on a pulse by pulse basis, a gradient of the relative ac Stark shift transverse to the beam causes no error in the separation. Similarly, an imperfect $\pi/2$ pulse size causes no error in the measured separation when the fields are spatially homogeneous. Furthermore, when the ac Stark shift varies with position along the beam the phase error due to an imperfect pulse size is one order lower in a small number. Although $\delta\varphi_{\text{off}}$ can be non-zero for single photon transitions, $\Delta(\delta\varphi_{\text{off}})$ is always zero in that case as long as the laser detuning is kept constant, because the terms which correspond to Ω^{AC} in the equations for single photon transitions are the fixed energies of the atomic levels.

3 Experiment

Before contributing to atomic interference fringes for measuring the photon recoil, the atoms undergo a significant amount of processing. See [46] for a brief summary and [2] for a more detailed discussion. Atoms are slowed, trapped, cooled and launched into a fountain trajectory using well-established laser cooling and manipulation techniques. On their way up they are prepared in a well-defined state and at the top of their trajectory they are given a series of interferometer pulses. On their way down their internal state is probed. The details of these various steps are presented in this section.

3.1 The atomic fountain

The overall experimental setup is similar to previous atomic fountain experiments (Fig. 13). A thermal beam of Cs atoms is slowed using the chirped slowing tech-
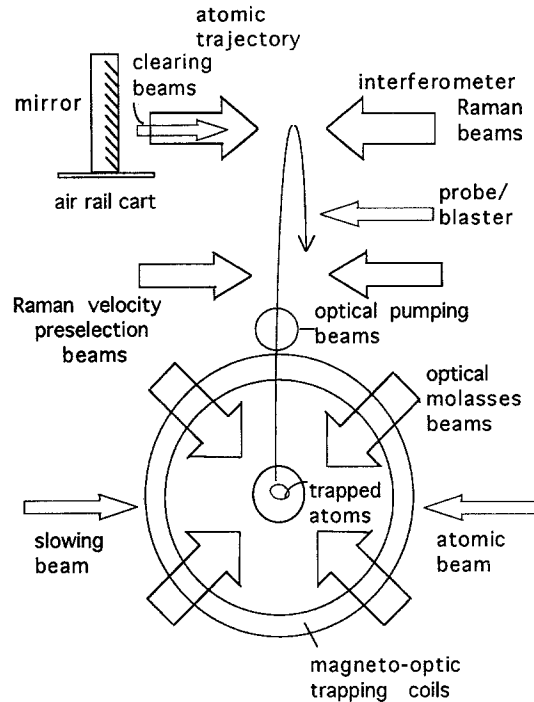
nique [47]. The primary slowing light is generated from a scannable single-mode Ti-Sapphire laser, locked near the $6S_{1/2}$, $F = 4$ to $6P_{3/2}$, $F' = 5$ resonance using an fm saturation technique (at 18 MHz) [48]. The 1 W Ti-Sapphire laser is also the source of the primary cooling beams, the probe/blasting beam, the Zeeman optical pumping beam, and the reference beam for the frequency lock of the Raman beams. The light necessary to repump the atoms out of the lower Cs hyperfine level is generated from a 50 mW diode laser with grating feedback [49] locked near the $6S_{1/2}$, $F = 3$ to $6P_{3/2}$, $F' = 4$ transition. The repumping beam is combined with the Ti-Sapphire beam in an acousto-optic modulator, so that both the slowing and cooling light contains both frequencies. The two carrier frequencies of the slowing light are 300 MHz above the $F = 4$ to $F' = 5$ and $F = 3$ to $F' = 4$ transitions, respectively, so that the unchirped part of the light is far from resonant with the slowed atoms, and will be less likely to heat them up and push them out of the way. A traveling-wave electro-optic modulator produces the sidebands with a modulation index of close to one. Slowing is accomplished by the lower sidebands, which are chirped from 550–340 MHz. The slowing light is circularly polarized and the resonant sideband has 100 mW and 1 mW in its two components, in a beam that converges from about 10 mm to 1 mm diameter over the 1 m interaction length.

The slowed atoms are captured in a Magneto-Optic Trap (MOT) [50] near the center of the 1×10^{-9} Torr vacuum chamber. The anti-Helmholtz coils for the MOT magnet consist of 10 turns of 3/16 inch diameter copper tubing, insulated by a loose fiberglass sheath and wrapped in three layers with a 10 cm inner diameter. The
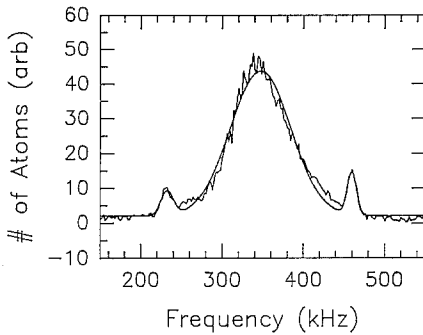
Fig. 14. Velocity distribution of fountain atoms. The temperature determined by the width of this signal is 4.0 μK, although because the distribution is not quite Gaussian, this is, strictly speaking, not a temperature. (The narrow side peaks are doppler-free resonances on magnetic-field sensitive transitions)

separation between the two halves is 3.5 cm. The typical current run through the water-cooled coils is 15 A.

The light for the trapping passes through three AOMs in series. The three downshifted first-order Bragg-diffracted beams are used successively for the horizontal molasses beams (≈ 3.5 cm diameter), and the upward propagating and downward propagating molasses beams (≈ 2.5 cm diameter), which are aligned 45° with respect to the horizontal. Because the frequencies of the beams need to be shifted for the launch, a short focal length lens images each AOM. In this way the angular change resulting from changing the AOM frequency is immediately converted to an acceptably modest spatial offset. The polarizations are adjusted by rotating quarter wave plates in each beam in order to maximize the trap lifetime[3]. The intensity in the diagonal trapping beams is approximately 25 mW/cm^2 per beam. The primary trapping light is typically detuned 20 MHz below the $F=4$ to $F'=5$ resonance.

After 200 ms of loading there are $\approx 5 \times 10^8$ atoms in the MOT. We block the slowing beam and shut off the magnetic field, and then wait for 50 ms before continuing the launch sequence so that any eddy currents induced by the switching magnetic field can die away. There are three orthogonal pairs of ≈ 1 m diameter Helmholtz coils around the apparatus, which are used to cancel the earth's magnetic field in the trapping region so that the optical molasses can cool most efficiently. The frequencies of the different molasses beams are then acousto-optically shifted to create molasses in a frame moving upwards, $\approx 5°$ off vertical at 2 m/s [21]. The intensity of the light is then decreased to further cool the atoms to ≈ 3.5 μK using the polarization gradient cooling mechanism. The temperature was measured, as shown in Fig. 14, using velocity-selective Raman transitions [18]. Then the light is blocked with a mechanical shutter and the atoms are left unperturbed on an upward ballistic trajectory. The repetition rate of the experiment is 2 Hz.

---

[3] Other work suggests that crossed linear polarizations are optimal, ultimately yielding up to 30% lower temperatures than opposite circular polarizations [51]

3.2 Atomic state preparation

Right after the atoms are launched we change the currents flowing through the Helmholtz coils in order to provide a bias field of ≈ 85 mG, so that the interferometer experiment can be performed using only magnetic field-insensitive transitions. On their way up the atoms are excited by a 1 cm diameter, 200 μW, linearly polarized horizontal beam that is resonant with the $6S_{1/2}$, $F=3$ to $6P_{3/2}$, $F'=4$ transition, so that it depletes the atoms in the $F=3$ level. This hyperfine pumping beam is overlapped with another linearly polarized beam that is resonant with the $6S_{1/2}$, $F=4$ to $6P_{3/2}$, $F'=4$ transition. This Zeeman pumping beam, with a few μW in its 1 cm diameter, increases by a factor of four the phase space density of atoms in the ground $F=4$, $m_F=0$ level. The two beams are slightly offset from each other, so that the atoms see the hyperfine pumping beam last. After the atoms have passed through both beams the light is shut off using AOMs.

A typical distribution of populations after Zeeman pumping is shown in Fig. 15. For this scan the bias magnetic field was aligned with the Raman beam propagation axis, and to the extent that this is achieved the $\Delta m = \pm 1$ transitions are not driven. Only half of the resonances are shown in the scan because the distribution is symmetric. Some population remains in the $m_F = \pm 1, 2$ levels, presumably because of the difference in the bias field direction between the optical pumping and Raman regions, which are separated by ≈ 7 cm. The temperature of the atoms after optical pumping is 4.0 μK.

If the Doppler-broadened width is significantly wider than the Rabi pulse widths in the interferometer, many atoms will be excited by off-resonant light. In this limit the maximum possible fringe contrast (the difference between the height of the peaks and valleys divided by their sum) is only 14% [42]. To reach the opposite limit, where the maximum possible fringe contrast is 50%, a preliminary velocity selection is made. A pair of velocity-selective Raman beams are made to counterpropagate just below the probe/blaster beam and the interferometer Raman beams (Fig. 13). The velocity
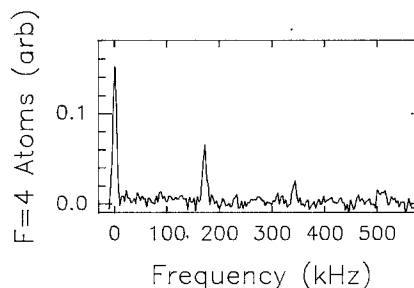

Fig. 15. Ground state populations after hyperfine pumping. The bias magnetic field is much larger than in Fig. 14, and it is aligned with the Raman beams. The peaks are each proportional to the number of atoms in a given sublevel, although the proportionality constants are different

selection light is $\approx 1/4$ of the intensity of the interferometer light. It is pulsed on to give a π pulse, which is typically 0.25 ms long. Atoms from within a velocity width of ≈ 500 µm/s are thereby transferred from the $F = 4$, $m_F = 0$ state to the $F = 3$, $m_F = 0$ state.

As the atoms continue upward through the probe/blaster beam, the beam is pulsed on for ≈ 6 ms with the light at $3I_{sat}$ in order to push the $F = 4$ atoms out of resonance and out of the way. Of the atoms that finish in the $F = 3$ state after blasting, the ratio of velocity pre-selected atoms to other atoms is typically ≈ 3. The residual background in the $F = 4$ state is $< 0.5\%$ of the pre-selected atoms. Overall, the internal and external state-selection leave about 10^6 useful atoms for the interferometer.

3.3 The Raman beams

The Raman beams are generated by two diode lasers, which are phase-locked to each other with a 9.2 GHz frequency offset. The reference frequency is the summed output of a fixed 9.14 GHz synthesizer and a low frequency digital synthesizer (≈ 60 MHz), the output of which can be changed between pulses without losing the phase lock. Our phase locking scheme is described in detail elsewhere [52], so we will only briefly describe the technique here. Both our laser diodes (SDL–5410–G1, GaAlAs) are spectrally narrowed using optical feedback from a gold coated, holographic grating in the Littrow configuration, which narrows their linewidths to < 1 MHz. Beams from the two lasers are overlapped in a polarizing beamsplitter cube and part of this light is split off and passed through a linear polarizer oriented at 45° to the polarization so that the two beams will interfere on a fast photodiode. This beatnote is mixed against a stable microwave reference, and the error signal is used to electronically feed back to one of the lasers. The feedback is accomplished in three bands. The low frequency ($\lesssim 500$ Hz) error signal is fed to a PZT on which the grating is mounted, the midband (0.5 kHz to ≈ 500 kHz) error signal is fed to the laser diode current controller, and the high band is ac coupled directly into the current lead to the laser diode. The final result is a phase lock with $\approx 5°$ phase noise which stays locked for several hours. The master laser in the phase lock is typically frequency locked from between 0.8 GHz and 3 GHz to the side of the $6P_{3/2}$, $F' = 5$ level.

The Raman beams are passed through an AOM that controls their intensity and then are coupled into an optical fiber to ensure that they are well-overlapped. After the fiber the beam is further spatially filtered to remove aberrations caused by the high numerical aperture optics. There is 15 mW total power after the filtering, and the beams are expanded to 2.3 cm Gaussian diameter. They are passed through the vacuum chamber and then retroreflected. These beams can drive the stimulated Raman transition with a Rabi frequency of ≈ 4 kHz.

Each of the counterpropagating Raman beams contains both frequencies, so the atom can in principle be excited by several combinations of beams. The velocity along the beam is made large enough so that only one of the two velocity-selective pairs is in resonance at any time. The direction of $\mathbf{k}_{eff}$ is determined by the choice of which velocity-selective pair is in resonance. The Doppler-free pairs and standing wave pairs are never in resonance. The Doppler-free transitions can also be suppressed using the appropriate polarization combinations for the Raman beams, but we have found these polarization tricks to be insufficient for avoiding unwanted transitions near zero velocity, due to residual polarization imperfection. The standing wave Raman transition, which depends on only one of the Raman beams, cannot be avoided using clever polarizations.

Crossed linear polarizations have at times been used in our measurements, with the retroreflected polarizations unchanged. Because there is no waveplate before the retroreflection, the polarizations of the two possible effective traveling waves are more reliably identical, so that some systematic errors are easier to diagnose. However, this polarization produces its own extra error because it creates optical standing waves, which will be discussed in the systematic errors section. We typically use opposite circular polarization for the two counterpropagating Raman beams, and avoid optical standing wave effects.

3.4 Phase noise and vibration isolation

Freely falling atoms in an atomic fountain provide an extremely good inertial reference. Their motion can be perturbed by inhomogeneous fields, but these perturbations are typically very small. For instance, a Cs atom in an $m_F = 0$ level that propagates for 0.5 s in a 100 mG bias field with a uniform gradient of 10 mG/cm will have its velocity changed as a result by 400 nm/s. It will be displaced from a perfect ballistic trajectory by only 100 nm. Vibrations of the field sources will in general have amplitudes less than 100 µm, even if the sources are mounted to a floating optical table, as are our Helmholtz coils. Assuming a field curvature of 2 mG/cm^2, the largest fluctuations in the atomic trajectories will be less than 2 nm for even the highest atomic fountains.

In contrast, the Raman light does not in general provide a very spatially stable wavefront. Any phase noise on the Raman beam difference frequency causes the effective wavefront to move. Since the phase of atomic interference fringes depends on the phase of the light at the point at which the atom interacts with the light, motion of the effective wavefront translates into noise on the interference fringes. If the phase noise approaches π, which is to say that the effective wavefront of the light moves by half an effective wavelength (which for counterpropagating beams is $2\pi/(k_1 + k_2)$) during the interaction time, the atomic interference fringes will be completely washed out. Of course, the momentum view can also be taken, where if the effective frequency ($\omega_1 - \omega_2$) of the light fluctuates by an interference fringe width, the interference cannot be seen. Sources of noise include phase noise on the reference frequency, noise in the phase

lock, and any Doppler shifts that are different for the two beams after they are combined for the phase lock.

The reference noise is negligible because our synthesizers are weakly locked to either a LORAN C signal or a stable crystal oscillator. As long as the experiment is triggered by the power line frequency, the phase difference between two fixed points in time is repeatable, leaving residual phase noise below 2°. The phase-lock noise, which is less than 5°, is largest at frequencies above a few hundred kHz [52]. Since this characteristic time is significantly shorter than typical pulse times, the noise is appreciably washed out during the atom's finite interaction time with the light.

Noise from the vibrations of mirrors can be a serious problem. The Doppler shifts on the two beams due to mirrors which they have in common are not identical, but the difference is small, reduced by a factor of $(k_1 - k_2)/(k_1 + k_2)$, which is 1.3×10^{-5} for Cs. In our experiment, the retroreflection mirror is the only mirror after the phase lock which is not common to the two Raman beams, so it is the only point in the apparatus which has stringent constraints on its inertial stability.

The first stage of vibration isolation is that the laser tables and the vacuum chamber are all rigidly mounted together and floated on a total of 9 Newport XLB pneumatic isolation legs. This removes most of the mechanical noise above 10 Hz. The residual vibrations are dominated by a table resonance at ≈ 3 Hz. The second stage of vibration isolation is an inertial platform that consists of a cart suspended on a precision air rail, oriented in the direction of the Raman beams. The cart is weakly trapped in a potential well created by permanent magnets. The resonance frequency for low amplitudes is greater than 5 s by an undetermined amount. With the air rail, there is no appreciable phase noise on the atomic interference signal with 25 ms separating a $\pi/2$ pulse pair.

The difference between the double atomic interferometer and the 3-pulse interferometer of Kasevich and Chu with regard to mirror vibrations is significant. In the 3-pulse interferometer, the first $\pi/2$ pulse and the first half of the π pulse set up state-labeled fringes in velocity space and the last half of the π pulse and the last $\pi/2$ pulse 'read out' these fringes. A uniform mirror velocity shifts both fringe patterns together, so the interference is unchanged. In the double atomic interferometer, the second pair of pulses propagates oppositely from the first pair, so the fringes shift in opposite directions due to the same mirror motion. Therefore, a uniform mirror velocity will change the phase relationship between the two sets of velocity fringes, thus changing the phase of the fringes as a function of the frequency of the final $\pi/2$ pair. So in the 3-pulse interferometer only a change in the mirror velocity during the time between the two $\pi/2$ pulses will cause phase noise on the interference fringes, while in the 4-pulse interferometer there is noise due to changes in the mirror velocity which occur on the time scale it takes to measure an entire interference fringe.

3.5 The double interferometer pulses

The atoms reach their apogee slightly above the center of the Raman beams, 10 cm and 145 ms from the launch point. 50 ms is available for interferometer pulses, which corresponds to a fountain height of 3 mm, measured from the location of the atoms at the first or last interferometer pulse. This is smaller than the spatial spread of the atoms we detect, which is ≈ 6 mm diameter. Outside of this range it takes more than 10% longer to drive a $\pi/2$ pulse, and the Rabi frequency starts to decrease rapidly. To avoid unwanted frequency sidelobes on our $\pi/2$ pulses each pulse is given a Blackman shape,

$$\Omega(t) = \Omega_{\text{eff}}\{0.5 \cos\left[\pi(2\,t/\tau - 1)\right] + 0.8 \cos\left[2\pi(2t/\tau - 1) + 0.42\right]\},$$

for $0 < t < \tau$ [53]. The pulse shaping is accomplished using an arbitrary function generator to drive the Raman beam's AOM.

The frequencies used in the pulse sequences when intermediate π pulses are added are illustrated in Fig. 16. Frequencies above and below the Doppler-free resonance frequency, ω_{DF} (defined as the hyperfine frequency separation when the ac Stark shifts of the two levels are equal) result in an effective wavevector in opposite directions. The two number lines in Figs. 16a, b correspond to the frequency sequences for two mirror symmetric interferometer pairs. The pre-selected velocity group is in resonance at the frequencies marked by 1 in either sequence, so 1 is the frequency of the first $\pi/2$ pair. In order for the next absorbed photon to have the opposite recoil, the frequency is reflected through ω_{DF} and then shifted either up or down by $\hbar k_{\text{eff}}^2/m$. The sequences that increase the absolute value of the atoms' velocity are marked above the number line, while those that bring the velocities closer to zero are marked below. The procedure of reflecting through ω_{DF} and shifting to account for the additional recoil velocity can be repeated many times. Frequencies for a three π pulse interferometer are shown
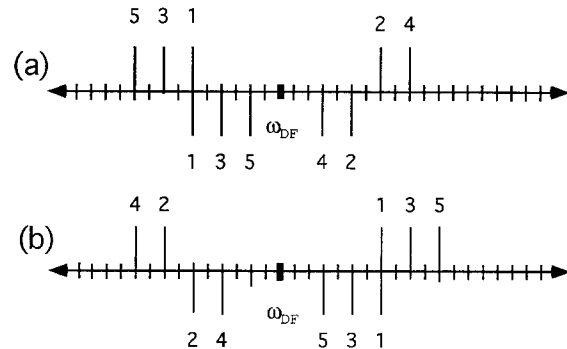

Fig. 16a, b. The frequency sequences for adding π pulses. Each number line gives the sequence for two interferometers whose center frequencies will be compared, one sequence marked above the line, the other below. In the rest frame of the pre-selected atoms, the interferometers corresponding to the two number lines are mirror symmetric to each other
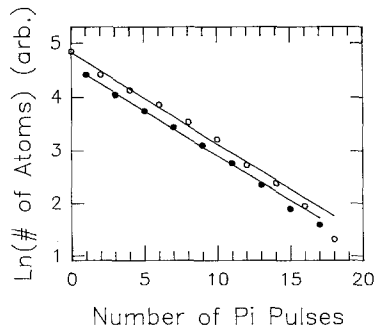
Fig. 17. Number of signal atoms vs number of π pulses. The difference between odd and even π pulses is due to uncertainty in the backgrounds
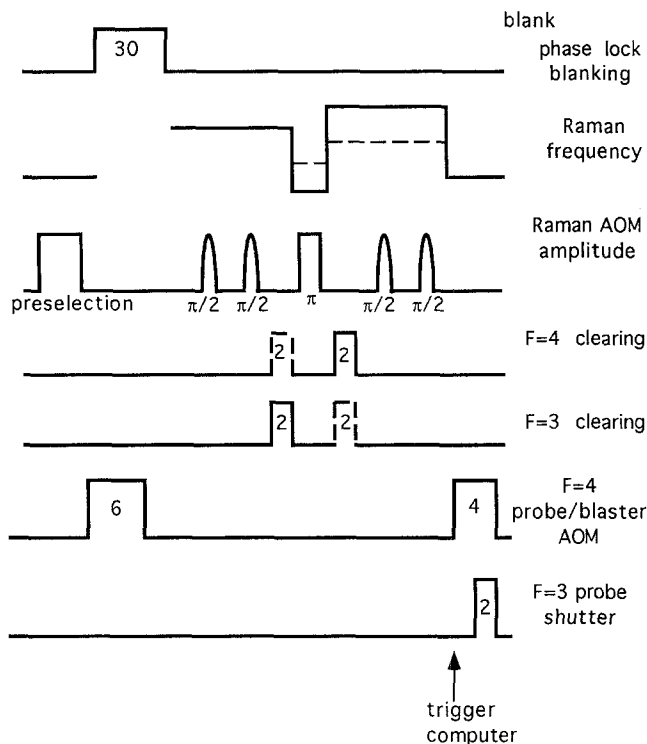

Fig. 18. Timing in the fountain after the launch. Numbers indicate time measured in milliseconds. The timing is not to scale, rather it serves to illustrate the relative positions of the various pulses. The *dashed lines* in the Raman frequency correspond to the other interferometer in the pair. See text for further details. As was discussed above in the subsection on Raman-beam polarization, it is basically undesirable for the Raman frequencies to be too close to ω_{DF}. In conjunction with the vacuum chamber windows, which limit the angle of the molasses beams and hence the initial velocity of the atoms along the Raman beams, this is currently the dominant constraint on the number of π pulses that can be given. If the Raman beams were vertical, the atoms could be accelerated through zero velocity by gravity (it only takes 3 ms to accelerate from $+2$ to -2 effective recoils) so this would not be a limitation

in the figure, where 5 designates the frequencies for the final $\pi/2$ pairs.

The state flip due to a π pulse is not perfect. The imperfection arises because the detected atoms sample a range of Raman beam intensities and because the pre-selected velocity width is a finite fraction of the Rabi

pulse width. Figure 17 shows the number of atoms that stay in resonance with a sequence of π pulses as a function of N, the number of π pulses. The loss per pulse is $\approx 15\%$, so that the signal is halved when $N \approx 4$. The difference between odd and even N results from differences in the background, which are primarily due to the difference in how unwanted atoms are cleared, as is discussed next.

Unwanted atoms can be cleared from the interferometer because the two interfering paths of each interferometer spend the time between the middle $\pi/2$ pulses in the same state. Atoms are cleared before and after the last π pulse (Fig. 18), so that any atom that does not make the appropriate transition at that π pulse is cleared. The $F = 4$ clearing is the same as the clearing which is part of the velocity pre-selection, where the atoms are cycled on the $F = 4$ to $F' = 5$ transition. The $F = 3$ clearing is slightly more complicated, because the $F = 3$ to $F' = 2$ transition tends to pump the atoms into a dark state. This optical pumping effect is avoided by making the polarization of the light linear and orthogonal to the bias magnetic field. The dark state then precesses in the bias magnetic field, so that within ≈ 1 μs it can again absorb photons. An atom need only absorb a few hundred photons before it is pushed out of resonance and well clear of the probe region, so that a ≈ 2 ms clearing pulse near saturation is enough to remove most of the atoms in the $F = 3$ state from the final signal. The $F = 3$ clearing beam is 452 MHz away from the repumping light, and is generated from a diode laser which is dedicated to that purpose (STC, nominally 50 mW) and locked to the $F = 3$ to $F' = 2$ transition.

The signal to noise does not significantly suffer from the loss of signal illustrated by Fig. 17 because of the combination of clearing and signal normalization. Atoms that are lost to the π pulse sequence are cleared, and the dominant noise is the residual amplitude noise after the normalization. Since this is not due to counting statistics it is largely independent of the total signal size.

After the clearing there remains a small number of background atoms. The background is $\approx 2\%$ of the cleared $F = 3$ atoms and $\approx 0.5\%$ of the cleared $F = 4$ atoms. In addition, there is a loss of atoms to the $F = 4$ state during the $F = 3$ clearing which is typically three times larger than what is left in the $F = 4$ state after the $F = 4$ clearing. The result is that the background levels, particularly in the $F = 4$ state, are different depending on the order of the clearing pulses, which are necessarily different for the two interferometers in a pair. None of the background subtractions that can be made are completely satisfactory, so that the vertical scale cannot be made a priori consistent for the two interference fringes in a pair. Also, the zero level or the unity level (depending on whether the off-resonant signal has all or none of the atoms in the $F = 4$ state) cannot be unambiguously determined. This imperfect knowledge of the scale and offset along the ordinate has no effect at all on the determination of the phase of the signal, and hence on the determination of the recoil.

3.6 Fluorescent detection and normalization

The atoms that remain at the end of the interferometer sequence fall back down through the lower clearing beam, which now becomes the probe beam (Fig. 13). Fluorescence from the beam is collected onto a photo-multiplier tube with a 10 cm focal length, 10 cm diameter doublet lens located outside of the vacuum chamber, ≈ 16 cm away from the fluorescence region. The PMT output is amplified and then smoothed with an RC filter with a 100 μs rolloff. It is then sent to an analog-to-digital card plugged into the computer, which digitizes it at 25 kHz. The digital signal during the pulse time is integrated and an offset, which is measured after the pulse, is subtracted.

The atomic cloud passes through the probe in ≈ 10 ms, full width at half maximum. However, when the high intensity probe is pulsed on, it cycles atoms on the transition at near the maximum rate, ≈ 1 cycle/100 ns. In a few hundred μs, all the atoms in the probe region receive enough momentum kicks to push them substantially out of resonance with the beam. After 2 ms the probe fluorescence has dropped by $\approx 95\%$, and it continues to drop thereafter. The exact detuning of the probe beam is set by looking at this raw signal, the goal being to place the peak of the signal pulse right at its beginning.

It is important that the fluorescence drops quickly because there is a second step in the detection. After 2 ms a mechanical shutter is opened that unblocks a repumping probe beam which is overlapped with the main probe beam. It requires significantly less ($\approx 0.01 I_{sat}$) power. Atoms which entered the probe region in the $F=3$ state require only a few photons to be dumped into the $F=4$ state, where they are detected just as before. The $F=3$ atoms detected in this way are from almost the same spatial volume as the originally $F=4$ atoms, so the area under these two peaks can be combined to give a signal with which to normalize the $F=4$ signal [54]. The typical fluctuations in the number of atoms launched is 15% peak to peak; normalization reduces the amplitude noise by a factor of 3 to 5. There are background atoms in each of the two signal peaks, and we will discuss the characterization of this background below.

3.7 Interferometer signals

An illustrative four $\pi/2$ pulse double interferometer signal is shown in Fig. 19 for 1 ms separating each pair of $\pi/2$ pulses. The microwave frequency of the first $\pi/2$ pair is fixed, at -50 kHz away from ω_{DF} in this instance, and the frequency of the final $\pi/2$ pair is scanned. The data in Fig. 19 was taken with a ≈ 4 kHz ac Stark shift difference between the two levels. Because the recoil measurement is a differential frequency measurement a uniform frequency shift due to the ac Stark effect will not shift the measured recoil. However, when there is such a shift, the phase of the interference fringes can be different for atoms in different parts of the beam. Thus, to prevent the interference fringes from washing out due to light inhomogeneities, we cancel the ac Stark shifts rou-
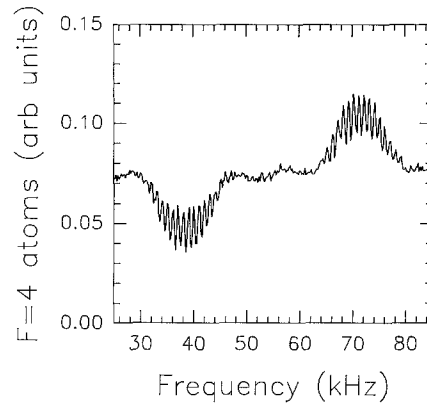
Fig. 19. Four-pulse double interferometer data. There is 1 ms between $\pi/2$ pulses in a pair. In contrast to the multiple π pulse interferometer data, this data was taken with square Raman pulses. Also, the atoms had an initial velocity along the Raman beams of only ≈ 3 effective recoils
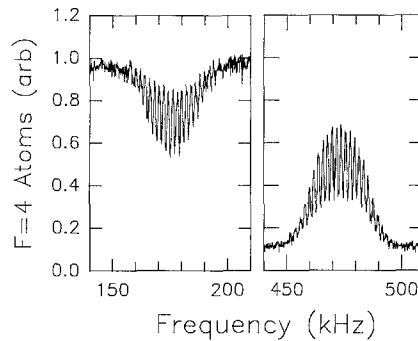
Fig. 20. The recoil doublet with 8 π pulses. The pulse sequences are different for the two sets of fringes. The frequency of only the final pair of $\pi/2$ pulses is scanned

tinely by scanning the frequency of a Doppler-free π pulse, and making sure the peak of the interferometer signal occurs when the Raman frequency difference is equal to the known hyperfine splitting. This is an adjustment of the relative intensities of the two Raman beams, which is accurate to $\approx 1/20$ of the Rabi width (<1 kHz). There is actually no observable change in the fringe contrast even when the ac Stark shift difference frequency is half of the overall ac Stark shift, so this routine adjustment is largely precautionary.

Illustrative data with 0.5 ms between $\pi/2$ pulses and 8π pulses is shown in Fig. 20. The separation between $\pi/2$ pulses was typically greater than 15 ms. The fringes on the left correspond to interferometer A in Fig. 3, while those on the right correspond to interferometer B. Before the final $\pi/2$ pulse pair the atoms are in either the $F=4$ state, $N+1$ recoil kicks away from the pre-selection velocity for the case of interferometer A, or in $F=3$, $N+1$ recoil kicks in the other direction away from the pre-selection velocity for interferometer B. This explains the off-resonant baselines, zero for interferometer B and a maximum for interferometer A. The fringes at the Rabi peak do not extend to the baseline because half the amplitude of the atoms that survive the clearing are in two trajectories that do not interfere.

3.8 Data collection and fitting

A typical scan of interference fringes is shown in Fig. 21. All such scans of interference fringes are taken in sets of four, consisting of two interferometer pairs which are mirror symmetric with respect to each other. A mirror symmetric interferometer results from a reversal of the direction of all of the interferometer light pulses. Points are taken from each of the four interferometers in succession, so that the four fringe patterns build up together. In under four minutes 101 points in each of the interferometers are collected. The frequency difference between the scans in a pair is set at the recoil separation to within at least a tenth of a fringe. (The recoil separation was originally determined to within a fringe by varying the time between $\pi/2$ pulses.) The frequency span is typically set to encompass three to five interference fringes. Two such sets are taken in succession, one with an even and one with an adjacent odd number of intermediate π pulses (N). Four of these pairs are usually taken with all experimental parameters the same, so that our data comes in blocks which take $\approx 1/2$ h to collect. We will refer to the two mirror symmetric pairs as 'left' and 'right' interferometers, and 'odd' and 'even' will refer
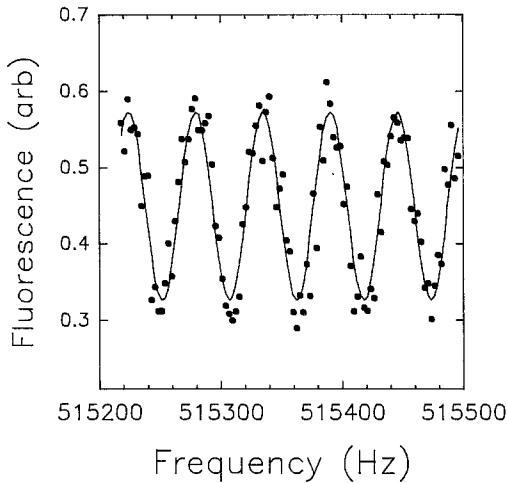

Fig. 21. Typical interference fringe pattern. These data were taken in one minute using 10π pulses and 18 ms between the $\pi/2$ pulses in a pair
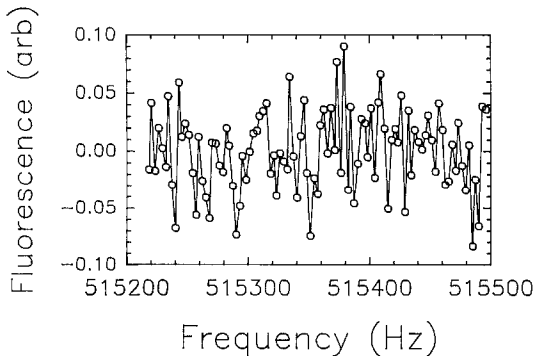

Fig. 22. A typical set of residuals from the least-squares fit

to the parity of N. The difference of the measured recoils between all possible combinations of these points are routinely computed in order to monitor potential systematic errors.

The four one-minute scans in a set are least squares fit together using 13 free parameters for four sine waves. The free parameters are the amplitude, vertical offset and phase of each of the four, and a fringe frequency offset common to all of them. The actual fringe frequency is well known (it is just the inverse of the time between $\pi/2$ pulses), but during the course of a scan the fringes drift to some degree, typically by <0.5 Hz, probably due to drifts in the Raman beams' power and polarization. The linear part of this drift is taken up by the 13th parameter, which is added to the known fringe frequency with opposite signs for the two interferometer pairs. Because we are only interested in the separation of the fringes and because we simultaneously build up the fringes that are to be compared, slow drifts have little effect on the result. The addition of the extra fit parameter does, however, improve the measured standard deviations. The residuals (data minus fit) for the typical scan shown in Fig. 21 are plotted in Fig. 22.

We are predominantly interested in the phase of the sine waves, which is labeled by a frequency near the middle of the scan. For convenience in our discussion we will refer to this as the 'central frequency', although it is not in general truly the frequency of the central fringe. The standard deviation of the center frequency is determined by assuming a Gaussian distribution of points and finding the curvature of the chi-square with respect to the fit center frequency [55]. The difference between the fitted center frequencies of the two interferometers in a pair is taken, adding or subtracting integral multiples of the fringe frequency if the difference is not within a half fringe of the recoil separation.

We adjust all our data so that we can compare all our recoil measurements with the same frequency unit. The coarse part of this adjustment is to normalize the results for all N values to $N=3$. A finer detuning correction is then made so that the data can be compared to that for Raman beams with an arbitrarily chosen detuning from the $6S_{1/2}$, $F=4$ to $6P_{3/2}$, $F'=5$ resonance of -2.186 GHz.

4 Determination of $\hbar/m$ and systematic errors in the recoil separation

4.1 Overview of the results

If we use the data we have taken with the parameters that yield the highest precision, 14 and 15 π pulses and 15 ms between $\pi/2$ pulses, our measured recoil is $132\,244.457 \pm 14$ Hz, normalized for 3π pulses with -2.186 GHz excited state detuning. The precision in two hours is 1.1×10^{-7} and the disagreement with the accepted value is at the 8.5×10^{-7} level. Since we do not yet have all of the systematic errors under control, this is not an absolute measurement. We expect to have a more

reliable result after the Raman beams are made vertical, which, as we will describe, should allow us to better diagnose these errors.

We have measured the recoil shift as a function of beam alignment, laser detuning, magnetic field, the relative ac Stark shift of the two levels, clearing beam intensity, time between $\pi/2$ pulses, and number of π pulses. In this section these results are presented along with calculations of how various imperfections are expected to affect the recoil measurement. At the current level of precision, we have made theoretical estimates that show many of the possible systematics to be unimportant. Other systematics have been ruled out experimentally. We have not yet placed upper limits on the errors from wavefront distortion and intensity gradients of the Raman beams. Also, we still observe systematic shifts with the number of π pulses, and have not clearly ruled out dependence on the laser detuning.

In our theoretical estimates we will give illustrative numbers where appropriate, and for this purpose we will define the following variables, and assign to them typical values that correspond approximately to those in the current experiment: for the time between $\pi/2$ pulses, $T = 20$ ms; for the number of intermediate π pulses, $N = 10$; for the time between the middle two $\pi/2$ pulses, $T' = 10$ ms; and for the $\pi/2$ pulse time, $\tau = 50$ μs. We will also discuss how the systematic errors are affected by changes in these parameters. Atomic Cs will be assumed throughout. We usually have velocity-selective Raman transitions in mind, although our use of $\mathbf{k}_{\text{eff}}$ typically makes the result for single photon transitions clear. We will consider both the cases of vertical and horizontal laser beams when there is a significant difference; we find that vertical laser beams typically lead to smaller systematic errors.

There are two convenient reversals that we conduct on a routine basis as we take data. We change the direction of all the pulses, which reflects both interferometers about the initial path of the atoms, and we change the parity of the number of π pulses we add. Both of these reversals change which side of the interferometers is occupied by which state during the time between the last two $\pi/2$ pulses, so we will associate the binary indicator 'spatial parity' with the combination of these reversals. Thus we can group the four experimental points in a set into three types of pairs that should behave characteristically with regard to various systematic errors.

Two parameters that are routinely scanned, T and N, should have characteristic effects on many different errors because they change the separations within and between interferometers, and it is typically spatial inhomogeneity that can lead to errors. Figure 23 shows the dependence on the time within a $\pi/2$ pulse pair. There is no significant change as a function of T and there does not appear to be any significant variation with any of the standard reversals. Figure 24 shows the recoil as a function of N. There is a clearly discernible dependence on N, although there is no significant variation with any of the standard reversals. We mostly took data for 14 and 15π pulses because it gives the highest resolution for a given measurement time. This dependence on N must be
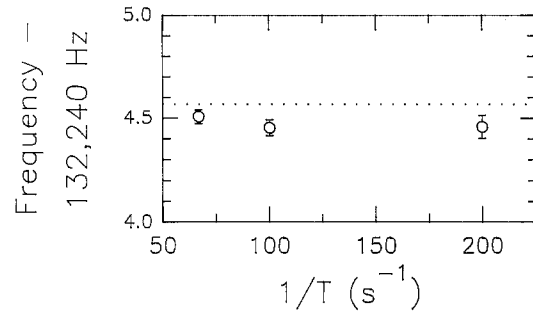

Fig. 23. Recoil as a function of T. All reversals are averaged together because there is no significant systematic shift in the reversals. The *dotted line* is the accepted value of the photon recoil, calculated from the accepted values of α and the other quantities listed in Table 1
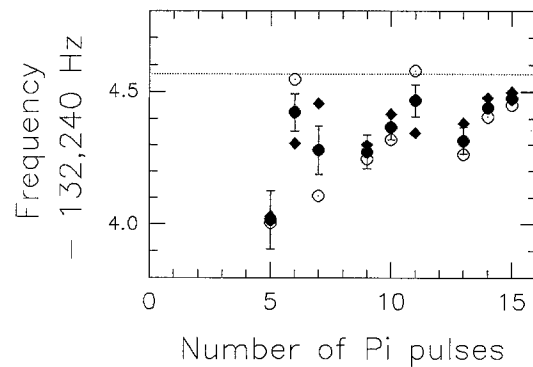

Fig. 24. Recoil as a function of N. The *open circles* are for the left interferometers and the *solid diamonds* are for the right interferometers. The error bars refer to their mean value. The *dotted line* is derived from the accepted values of fundamental constants

eliminated before an absolute accuracy can be assigned for our recoil measurement.

4.2 Magnetic fields

Magnetic field gradients can change the measured recoil due to the quadratic Zeeman shift, which is different for the two states used in this experiment, the $F = 3$, $m_F = 0$ and the $F = 4$, $m_F = 0$. When the shifts are small compared to the hyperfine structure, the relative shift of the two $m = 0$ levels is $\Delta U_{\text{QZ}} \approx 2(\mu_J B)^2/\Delta W$, where ΔW is the hyperfine splitting, μ_J is the Bohr magneton and we have ignored the relatively small nuclear moment [37]. For Cs, $\Delta v_{\text{QZ}}[\text{Hz}] \approx \alpha B^2[(\text{mG})^2]$, where $\alpha = 4.27 \times 10^{-4}$. With magnetic shielding one can make the bias field in an atomic fountain apparatus very small (less than 1 mG), [56] but in the present apparatus the bias field is 100 mG along $\mathbf{k}_{\text{eff}}$. So the approximate size of the phase shift in each interferometer due to the magnetic field is $\varphi_B = (4.27 \text{ Hz}) 2\pi(2T + T')$. As with all phase shifts we consider, a constant field has no effect on the recoil measurement.

Magnetic field gradients can affect the recoil measurement in two somewhat different ways. First, a linear field gradient shifts the mean field value in each of the two

interferometers differently, which results directly in an error in the recoil measurement, $\Delta\varphi_B$. Second, there can be a different average field along the two paths within each interferometer, $\delta\varphi_B$. For a linear field gradient $\delta\varphi_B$ is the same for the two interferometers, so only higher order spatial derivatives affect the recoil measurement in this manner. Magnetic fields experienced by the atom between the last two $\pi/2$ pulses, when the two paths of each interferometer are in different internal states, can shift the recoil measurement by the first mechanism. In contrast, shifts in the interference fringes due to field gradients experienced by the atom between the middle $\pi/2$ pulses can not be due to the first mechanism, because both paths within an interferometer occupy the same state during that time. Therefore we are predominantly concerned with the magnetic fields seen by the atom between the last two $\pi/2$ pulses, when the recoil measurement is sensitive to linear gradients.

4.2.1 Linear gradients. In between the final two $\pi/2$ pulses, the average separation between the two interferometers is $\Delta z(N, T, T') \approx 2(N+1)\,(\hbar k_{eff}/m)\,(T/2+T'/2)$, where the T' term comes from the assumption that many π pulses are equally spaced throughout the intermediate time. For our typical parameters, $\Delta z = 2.3$ mm. If the bias field is much larger than the gradients, the difference between the phase shifts in the two interferometers is

$$\Delta\varphi_B \approx 2\alpha B_0 \left(\frac{dB}{dz}\right) \Delta z(N, T, T')\, 2\pi T. \tag{28}$$

For a linear field gradient of 10 mG/cm, $\Delta\varphi_B \approx 30$ mrad, which corresponds to a fractional error in the recoil measurement of 5×10^{-7}. Since the phase shift is in fact due to a change in wavepacket momentum, we are using the approximation that these energies are small compared to the atom's kinetic energy.

From (28) we see that the absolute frequency shift in the recoil measurement grows approximately linearly with N, but so does the frequency separation of the interferometers, so the fractional error is independent of N. If we increase T, the phase difference due to the field gradient grows approximately quadratically. However, each interference fringe is a linearly decreasing fraction of the total recoil, so the sensitivity to magnetic fields only grows linearly with T.

We can change the sign of the error by changing which state is on which side of the interferometer during the time between the last two $\pi/2$ pulses (the spatial parity reversal). Figure 25a shows the two pairs of interferometers (1–3 and 2–4) in the reference frame of the initial atomic velocity. Changing the direction of all the pulses transforms one pair into the other. The resonance frequencies at the final $\pi/2$ pulse pair are shown in Fig. 25b for a situation where the resonances are shifted due to the magnetic field by a greater amount in region A than B. The same field gradient tends to push frequencies 1 and 3 together and pull frequencies 2 and 4 apart. An additional π pulse will shift all the frequencies by $\hbar k_{eff}^2/m$ and flip all the resonances through the origin, so the same field gradient will then pull 1 and 3 apart and
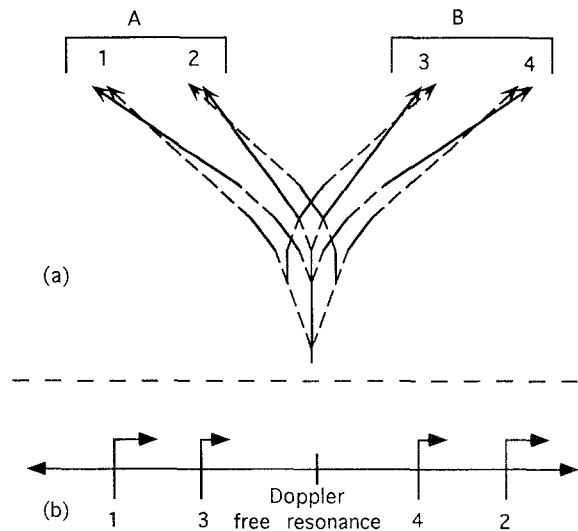

Fig. 25a, b. Flipped interferometer pairs. **a** Spatial picture of the two interfering pairs (*1* and *3*, and *2* and *4*), drawn in the reference frame of the interfering atoms. **b** The final frequencies at which each of the interferometers interferes. The *length of the arrows* indicates the size of the shift of the resonance due to the magnetic field, which is taken to be larger in spatial region A than B
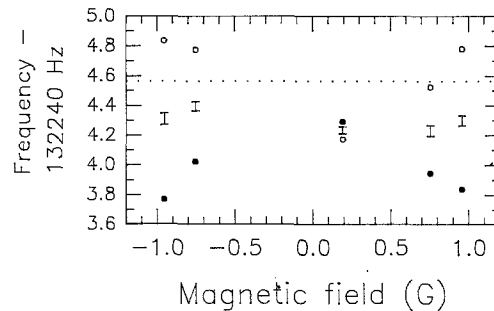

Fig. 26. Recoil as a function of magnetic field. The *open* and *closed circles* are spatial parity opposites. The *dotted line* is derived from the accepted values of fundamental constants

push 2 and 4 together. If the 1–3 and 2–4 pairs were exactly spatially overlapped, spatial parity reversals would perfectly cancel all magnetic field gradients.

The measured dependence on B is shown in Fig. 26. The open and closed circles are spatial parity opposites. The salient feature of the curve is that at high B field the spatial parity pairs split from the mean just as expected. The linear magnetic field gradient empirically determined in this way is 10 mG/cm.

4.2.2 Quadratic gradients. To the extent that the overlap between the 1–3 and 2–4 pairs is imperfect, errors due to spatial second derivatives of the field can be studied by varying the size of the bias magnetic field. To estimate the magnitude of these errors, we must follow the phase evolution more carefully than is necessary for linear gradients. If $\mathbf{k}_{eff}$ and $\mathbf{B}_0$ are along the z-axis, then we can Taylor expand $|\mathbf{B}|^2$ around small displacements in the x_i directions,

$$|\mathbf{B}|^2 \approx B_0^2 + 2x_i \frac{B_0 \partial B_z}{\partial x_i} + x_i x_j \frac{\partial B_k}{\partial x_i} \frac{\partial B_k}{\partial x_j} + x_i x_j \frac{B_0 \partial^2 B_z}{\partial x_i \partial x_j}.$$

$$(29)$$

The magnetic-field-dependent phase shift in a single interferometer is

$$\varphi_B = 2\pi\alpha \int_{\substack{\text{mean} \\ \text{path}}} |\mathbf{B}(\mathbf{r})|^2 \, dt. \tag{30}$$

The calculation of this shift is straightforward but can be messy. For the case where z is vertical and the transverse velocity spread is negligible, the answer is relatively simply expressed. For simplicity we ignore the initial separation at the third $\pi/2$ pulse. The phase shift difference between the two interferometers is then

$$\Delta\varphi_B = 2\pi\alpha \left\{ \frac{B_0 \partial B_z}{\partial z} \Delta v T^2 + \left[(2v_0\Delta v + \Delta v^2) \frac{T^3}{3} - \Delta v g \frac{T^4}{4} \right] \right.$$

$$\left. \times \left[\left(\frac{\partial B_z}{\partial z}\right)^2 + \frac{B_0 \partial^2 B_z}{\partial z^2} \right] \right\}, \tag{31}$$

where $\Delta v = 2(N+1)\hbar k_{\text{eff}}/m$ and v_0 is the mean initial velocity of the atoms in the interferometer. There exists an initial velocity for any given T and Δv for which the second derivative terms cancel; this occurs when $v_0 = 3gT/8 - \Delta v/2$. The optimal condition is when the atoms pass their apogee between the last two $\pi/2$ pulses. When k_{eff} is horizontal so that the atoms are obliged to have non-zero initial horizontal velocity, and to a lesser extent when there are transverse velocity spreads, there is a proliferation of cross derivative terms in (29). The additional terms depend on Δv and T like the T^3 term in (31). Because $\mathbf{g} \perp \mathbf{k}_{\text{eff}}$ there is no T^4 term for these extra terms and hence no optimal launch velocity in that case. To give a rough idea of the size of these shifts, we can calculate the size of the T^3 term of (31) for our approximate conditions of $v_0 = \Delta v = 14$ cm/s. If we take a plausible value for the field curvature of $\partial^2 B/\partial z^2 \approx 0.2$ mG/cm^2, then the resulting phase shift is 0.5 mrad, which represents a fractional error in the recoil measurement of 1.1×10^{-8}.

4.2.3 Magnetic fields and line pulling.

Line pulling from other Zeeman levels can be from either the Doppler-sensitive features or the Doppler-free features. The latter are more worrisome because they can contribute $\pi/2$-$\pi/2$ fringes with the same periodicity as our interferometer fringes. The effect of these fringes, however, is washed out to some degree by field inhomogeneities, which cause different atoms in the ensemble to be Zeeman shifted by different amounts. We find only $\approx 10\%$ contrast in these Zeeman shifted fringes with $T = 15$ ms. To avoid line pulling from these atoms we make sure that the frequencies of all the $\pi/2$ pairs are more than a Rabi width displaced from all Doppler-free resonances. The Blackman pulse shapes avoid potential trouble from sidebands, which could make it difficult to avoid resonances.
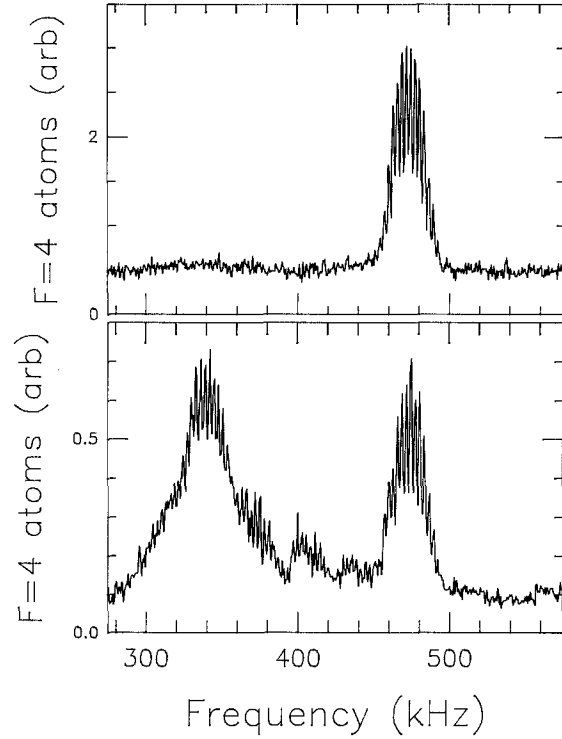

Fig. 27. Effect of clearing on the background. The *upper curve* is a ten π pulse interference signal with clearing. As usual, the frequency of the final two $\pi/2$ pulses is scanned. The *lower curve* is the same scan with no clearing of the $F = 3$ state. The broad feature at 340 kHz is the Doppler-sensitive excitation of the background atoms which remain in the $F = 3$ state after the optical pumping into the $F = 4$ state. The difference in scales between the two curves results from normalization with and without the background. There is aliasing of the fringes

Another straightforward way in which we suppress line pulling from other Zeeman levels is by removing potentially offending atoms. The blasting and clearing beams allow very few atoms in the wrong magnetic sublevels to be present at the final signal. Nonetheless, some do remain as part of the uncleared background. The wrong Zeeman level atoms are present because they are either left in the $F = 3$ state after the optical pumping before the pre-selection or they are dumped into the wrong sublevel by spontaneous emission during the Raman pulses. Either way, they have a high probability of being cleared before and after the last π pulse. Figure 27 illustrates the effectiveness of this final clearing in removing most of the unwanted background. We have taken recoil measurements with and without the $F = 3$ clearing, so that the background changes as it does between Fig. 27a and b, and there was no observable shift in the recoil measurement.

Still, some atoms do remain, which amount to less than 20% of the signal atoms after 10π pulses, but as large as 40% after 15π pulses. If they cause line pulling it will be worse for higher N, where the signal to background ratio is lower, although since the locations of the final frequencies relative to the Zeeman resonances change as a function of N, the dependence is likely to be erratic. Our measurements have repeatable behavior as

a function of N, and our measurements do not drift over time even when the magnetic field does, so we have further reason to rule out line pulling from Zeeman shifted levels as a significant source of error.

4.3 Wavefront irregularities

The recoil measurement is commensurate to a measurement of the number of effective photon wavelengths between the endpoints of the two interferometers in the double interferometer. If the wavefronts of the exciting light are not planar, the number of wavelengths between two points may not properly reflect the distance along the beams separating the two interferometers. Systematic errors can thereby be introduced into the measured recoil.

The wavefronts of a perfect Gaussian beam are spherical, with the radius of curvature going to infinity at the beam focus. Imperfections in the beams due to imperfectly smooth optics or point scatterers will also lead to wavefronts that are approximately spherical in the far field. In the near field, however, a single scatterer gives rise to more complicated wavefronts. The near field interference of the fields due to many coherent scatterers, laser speckle, is still more complicated and can typically only be described using statistical methods. Because of its fine spatial structures and their associated large curvatures, speckle is likely to be the type of wavefront curvature most damaging to the recoil measurement. However, to convey the underlying physics of wavefront curvature systematic effects, we will primarily consider spherical wavefronts, applying the result to both imperfectly collimated beams and scattered light in the far field. We will assume that the local field can be described by a single k-vector, so we can ignore the non-linear processes that occur when there are multiple k-vectors at a single point in space. Furthermore, we will start by assuming k is due to only one laser beam exciting a single photon transition, and then we will generalize this to the case of Raman transitions with two counterpropagating beams.

4.3.1 Uniform wavefront curvature. The dominant spatial separation between the two interferometers is accrued between the last two $\pi/2$ pulses, so we will concentrate on these two pulses now. The local radius of curvature of the beam that the atom sees during the third $\pi/2$ pulse is R, which we take to be roughly the same for each path of each interferometer. By the time of the fourth $\pi/2$ pulse the atom will have moved a distance Δx perpendicular to k, and the paths of the two interferometers will be separated along the beam by a distance Δz (near 3 mm for the typical conditions we have been using). We see from Fig. 28 that at the last $\pi/2$ pulse each path will be shifted by δz with respect to where they would be if the wavefronts were planar. For $R \gg \Delta x$ and Δz, the phase shift difference between the two interferometers due to the curvature is given by,

$$\Delta\varphi_{\mathrm{wfc}} = (\delta z_2 - \delta z_1)k = \frac{(\Delta x)^2 \Delta z}{2R^2}k. \quad (32)$$
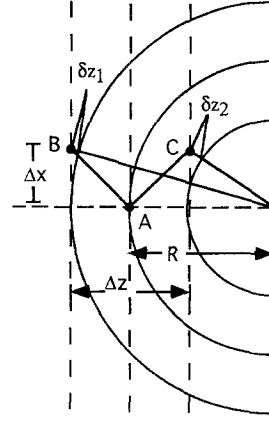

Fig. 28. Illustration of the relative phase change due to wavefront curvature at the final vertex of two interferometers. The *filled circle* is the effective source for some curvature. Point A corresponds to the vertex at the third $\pi/2$ pulse for two interferometers, which are assumed to be approximately overlapped at that point. The difference in the distance of B and C relative to the constant phase fronts will lead to an error in the measured recoil

For a Gaussian beam with a large waist, the Rayleigh range $(z_0 = \pi w_0^2/\lambda)$ can be quite large on a laboratory scale. For instance, for 852 nm light and a 1.3 cm beam radius, z_0 is 625 m. Because the Rayleigh range sets the scale over which the phase front is mostly planar, R can be made larger than z_0. If the atoms traverse 2 mm perpendicular to the laser beam, the separation between the interferometers is 3 mm, and R is 100 m, then $\Delta\varphi_{\mathrm{wfc}}$ is 10^{-5} rad, which corresponds to a fractional error in the recoil measurement of 2×10^{-10}. For a Raman transition it is the relative phase of the two laser fields that is important to the interference, so we must find a δz for each beam. In our experimental case, where the beams copropagate and are retroreflected, the error is just double what one would expect for a single photon transition.

Now suppose that near the center of the laser beam a large distance d_S away from the interaction region there is a circular diffusive scatterer of radius $a \ll w_0$. Since we are taking the far field limit we can apply Babinet's principle, and consider the additional spherically curved wavefront due to the removal of light by the scatterer. The scattered light in the far field varies like an Airy pattern. It has an integrated power of $\approx \pi a^2 I_0$, where I_0 is the central intensity of the beam. Its central disk has an area of $\pi(d_S\lambda/a)^2$, so its average intensity in this region is $I_0(a^2/d_S\lambda)^2$. The amplitude of the scattered field is thus $a^2/d_S\lambda$ of the main beams. The radius of curvature of the scattered light in the far field is approximately d_S. An atom in the central Airy disk will see a phase front that has an amplitude weighted contribution from this higher curvature beam. Applying (32), we find the contribution from the scatterer to the phase shift difference between the two interferometers,

$$\Delta\varphi_{\mathrm{scat}} = \frac{a^2(\Delta x)^2 \Delta z}{2\lambda d_S^3}k. \quad (33)$$

For $d_s = 0.4$ m and $a = 10$ μm, $\Delta\varphi_{scat} = 2 \times 10^{-4}$ rad, which is a fractional error of 5×10^{-9}. This phase shift increases quadratically with the scatterer size, and there is obviously a significant advantage to being far from all scatterers.

In a measurement with a single pair of horizontal Raman beams the distance traversed transverse to the beams, Δx, grows approximately quadratically with T due to gravitational acceleration. Therefore, if we assume that the curvature of each wavefront is constant, (32) implies that $\Delta\varphi_{wfc}$ increases like T^4. The number of cycles in a recoil separation increases linearly with T, so the relative error in the recoil measurement increases like T^3. When the number of π pulses, N, is increased, Δz increases linearly. The sensitivity to the recoil also increases linearly, so the relative error should be basically independent of N.

If vertical Raman beams are used then the transverse travel is only caused by atoms' transverse velocities, so Δx is linear in T and the relative error increases as T. In the vertical configuration there is a further experimental handle on this systematic error, because the initial transverse velocity spread can be limited and varied. The error from uniform wavefront curvature should decrease linearly with transverse velocity spread. With horizontal Raman beams, Δx cannot be independently limited in this way.

To understand the behavior of this systematic error with changes in spatial parity, consider the wavefronts shown in Fig. 28, which correspond to those for a single beam. At the final $\pi/2$ pulse the two interferometers are separated by fewer wavelengths than they would be if the wavefronts were parallel. Therefore, the measured recoil separation will be smaller than the true value. This is a statement about the distance between the wavefronts; it is independent of the direction of beam propagation. So if the beam were exactly reversed in such a way that the wavefronts were unchanged, the measured recoil would be unchanged. Thus the error due to wavefront curvature is invariant under spatial parity reversal. The geometric argument also implies that curvature will always lead to smaller measured recoils. That the recoil is always smaller can also be understood by the obvious fact that the dot product of the **k**-vector at the third $\pi/2$ pulse with the **k**-vector at the fourth $\pi/2$ pulse is maximized when they are parallel.

The argument carries over completely for the case of Raman transitions, where $\varphi_{eff} = \varphi_1 - \varphi_2 = (\omega_1 - \omega_2)t - (\mathbf{k}_1 - \mathbf{k}_2) \cdot \mathbf{x}$, and $\mathbf{k}_{eff} = \mathbf{k}_1 - \mathbf{k}_2$ replaces **k** in the above argument. When the spatial parity is changed, the wavefronts will reverse more cleanly when counterpropagating Raman beams excite a transition than they will for a single beam and a single photon transition. Wavefront irregularities will in general be different for beams propagating in different directions, but if the two frequency components are well overlapped and retroreflected, the wavefront shapes will be the same for beams that travel in the same direction, as long as their frequency difference is small enough that there are no chromatic effects.

4.3.2 Laser speckle. Chromatic effects may arise due to the interference of many scatterers. The location of interference features will vary on the scale of the wavelength associated with the difference frequency. Many wavelengths away from the scatterers, the details of speckle patterns for the two frequencies could look very different, so spatial parity reversals may result in a change in the measured recoil. Furthermore, the error in the recoil measurement due to a wavefront with a complicated shape can have either sign.

Since we began this experiment we have changed the Raman beam optics several times to improve the beam quality. With each change the measured recoil has changed, generally moving closer to the accepted value. With worse quality beams there are systematic dependencies on the reversals. The deviation from the accepted value has had both signs.

We have yet to make detailed calculations of speckle effects, but we can make some general observations. A speckle pattern is characterized by spatial correlation functions of the intensity and phase of the light. At separations greater than the scale of the second order correlation functions, the relative phase shifts of two points will start to have a random relation to each other. So the phase shift may not continue to increase with separation like those due to spherical wavefronts. If the magnitude of the average phase shift levels off for large separations, the fractional error in the measurement will become independent of T and will decrease linearly with N.

It may be possible to independently characterize the speckle patterns in the beam under conditions nearly identical to the recoil measurement, also using interfering atoms. The technique would rely on a fundamental difference between the double atomic interferometer and the 3-pulse interferometer of Kasevich and Chu. In the recoil measurement the spatial separation between the interferometers is essential; the greater the separation, the more precise the measurement. In the 3-pulse interferometer, the fringes are sensitive to the phase difference between the pulses at different times, but the difference in space is not important. For instance, the measurement of g is just as precise near the top of a fountain trajectory as far from it. One could perform the g measurement at different times during the fountain trajectory and compare the results. Unfortunately, it is not possible to cancel out the shifts completely, because the phases of the first and the last pulses add. It should, however, be possible to decrease the phase shift by half by making the middle pulse spatially coincide with one of the $\pi/2$ pulses.

The data's general insensitivity to the sign of the detuning suggests (as we shall see in the next section) that if beam distortion causes a shift, it is through wavefront curvature. It is clearly essential to be able to control the transverse velocity spread and location of the signal atoms, as can be done with vertical Raman beams.

4.3.3 Beam misalignment. The dominant effect of beam alignment on the recoil shift is explicit in the definition of $\mathbf{k}_{eff}$. If there is a small angle θ between the two Raman beams, then the recoil shift changes proportional to the
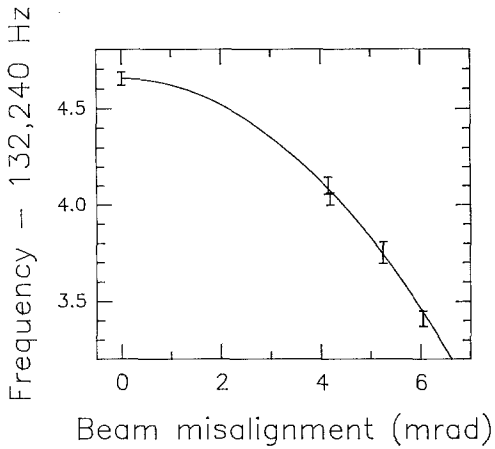
Fig. 29. Data for different Raman-beam angles. The curve is a parabola, and only the offset is a free parameter in the least-squares fit
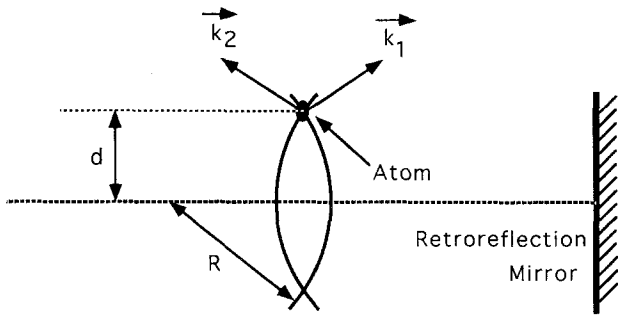

Fig. 30. Error from wavefront curvature when an atom is offset from the beam axis

square of k_{eff}.

$$k_{eff}^2 = k_1^2 + 2k_1 k_2 \cos\theta + k_2^2 \approx (k_1 + k_2)^2 - k_1 k_2 \theta^2$$

$$\approx (k_1 + k_2)^2 \left(1 - \frac{\theta^2}{4}\right), \tag{34}$$

where the last step assumes $k_2 - k_1 \ll k_2$.

Data taken at different angles is shown in Fig. 29, where the data has not been corrected to take into account the deviation from retroreflection. Therefore, to the extent that the data fits the quadratic, it yields a consistent value for the recoil. The fit shown has only one free parameter, the offset, which determines the size of the photon recoil. Each data point for misaligned beams has an uncertainty in its alignment that leads to a $\approx 2.0 \times 10^{-7}$ uncertainty in the recoil. However, when the beam is retroreflected to within 1×10^{-4} radians, which is our standard condition and fairly straightforward to achieve using the available 3.5 m lever arm, the uncertainty due to the beam alignment is 2.5×10^{-9}.

Uniform wavefront curvature also mimics beam misalignment for atoms that are not along the central axis of the Raman beams. Figure 30 illustrates this effect, where for a radius of curvature R and a displacement d, the angle between the k-vectors of the two beams is $\theta = 2d/R$. Using (34) and taking $d = 3$ mm and $R = 100$ m, the fractional error in the recoil due to this effect is 10^{-9}.

4.4 ac Stark shifts

Fringes in an atomic interferometer can be shifted by ac Stark shifts in two distinct ways. A shift can result from the average ac Stark shift term, $\varphi_{acs} = (\Omega_a^{AC} + \Omega_b^{AC})\tau/2$, which multiplies every path at every vertex. For our experimental parameters the average ac Stark shift is about twice the Rabi frequency, which makes φ_{acs} approximately equal to π for a $\pi/2$ pulse. A shift can also come from φ_{off}, which affects those paths which do not make a transition at a pulse. Near resonance

$$\varphi_{off} \approx \frac{\delta^{AC} - \delta}{2\Omega_{eff}}, \tag{35}$$

which we find using (20) and (17). The difference between the ac Stark shifts of the two levels, $\delta^{AC} = \Omega_b^{AC} - \Omega_a^{AC}$, appears in this term, so it is zero if we are tuned to the Stark shifted resonance. Hence, for spatially uniform fields, it is possible to make $\varphi_{off} = 0$, but φ_{acs} cannot be made zero. When there are intensity gradients in the fields, both of these terms can contribute to systematic errors.

Spatial variations in the ac Stark shift occur on the same scales as the curvatures discussed in the previous section. In addition, subwavelength variations will arise if there are any standing wave components in the light. Other sources of light, like the clearing beams, can also affect the measurement through these terms.

4.4.1 Large-scale Raman-beam intensity gradients. A diverging laser beam is the easiest slowly varying perturbation to characterize. For simplicity, we will start by considering the intensity variation due to a single beam. The effect of the Raman beams themselves can be understood as a generalization of this case. The two Raman beams start with the same spatial mode, but one of them interacts with the atoms only after being retroreflected, so the spatial intensity gradients for the two beams have opposite signs. Therefore, when we apply these results to the Raman beam pairs, they will be too optimistic for φ_{off} and too pessimistic for φ_{acs}.

Using ray optics, for a beam of radius w_0 which has a half angular divergence θ, the normalized spatial derivatives of the beam area are

$$\frac{dA}{A\,dz} = \frac{2\tan\theta(w_0 + z\tan\theta)}{w_0^2} \approx \frac{2\theta}{w_0}, \tag{36}$$

$$\frac{d^2 A}{A\,dz^2} = -\frac{2\tan^2\theta}{w_0^2} \approx -\frac{2\theta^2}{w_0^2}. \tag{37}$$

As can be seen from Fig. 12, the difference in φ_{off} is manifested at all the $\pi/2$ pulses but the first. Because this phase shift only accrues when a path does not make a transition, none of the π pulses contribute. Like φ_{wfc}, the large spatial separation of the two interferometers at the fourth $\pi/2$ pulse contributes most of the error. The separation of the interferometers at the fourth $\pi/2$ pulse is $\Delta z \approx 3$ mm. For 1.3 cm radius Raman beams that diverge with an angle of 0.1 mrad, the interferometers see a relative

intensity change of 5×10^{-5} [using (36)]. Therefore, $\Delta \varphi_{\text{off}} \approx 1.2 \times 10^{-4}$ rad, and the associated fractional error is 2.5×10^{-9}. This is about an order of magnitude larger than φ_{wfc} for comparable beams and these parameters. The functional form of the error is, however, different from that for φ_{wfc}; both $\Delta \varphi_{\text{off}}$ and the total interferometer phase are linearly proportional to N and T, which makes the fractional error from this effect independent of N and T. The systematic error $\Delta \varphi_{\text{off}}$ associated with uniform intensity gradients approaches zero near the waists of diffraction-limited Gaussian beams. Therefore, as with $\Delta \varphi_{\text{wfc}}$, the major concern is the steeper gradients associated with laser speckle.

For φ_{acs}, the difference is only manifested at the π pulses and at the third $\pi/2$ pulse, because at the first and last $\pi/2$ pulses, the vertices are at the same spatial point for the two paths in an interferometer, and at the second $\pi/2$ pulse the difference between the paths is the same for the two interferometers. The separation within an interferometer, δz, is $\hbar k_{\text{eff}} T/m$, and the separation between two corresponding paths in the two interferometers, Δz, increases with each π pulse to $\approx (N+1)\hbar k_{\text{eff}} T'/m$ at the third $\pi/2$ pulse. The sensitivity to the recoil is independent of T', but as $T' \to 0$, so that $\Delta z \to 0$ at the third $\pi/2$ pulse, the systematic errors in the recoil measurement due to φ_{acs} will also approach zero. The critical difference between $\Delta \varphi_{\text{off}}$ and $\Delta(\delta \varphi_{\text{acs}})$ errors, and what makes the former much more severe, is that it is sensitive to differences in intensity between two interferometers, while the latter is sensitive to the difference between the two interferometers of the intensity difference between two paths. Typically, the spatial separation between the two paths in each interferometer during the time between the middle $\pi/2$ pulses is 140 μm, and the spatial separation of the two interferometers at the third $\pi/2$ pulse is 840 μm. Using (36) and (37) and taking $\theta = 0.1$ mrad and $N = 10$, we find $\Delta(\delta \varphi_{\text{acs}}) \approx 4 \times 10^{-10}$ rad, which corresponds to a fractional error some six orders of magnitude below $\Delta \varphi_{\text{off}}$ due to the same imperfect beam.

To first order, all ac Stark-related phase shifts are independent of the magnitude of the detuning Δ if the Raman beam intensity is fixed, because although the ac Stark shift decreases with higher Δ, the Rabi pulse time must be increased. However, in our experiment both Raman beams shift both levels, so the ratio $\varrho = \Omega_{\text{eff}}/\Omega^{\text{AC}}$ of the Rabi frequency to the ac Stark shift is Δ-dependent. The ratio of intensities of the two Raman beams is empirically adjusted at each detuning so that the Stark shifts of the two levels are equal. To satisfy this condition,

$$\frac{I_1}{I_2} = 1 + \frac{2\Delta}{(H-\Delta)}, \tag{38}$$

where H is the hyperfine frequency splitting, the subscripts of the intensities conform to Fig. 6 and the detuning is taken to be positive. Thus,

$$\varrho = \frac{\dfrac{\sqrt{I_1 I_2}}{\Delta}}{\dfrac{I_1}{\Delta} - \dfrac{I_2}{H-\Delta}} \approx 1 - \frac{1}{2}\left(\frac{\Delta}{H}\right)^2, \tag{39}$$
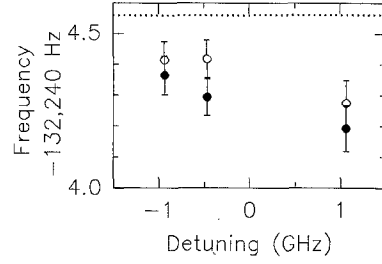

Fig. 31. Recoil measurement as a function of detuning from the center of mass of the excited state. The *dotted line* is derived from the accepted values of fundamental constants

in the limit where $\Delta \ll H$. Therefore, the φ_{off} and φ_{acs} terms increase with Δ in this limit.

To date, measurements have been taken using cork-screw polarization at only a few different detunings. As can be seen in Fig. 31, there is weak evidence for a dependence on the sign of the detuning, so further study is clearly needed.

Errors from φ_{off} change sign under spatial parity reversals because $\Delta \varphi_{\text{off}}$ is proportional to the gradients of the ac Stark shifts. When the directions of all of the pulses are reversed, then the resulting interferometer is mirror symmetric to the original interferometer, except that the spatial gradients of the Stark shifts change sign. Consequently, $\Delta \varphi_{\text{off}}$ must change sign as well.

Because the errors from φ_{acs} are insensitive to the atom's internal state, they have a spatial structure similar to the φ_{wfc} error. If two points in space appear to have more cycles between them because of the difference in φ_{acs}, this fact will not change if the interferometers are flipped, or if the internal states are flipped by an extra π pulse.

The fact that all the φ_{off} and φ_{acs} terms change sign with the detuning offers some promise for keeping track of these systematic errors. Unfortunately, the reversal may be imperfect for the complicated intensity gradients caused by speckle, because the absolute frequency change associated with a sign change in the detuning may cause the speckle pattern to change.

4.4.2 Standing waves. If there are standing wave components in the Raman fields, there can be a considerably more complicated and potentially larger systematic error than those due to more gradual gradients. When the two Raman beams are oppositely linearly polarized and retroreflected, then Doppler-sensitive, Doppler-free, and standing wave Raman transitions can all be excited. The last two are only resonant when the atoms have velocities along the beam axis of 0 and $\pm \hbar k$, respectively, so they will be suppressed if the velocities are large enough. If the Rabi pulses are shaped to minimize sidebands, the individual unwanted processes can be essentially completely avoided. However, there is not a complete separability among these processes; beams that do not cause transitions can affect transitions that do occur [57]. This kind of interplay can lead to a physically interesting phase shift which can appear as a systematic error in the recoil measurement.
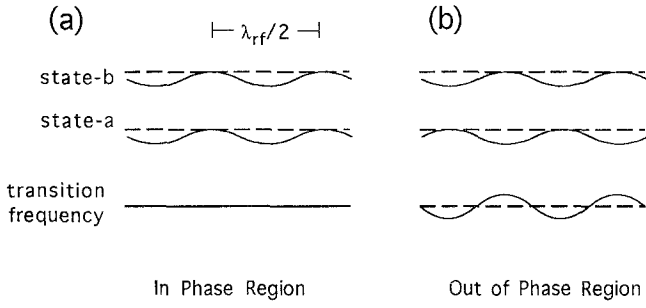
(a)

$\vdash \lambda_{rf}/2 \dashv$

(b)

state-b

state-a

transition
frequency

In Phase Region   Out of Phase Region

Fig. 32a, b. Systematic error due to optical standing waves. The upper two curves are the ac Stark shifts of the two levels caused by different standing waves. **a** When the standing waves are in phase, the transition frequency, which is proportional to the difference of the energies of the two levels, is position insensitive. **b** For two standing waves π out of phase, the transition frequency varies with position

The field for this polarization configuration consists of two standing waves with spatial periodicities of $\lambda_1/2$ and $\lambda_2/2$, where $\lambda_k = 2\pi/k_k$. The two standing waves come in and out of phase with a periodicity of $\lambda_{rf}/2 = 2\pi/(k_1 - k_2)$, which corresponds to 1.55 cm if the two frequencies drive a Raman transition between the ground state hyperfine levels in Cs. In the regions where the two standing waves are in phase, the two atomic levels shift together, as shown in Fig. 32a, so the Raman transition resonance frequency is independent of position. In contrast, in the regions where the two standing waves are out of phase (Fig. 32b), there is a position dependence to the Raman transition frequency, which varies from $+2\Omega^{AC}$ to $-2\Omega^{AC}$ with the periodicity of the standing waves. As is illustrated in Fig. 7, after a single Rabi pulse in the limit where the atomic velocity is much greater than $\hbar k_{eff}/m$ the atom is delocalized over many wavelengths. Therefore, periodic changes in the resonance frequency on the scale of the optical wavelength are averaged by each atom. This is important because $\Omega^{AC} \gg 1/T$, and were the average of the resonance frequencies taken over an ensemble of atoms, rather than by each atom, the interference fringes would be washed out.

If the amplitude of the atom's wavefunction were constant over a standing wave period, the sinusoidal variation in the resonance frequency would average to zero. But the wavefunction is not constant. Just as a classical particle rolling over a series of hills spends less time near the valleys than near the peaks, where it moves relatively slowly, the atomic wavefunction has a higher amplitude in the standing wave peaks. The amplitude weighted spatial average of the resonance frequency will therefore be changed by the standing waves. The size of this change depends on how much the atom's amplitude varies across the standing wave, and these fluctuations are larger when the atom moves more slowly. Because the absolute velocities in the two interferometers are different, this can cause an error in the recoil measurement.

Near resonance, the transition frequency only acts through the φ_{off} terms, which only accrue to paths that do not make a transition during a pulse. From Fig. 12, we see that this error in the recoil measurement can enter at all of the $\pi/2$ pulses except for the first.

Even though the atom is highly delocalized, we are still in a regime where its de Broglie wavelength is much shorter than the optical wavelength, so we can determine the appropriate weighting function for calculating the expectation value of φ_{off} by working in the semi-classical limit. For simplicity, we will assume that a semi-classical path that does not make a transition never leaves its initial state, even though these paths do have some amplitude in the other state during the light pulse (Fig. 7). The actual phase shift should thus be slightly smaller than the value we calculate. If we follow any initial position component of the atom across the standing wave, its velocity varies like that of a classical particle,

$$v(z) = \sqrt{v_0^2 - \frac{2\hbar\Omega^{AC}}{m}(2\cos^2 k_{1,2}z)} \approx v_0 - \frac{\hbar\Omega^{AC}}{mv_0}$$

$$\times (1 + \cos k_{eff}z \cos k_{rf}z \mp \sin k_{eff}z \sin k_{rf}z), \tag{40}$$

where we are in the limit that the energy perturbation is much less than the atom's initial kinetic energy, and minus refers to k_1, plus to k_2. We have assumed that the intensities of the two beams have been adjusted to give the same ac Stark shift to both levels, Ω^{AC}, and we have ignored for now the fact that each state is shifted by both beams. The probability of finding any given initial position component at a given position along the standing wave is inversely proportional to its velocity at that position, so the normalized weighting function in this limit is

$$g(z) = 1 + \frac{\hbar\Omega^{AC}}{mv_0^2}(1 + \cos k_{eff}z \cos k_{rf}z \mp \sin k_{eff}z \sin k_{rf}z). \tag{41}$$

The value of δ^{AC} as a function of position is

$$\delta^{AC}(z) = 2\Omega^{AC} \sin k_{eff}z \sin k_{rf}z, \tag{42}$$

so the expectation value of φ_{off} is

$$\varphi_{SW} = \langle\varphi_{off}\rangle_{SW} = \left(\frac{1}{\lambda}\right)\int_0^\lambda g(z) \frac{-\delta^{AC}(z)}{2\Omega_{eff}}dz$$

$$= \pm \frac{\hbar(\Omega^{AC})^2}{4mv_0^2\Omega_{eff}}(1 - \cos 2k_{rf}z), \tag{43}$$

where the integration has been done over a region where the change in z is much less than λ_{rf}, and the plus sign corresponds to φ_{SWa}, the minus sign to φ_{SWb}. As expected, when the optical standing waves are π out of phase, which corresponds to $k_{rf}z = \pi/2$, the magnitude of φ_{SW} is maximized.

Unlike all the other phase shifts we consider in this paper, φ_{SW} would cause an error in the recoil even if it had the same magnitude everywhere it accrues. Recall from (27) that when φ_{off} terms result from a simple detuning from resonance the fringes of each interferometer shift, but by the same amount for the two interferometers. When the error is caused by standing waves, the signs of

the φ_{off}'s that apply in Fig. 12 depend on the atom's internal state, so there is no longer a cancellation between the two interferometers. In fact, the nature of the fringe shift in each interferometer is different from all the others considered in this paper, because a change in exit path changes the sign of the φ_{sw} term added at the fourth $\pi/2$ pulse. The accumulated phase shift therefore depends on the state in which the atom exits the interferometer, which has the result that the interference fringes are distorted from a sinusoid. Inspection of Fig. 12 in this light shows that the absolute value of the relative shift of the nodes and antinodes in a given interferometer is $2|\varphi_{\text{sw}}|$ leading to an average phase shift, $\delta\varphi_{\text{sw}}$, of half that magnitude. The error in the recoil measurement, which is invariant under any of our standard reversals, is

$$\Delta(\delta\varphi_{\text{sw}}) = 2(\varphi_{\text{sw}a} - \varphi_{\text{sw}b}). \tag{44}$$

The assumption that the magnitude of φ_{sw} is constant for all the vertices is not generally a good one, so we will now consider corrections to the above derivations. We will start by ignoring the spatial separations of the atomic paths and concentrating on the more important effect of unequal final velocities. For an interferometer pair where the first recoil is opposite the initial velocity of the atoms selected at the start of the interferometer sequence, v_i, the velocities of the two interferometers at the final two pulses are $v_i + Nv_{\text{rec}}$ and $v_i - (N+1)v_{\text{rec}}$, where $v_{\text{rec}} = \hbar k_{\text{eff}}/m$. If all the paths are near where the standing waves are out of phase then, using (43), the error in the recoil shift will be

$$\Delta(\delta\varphi_{\text{off}})_{\text{sw}} = \frac{\hbar(\Omega^{\text{AC}})^2}{m\Omega_{\text{eff}}}$$

$$\times \left(\frac{1}{[v_i - (N+1)v_{\text{rec}}]^2} + \frac{1}{v_i^2} + \frac{1}{(v_i + Nv_{\text{rec}})^2} \right). \tag{45}$$

It is independent of N for $Nv_{\text{rec}} \ll v_i$, but for large N the first term, which corresponds to the slower interferometer, dominates and leads to a strong N-dependence. When the first recoil in the interferometer sequence is along the initial velocity the N and $N+1$ terms are reversed, so there will be a change in the size of this error with the reversal from left to right interferometers.

If in (45) we use values from our experiment for which we observe a large error due to this effect, which include $\Omega^{\text{AC}} \approx 2\pi \times 10$ kHz, $v_i = 20v_{\text{rec}}$, $N = 15$, and $\Omega_{\text{eff}} = 2\pi \times 4$ kHz, we calculate $\Delta(\delta\varphi_{\text{sw}}) = 0.10$ rad. The observed phase shift is 0.14 rad. The theoretical and experimental values for the comparable mirror flipped interferometer pair are 0.07 rad and 0.04 rad, respectively.

The observed dependence on N is shown in Fig. 33. The experimental data matches quite well the prediction of (45) that the error should rise rapidly when the atom's velocity along the standing waves approaches zero.

To incorporate the spatial separation of the different interferometer paths it is necessary to include the factor of $(1 - \cos 2k_{\text{rf}}z)/2$ from (43) for each of the six φ_{off} terms
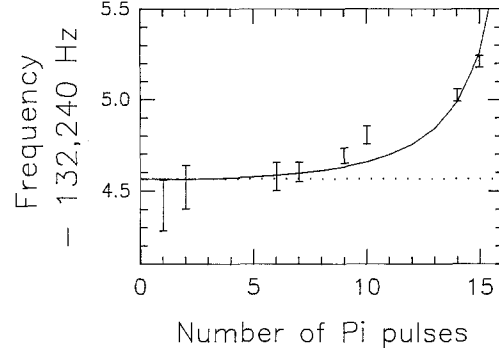

Fig. 33. Data vs number of π pulses, with optical standing waves. For clarity, all four spatial parity points are combined to yield each point. $T = 5.7$ ms and $\Delta = -1.0$ GHz. The fit is to (45) with v_i fixed, but allowing an offset and overall amplitude scale factor. The *dotted line* is derived from the accepted values of fundamental constants
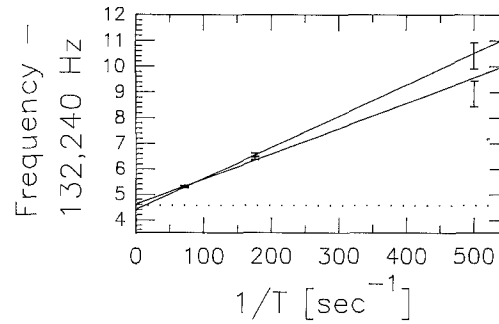

Fig. 34. Data vs time between $\pi/2$ pulses, with optical standing waves. The steeper curve corresponds to $N = 15$, the shallower curve to $N = 14$. The *dotted line* is derived from the accepted values of fundamental constants

which contributes to (45). When the slower interferometer dominates (45) and the separation between its two paths is much less than λ_{rf}, this spatial separation only slightly reduces the peak error. For the largest separations in this experiment this correction is less than 3%. The absence of a significant dependence on spatial separation implies that the phase shift is independent of T, as in (45). Therefore as T is increased $\Delta(\delta\varphi_{\text{sw}})$ represents a linearly smaller fractional error. The observed change in the error as T is varied, shown in Fig. 34, agrees well with the expected linear dependence.

The fact that both Raman beams shift both levels complicates the above description. The two ground state levels will be ac Stark-shifted differently by the other frequency component, which changes the phase relationship between the transition frequency and the standing waves. Some algebraic manipulation shows that the magnitude of δ_{sw} is different for paths in the two atomic levels. Specifically,

$$\varphi_{\text{sw}a} = -\frac{\hbar(A^2 + AB)}{8mv_0^2\Omega_{\text{eff}}}(1 - \cos 2k_{\text{rf}}z),$$

$$\varphi_{\text{sw}b} = -\frac{\hbar(B^2 + AB)}{8mv_0^2\Omega_{\text{eff}}}(1 - \cos 2k_{\text{rf}}z), \tag{46}$$

where $A = \Omega_{1a} - \Omega_{2a}$, $B = \Omega_{2b} - \Omega_{1b}$, and Ω_{kj} are the ac Stark shift of the $j = a$ or b ground state by the $k = 1$ or 2 Raman beam. Using the relations in (46) in (44) illustrates that in the limit where differences in v_0 and z among the paths are insignificant, this complication does not change the error. In the more experimentally important case where it is appropriate to use (45) in the limit where only the slower interferometer contributes a significant φ_{sw}, the errors depend on which internal state the slow interferometer's paths are in when they reach the final $\pi/2$ pair. This state changes under spatial parity reversal. Straightforward calculations reveal a difference in $\Delta(\delta\varphi_{\mathrm{sw}})$ under spatial parity reversal proportional to $2(A^2 - B^2)$, which for $A \ll H$ (where H is the hyperfine splitting) is equal to $16(\Omega^{\mathrm{AC}})^2 A/H$. For $A = H/8$, this would make the absolute size of the change with spatial parity close to 50% of the size of the error. We observed closer to 10%. Perhaps this overestimation could be corrected by a more exact treatment of the phase shifts during the time of the pulses.

The error depends on $(\Omega^{\mathrm{AC}})^2$, so it is independent of the sign of the detuning from the excited state resonance (43). The sign independence comes about because the effect depends upon the product of the spatially dependent energy shift and the spatially dependent transition frequency, both of which change sign with detuning. The observed dependence on Δ is shown in Fig. 35. The data are independent of the sign of Δ, and there is the expected decrease in the error as Δ increases.

The most unique feature of the standing wave error is its periodicity with a spatial frequency of $2k_{\mathrm{rf}}$. We set the parameters to where the systematic error was relatively high ($T = 5.7$ ms, $N = 15$, $\Delta = -1.0$ GHz) and took points as we scanned the location of the retroreflection mirror. The data is shown in Fig. 36. It behaved as expected, with the error oscillating with a period of half the rf wavelength. In addition to the large changes in the mean values of the recoil, there is also a statistically significant difference between right and left interferometers, of the size expected due to the associated change in the velocity of the slower interferometer.

We are able to nearly completely avoid this systematic error by using opposite circular polarizations in the two Raman beams. In this case the net polarization is linear everywhere and the direction of the polarization spirals
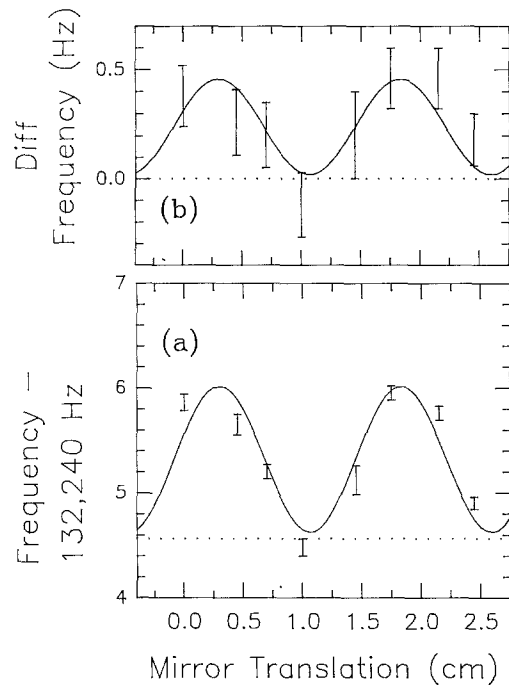

Fig. 36a, b. Standing wave recoil error as a function of mirror position. a The mean value of the recoil as a function of distance from the mirror. $N = 14$ and 15, $T = 5.7$ ms and $D = -1.0$ GHz. b The frequency difference between left and right interferometers, taken from the data in (a)
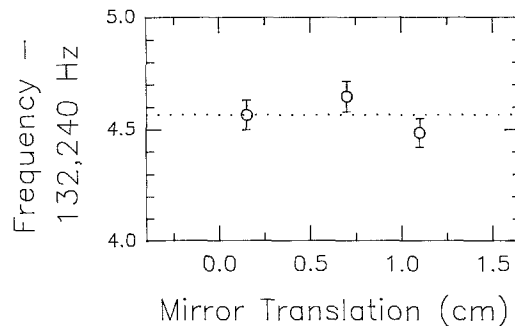

Fig. 37. Recoil as a function of mirror position using corkscrew polarization. Comparison with Fig. 36 reveals that the systematic error is at least an order of magnitude reduced. The *dotted line* is derived from the accepted values of fundamental constants

along the propagation axis. An atom in the $m_F = 0$ state has the same ac Stark shift everywhere along this 'corkscrew' polarized beam. The residual amplitude of the standing wave component of the light is then less than 10% of the non-standing wave component. A curve comparable to Fig. 36 for this new polarization is shown in Fig. 37. Evidently, the large error is gone. For most of our data collection the mirror was placed at the location corresponding to the minimum in Fig. 36.

There is another potential systematic error due to standing waves. If the two paths in an interferometer see a significantly different phase relationship between the two standing waves, the depths of the potential wells they pass when they are in a superposition of the two ground states will be different. They will be delayed by different
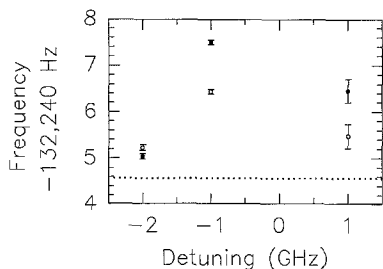

Fig. 35. Data vs detuning with optical standing waves. The detuning is measured with respect to the center of mass of the excited state. The *open circles* are for left interferometers, $N = 14$ and 15, and the *closed circles* are for right interferometers. The *dotted line* is derived from the accepted values of fundamental constants

amounts, and the resulting deviation from overlap of the recombined paths is equivalent to an interference fringe shift. This mechanism is less important than the one described above because it requires there to be a significant difference in the depth of the potential wells not just between the two interferometers but between the two paths within an interferometer. Unlike the dominant standing wave mechanism, this shift should accrue at every π pulse and at the third $\pi/2$ pulse.

4.4.3 The clearing beams.

The clearing beams can cause errors because of the Stark shifts they induce on the atoms they do not clear. Unwanted vacuum window reflections from these beams do not intersect the atoms so they can cause no standing wave shifts. The clearing beams are pulsed on just before the third $\pi/2$ pulse, so any systematic errors they cause will be proportional to the separations between and within the interferometers at that time, which vary approximately linearly with N and T, respectively. The intrinsic resolution improves with higher N and T, so any error due to the clearing beams should be insensitive to changes in N and T. Like other ac Stark shift effects, any systematic error they cause should not reverse sign with spatial parity reversals. Furthermore, because the $F=3$ clearing light is to the blue of the $F=4$ resonances, if it has uniform curvature it will lead to a systematically lower recoil measurement. Similarly, uniform curvature of the $F=4$ clearing beam will lead to a systematically higher recoil measurement. Although shifts due to speckle on the clearing beams will not change under spatial parity reversal, they will not have the same predictable signs as do shifts due to uniform curvature, nor necessarily the same predictable dependences.

We have checked in several ways to see if the clearing beams introduce a systematic error. The most reliable method is to increase the intensity of the clearing beams, which should linearly increase the size of any shift. In doing this we have more dynamic range on the $F=4$ clearing, and we find no change at the 1.5×10^{-7} level even with an order of magnitude increase in intensity above normal operating conditions. For the $F=3$ clearing we can only increase the intensity by a factor of four, and this tends to increase feedback to the laser diode which adds noise to the clearing. Still, we do not see a change in the signal at the 2.5×10^{-7} level. We have also completely blocked the $F=3$ clearing, which has only a mild effect on the noise but leaves a substantial background with a lot of frequency structure (Fig. 27). The measurement is unchanged within the 2×10^{-7} level when there is no $F=3$ clearing.

4.4.4 Beam misalignment.

When the beams are misaligned there will be an intensity gradient along $\mathbf{k}_{eff}$, as illustrated in Fig. 38. Consider an atom located on the z-axis, where the mirror is the origin. Assume a Gaussian beam with radius w_0. Then the intensity and the normalized spatial gradients of the intensity along the z-axis are

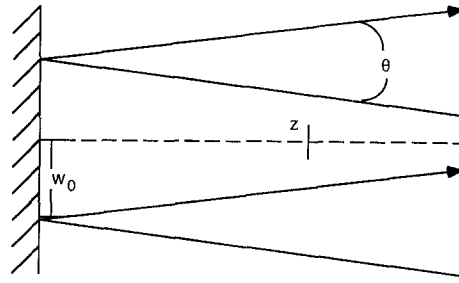$$I = I_0 \exp \left\{ -2 \left[z \sin \left(\frac{\theta}{2} \right) \right]^2 / w_0^2 \right\},$$

Fig. 38. Illustration of the axial variation in intensity due to beam misalignment. The relative intensity of the two beams, and hence φ_{off} and the ac Stark shift, depends on the axial position along the beams

$$\frac{dI}{Idz} \approx -\frac{z\theta^2}{w_0^2},$$

$$\frac{d^2I}{Idz^2} \approx \frac{-\theta^2}{w_0^2}. \tag{47}$$

For $\theta = 3$ mrad, $w_0 = 1.3$ cm, and $z = 60$ cm, the fractional difference in the intensity seen by two interfering paths that are separated by 140 μm at the time of the pulse is 4.5×10^{-6}. If this difference prevails for 10 π pulses, then the accumulated phase difference due to the ac Stark shift is 3×10^{-4} rad. The phase shift difference between two interferometers that have an average separation in the middle period of 420 μm is then 3×10^{-9} of the total ac Stark shift, or 2×10^{-7} rad, which represents a fractional error in the recoil measurement of 5×10^{-12}.

4.5 Line pulling

In precision frequency measurement there is often the concern that the measured center of one resonance will be shifted by nearby resonances or other sloping backgrounds. Since the center of a symmetric feature is primarily determined using the high slope sections on either side of the peak, a linearly sloping background will change the amplitude on either side differently, thus changing the apparent center. This problem is significantly reduced when the resonance being measured is not the center of a single peak but the phase of a sine wave, as in the case of our recoil measurement. For a sine wave, the shift of the centers of the maxima will be opposite the shift of the centers of the minima. As long as an integral number of cycles are measured, a linear background will cause no systematic shift of the measured phase, although the quality of the fit to a sine wave may suffer.

If there are higher order terms in the background there is the possibility that they will cause a shift, but this will be leveraged down because of the periodicity of the function. Figure 39 illustrates how this comes about. Each successive extrema is shifted one way or the other by a linearly increasing amount, and the fitted phase is assumed to be the average of the shift of all the extrema. If, as in Fig. 39b the frequency is scanned over an integral
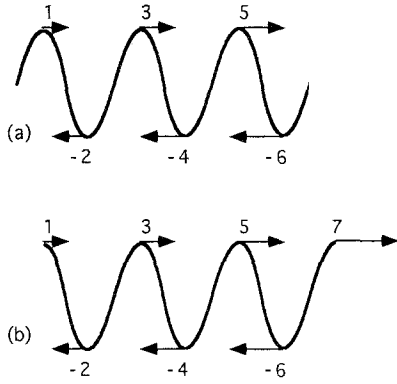
Fig. 39a, b. Line pulling due to a quadratically varying background with positive curvature. The relative size and direction of the shifts of the fitted phase of each peak due to a quadratic background is indicated by the *arrows*. **a** If an integer number of cycles is fit with this phase there is a net shift in the fitted phase. **b** With this phase, because the first and last upper peaks are only fit with half weight, the net shift is zero

number of cycles starting at a minima or maxima (so that the shifts of the first and last extrema are weighted by $1/2$), then the shift due to a second-order background exactly cancels. If, as in Fig. 39a, the scan is started at the point of maximal slope then the shift is the average of the shifts over a single cycle.

The Doppler-free and velocity-selective resonances of various magnetic sublevels are potentially problematic for this experiment, and their avoidance is discussed above. Here, we consider the contribution to the signal from the non-interfering paths which diverge from the interfering paths at the third $\pi/2$ pulse. The non-interfering paths contain a total amplitude equal to the interfering paths' amplitude. Furthermore, they come into resonance at the same frequency as the interference fringes, so they can only be removed from the final detection if there is very fine spatial resolution[4]. Because there is no interference for these paths at the final $\pi/2$ pulse, their lineshape is simply that due to a single Rabi pulse, which depends on the shape of the pulse, typically either square or Blackman [58].

From (16) we find that the transition probability P for a square $\pi/2$ pulse near the resonance peak is

$$P(\delta') = \frac{1}{2}(1 - a_2 \delta'^2),\tag{48}$$

where

$$\delta' = \delta^{AC} - \delta, \quad a_2 = (1 - \pi/4)/(2\,\Omega_{eff})^2.\tag{49}$$

Assuming perfect clearing before the final pair of $\pi/2$ pulses, the wavefunction amplitude along all the possi-

---

[4] To isolate these paths the spatial extent of the useful atomic ensemble must be less than $(\hbar k_{eff}/m)T$, which is a condition that is not satisfied in our experiment by about two orders of magnitude. Performing this spatial resolution can likely be realized using some combination of lighter atoms or longer times between $\pi/2$ pulses. Additional intermediate π pulses do not improve the separation
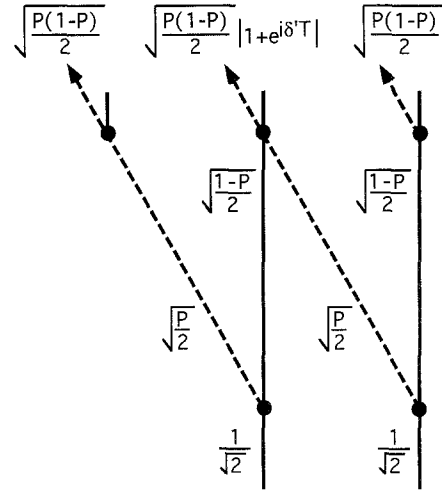

Fig. 40. The wavefunction amplitude for an atom in an interferometer during the final pair of $\pi/2$ pulses, written in terms of the transition probability P for the "$\pi/2$" pulses near resonance. The atom enters the interferometer in state $|a\rangle$ (*solid lines*) along one of two paths. We determine the amplitudes for an atom leaving the interferometer in state $|b\rangle$ (*dashed lines*), either along the non-interfering paths on the left and right, or the interfering paths in the center

ble atomic paths in the left interferometer is shown in Fig. 40. The total probability of an atom ending up in state $|b\rangle$ is

$$P_b(\delta') = P(1-P) + \frac{1}{2} P(1-P)\,|1 + e^{i\delta'T}|^2$$

$$\approx \frac{1}{4}(1 - a_2^2\,\delta'^4)(2 + \cos\delta'T).\tag{50}$$

We fit experimental fringes to a pure sinusoid, rather than to the more complicated feature described by (50). The fringes are measured as close as possible to the center fringe in order to minimize their non-sinusoidal characteristics. Since we do not perfectly locate the center fringe, we estimate here the phase error that results from taking data off to the side. Since the least squares method used to fit the curves is most sensitive to the points of maximum slope, or inflection points, it pushes the inflection points of the sinusoidal fitting function as close as possible to those of P_b. Let $\delta_\pm$ be locations of inflection points of $\cos\delta'T$ with slope $m \gtrless 0$, and let $\delta_\pm + \Delta\delta_\pm$ be the corresponding inflection points of P_b. Then the error caused by the fit will approximately equal the offsets $\Delta\delta_\pm$. The inflection points of P_b are given by the condition

$$\frac{d^2 P_b}{d\delta'^2}\bigg|_{\delta_\pm + \Delta\delta_\pm} = 0.\tag{51}$$

Substituting (50) into (51) and expanding to lowest order around $\delta' = \delta_\pm$ gives the left interferometer phase shifts

$$\delta\Phi_\pm = T\Delta\delta_\pm \approx -\frac{8\,a_2^2\,\delta_\pm^2}{T^2}(\delta_\pm T \pm 3),\tag{52}$$

where the first term is from the amplitude envelope of the fringes, and the second term is from the curvature of the background. The right interferometer has the same amplitude envelope for the fringes, but opposite background curvature. Consequently, the second term of (52) has reversed signs for the right interferometer. Then the difference between the shifts of corresponding points for the two interferometers is

$$\Delta(\delta\Phi_\pm) = \pm 48\, a_2^2 \delta_\pm^2/T^2. \tag{53}$$

Over an entire fringe, the fitting error is approximately the average of $\Delta(\delta\Phi_+)$ and $\Delta(\delta\Phi_-)$, which only differ in magnitude because of the difference $|\delta_+ - \delta_-| = \pi/T$. Using (49) and $\tau = \pi/4\Omega_{\text{eff}}$ for a $\pi/2$ pulse in (53) gives the net phase error over an integral number of fringes caused by the non-interfering paths,

$$\Delta\Phi_{\text{ni}} = \frac{192}{\pi^2}\left(1 - \frac{\pi}{4}\right)^2\left(\frac{\delta^{\text{AC}} - \delta}{\Omega_{\text{eff}}}\right)\left(\frac{\tau}{T}\right)^3. \tag{54}$$

In the current experiment $\tau/T \approx 0.0025$, and we can locate the center fringe to at least within 500 Hz, which gives $\Delta\Phi_{\text{ni}} = 3 \times 10^{-9}$ rad. The fractional error in the recoil measurement is thus 6×10^{-14}, which is far beyond our measurement precision.

4.6 Inertial phase shifts

One of the areas of great promise for atomic interferometry is inertial sensing of external forces and fields. One might think that the potentially high sensitivity could be a problem for the recoil measurement, but the differential nature of the measurement makes these errors insignificant. By far the largest inertial shift in a light-pulse atom interferometer is the first-order Doppler shift of the light beams due to gravity, which changes linearly in time according to,

$$\Delta(\mathbf{k}_{\text{eff}} \cdot \mathbf{v}) = \mathbf{k}_{\text{eff}} \cdot \mathbf{g}\Delta t. \tag{55}$$

But since the two interferometers in a double atomic interferometer essentially only differ in their mean velocities, the phase shift due to gravitational acceleration is the same for both of them.

The second-order Doppler shift has the same sign and almost the same size for the two Raman beams, so it predominantly has the effect of changing the detuning from the excited state resonance. For atoms moving at 2 m/s, which is about the fastest they get in a fountain, the second-order Doppler shift for a single beam is $2.2 \times 10^{-17}\omega$, or 8×10^{-3} Hz for Cs light. This is an insignificant change in the excited state detuning, so certainly the difference of this effect between the two interferometers is insignificant. The gravitational red-shift is also insignificant, causing a fringe frequency shift of $(g\Delta z/c^2)\omega_{\text{rf}} = 0.3$ μHz between two interferometers separated by 30 cm.

The calculation of the Sagnac effect for atoms launched at an angle in an atomic fountain is not straightforward. Because the trajectories are very curved, one can-
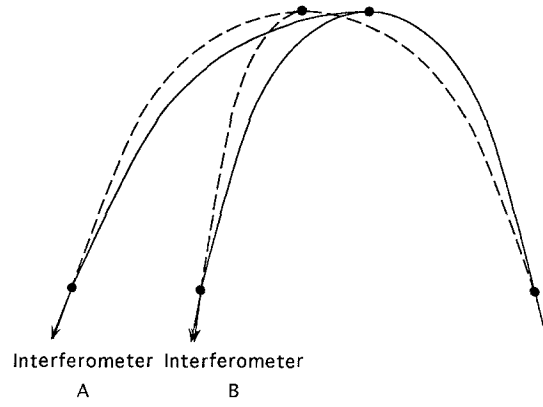

Interferometer   Interferometer
       A   B

Fig. 41. Atomic fountain double interferometer in the lab frame. For simplicity, there are no π pulses, and the second and third $\pi/2$ pulses are nearly overlapped in time, so that the middle two vertices in the usual double interferometer diagram (Fig. 3) are condensed into one

not make the simple analogy to the optical Sagnac effect, where the size of the effect is proportional to the area enclosed by the interferometer [45]. Figure 41 shows the approximate shape of our interferometers in the lab frame, as opposed to the falling frame in which we typically consider them. For clarity there are no π pulses and the time between the middle two $\pi/2$ pulses is made negligible. The paths in each interferometer cross each other, so the area of the interferometers in the lab frame is not even defined. However, we do not need to calculate the size of the Sagnac shift to show that it will not cause a systematic error in the recoil measurement.

In the gravitationally accelerating frame the area swept out by the two interferometers is the same, which has been shown analytically [43] and is also easy to demonstrate with simple geometry. Furthermore, because this holds true regardless of T or T', the equality holds during any given time interval. Therefore, since this result is independent of a uniform change of the velocity, it must also be independent of a uniform acceleration. So the cancellation of the Sagnac effect holds in the laboratory frame in the presence of gravity.

4.7 Atoms that miss photon kicks

There is a scenario by which unwanted Doppler-sensitive atomic interference can be created, leading to interference fringes which can pull the center fringes in the desired interferometers. The problem can come about in several similar ways. For pedagogical reasons we will start our explanation with the clearing beams blocked. At each real, imperfect π pulse some of the population is left behind, which is illustrated in Fig. 42, where we follow only one of the interferometers in the double interferometer. In the limit where $\Omega_{\text{eff}} \ll 2\delta_{\text{rec}} = \hbar k_{\text{eff}}^2/2m$, these lost atoms are never in resonance again, so the final $\pi/2$ pulse pair does not excite them, and they never interfere. When $\Omega_{\text{eff}} \geq 2\delta_{\text{rec}}$, however, these atoms are not left behind completely. Paths that are missed by the
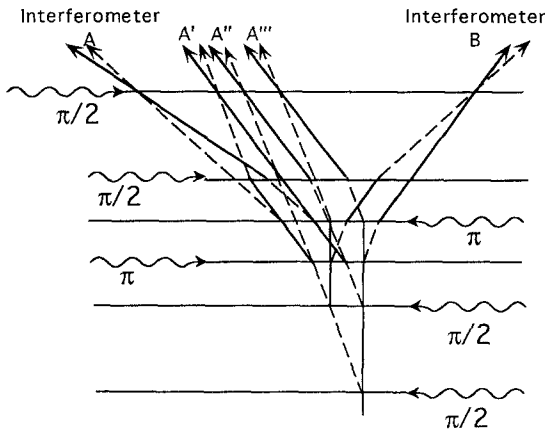
Interferometer   Interferometer

Fig. 42. Interference from atoms which miss π pulses. Atoms that interfere as in A''' may start with a velocity of $2\hbar k/m$ away from the peak velocity. After these atoms miss two pulses they are indistinguishable from the interferometer A atoms, except that they contribute to fringes with a different phase

last π pulse, are to some extent resonant with the final $\pi/2$ pulse pair, and they can form their own interference loops, as illustrated in Fig. 42. These paths, labeled A', form an interferometer akin to the 3-pulse interferometer of Kasevich and Chu [59], except that now the frequency of the final half of the π pulse (which is our third $\pi/2$ pulse) is scanned along with the final $\pi/2$ pulse, so there are fringes as a function of the final frequency. The fringes corresponding to A and A' will be separated in frequency by $2\delta_{eff}$ and they will have a phase relation with respect to each other which will be periodic in $1/T$. When the fringes are out of phase, the measured center frequency will be shifted by A'. For 15% loss per π pulse and $\Omega_{eff} \gg 2\delta_{rec}$ the shift can be as large as 0.1 rad.

If we turn on the clearing beams the paths in interferometer A' will be pushed away by the last clearing pulse, and the phase shift just described will not appear. Similarly, the atoms in what would be interferometer A'' are pushed away by the next to last clearing pulse. However, atoms which miss two earlier pulses in succession yet manage to keep up with the remainder of the π pulses, like those in interferometer A''', can still interfere at the final pulse. The most likely scenario is that an atom that is part of the background after the pre-selection and has a velocity near $2\hbar k_{eff}/m$, will evolve according to the double atomic interferometer diagram for the first two $\pi/2$ pulses, albeit with unequal populations in the four arms. Then whatever amplitude is still left in that same state after the next two π pulses will be indistinguishable from the intended signal atoms, except for the phase of their fringes. The unwanted atoms must first be excited far from resonance and then twice miss being excited as the light comes closer to resonance. Nonetheless, when the on-resonant π pulse is imperfect, there will be some amplitude for this to occur. This problem clearly gets worse when there is no clearing (even if the two interferometers are spatially resolved), and when either the Rabi frequency or the initial spread in atomic velocity is large.

Varying T by a small amount will change this phase difference and hence any related systematic error. We see no evidence of significant changes of the measured recoil which are correlated with small changes in T.

4.8 Instrumental systematic errors

4.8.1 Phase-lock imperfections.
If the diode phase lock does not settle after the final change in frequency, which is after the last π pulse and before the third $\pi/2$ pulse, a systematic error can result. A time lag or overshoot in the phase lock frequency compared to the reference will mean that the number of cycles of the beatnote between the third and fourth $\pi/2$ pulses will not equal the number of cycles of the reference. Since the final change in frequency is larger for the pulse sequences which lead to higher velocity than for those which lead to lower velocities (Fig. 16), a lag or overshoot will be more pronounced for those interferometers, so that the wrong frequency difference will be measured. Since the lag or lead will be a fixed phase shift, as long as the phase lock has equilibrated by the last $\pi/2$ pulse, this mechanism would cause an error in the measurement which increases inversely with T.

The error from this mechanism would not change sign with reversal of all the pulses (i.e., flipping the interferometers), because the lock would presumably overshoot or undershoot independently of the direction of the final change in frequency. An overshoot, for instance, would increase the average beatnote frequency separation between the interferometers in a pair, so that the measured recoil separation would be smaller, regardless of whether the final change is to a higher or lower frequency. For the same reason, such an error would always change the recoil measurement in the same direction.

The empirical evidence exonerates this mechanism. It is straightforward to look at the error signal from the phase lock and check the transient features associated with the frequency changes. The first clear feature of this signal is that there is a frequency dependent phase offset in the lock of $\pi/20$ per MHz. This in itself is inconsequential as long as the phase offset is the same at the final two $\pi/2$ pulses. However, the error signal takes at least two milliseconds to settle at the new level, depending on the gain settings in the phase lock. One millisecond after a 500 kHz frequency switch there can be a phase shift of 10 mrad, which can be worse still if the phase lock is poorly adjusted. By 3 ms, which is the typical time we wait after the last π pulse, no phase shift is observable even after 250 switches have been averaged, which places a limit on the shift from this source of 3 mrad.

We can also delay the third $\pi/2$ pulse to allow more time for the phase lock to settle. There is no change in the recoil measurement as a function of this delay, which seems to rule this out as a source of error.

4.8.2 Frequency-dependent amplitude changes.
If the amplitude in the slave Raman beam changes as a function of its frequency, then the relative ac Stark shifts of the two ground state hyperfine levels will be different for

different interferometer final frequencies. As a result the central fringe frequencies will be ac Stark shifted differently and the measured recoil will be wrong. The amplitude dependence on the frequency can come about in at least two different ways. First, the laser diode current affects both the frequency and amplitude of the output, so when the frequency is adjusted by changing the current, as the phase lock does in the mid-band, there is an amplitude change. Typically for these lasers (SDL–5410) it requires less than 1 μA to change the frequency by 1 MHz, so that the corresponding fractional change in power out is minuscule at $< 10^{-4}$. Second, when the frequency is changed by moving the PZT, this can change the alignment of that laser into the optical fiber. The size of this change is more difficult to estimate a priori. We have measured the amplitude change after the optical fiber when the frequencies are switched by ≈ 500 kHz, which corresponds to the separation of two interferometers in a pair after 15 π pulses. It is less than 0.25% of the total amplitude.

A 0.25% change in the amplitude of one of the Raman beams will to first order simply cause a shift of 0.25% in the ac Stark shift of the corresponding ground state hyperfine level. If the Stark shifts have been set to be approximately equal for the two levels, which they typically are, then the frequency shift of the fringes will be 0.25% of the absolute Stark shift, weighted by the fractional time that the Raman light is on during the Ramsey period. The actual effect of the light is somewhat more complicated, because both beams affect both levels, but this is less than a factor of two correction so we will ignore it. The measured value of the ac Stark shift with 1.3 GHz detuning and at our typical intensities is ≈ 10 kHz, which we determine by attenuating one Raman beam by a known amount and observing the shift of the resonant Raman frequency with a single π pulse. For T = 15 ms, a Rabi time of 50 μs, and a 0.25% amplitude dependence, the shift of the fringe will be 0.17 Hz, which corresponds to a 0.04 Hz shift in the recoil normalized to 3 π pulses. This fractional error of 3×10^{-7} is within our current precision. If the frequency dependence of the amplitude is linear, as shown in Fig. 43, then the error in the recoil will be the same under spatial parity reversals [2]. If this error is a problem or becomes a problem, it could be corrected by actively stabilizing the relative amplitudes of the two Raman beams after the optical fiber.
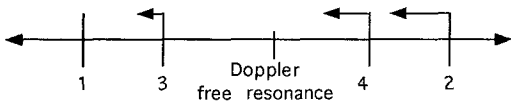

Fig. 43. Illustration of the effect of a frequency-dependent Raman-beam amplitude on the sign of the resulting error in the recoil. The numbers label the center frequencies of the interferometers of two spatially flipped pairs, 1 and 3, and 2 and 4. Diagrams of these interferometers can be found in Fig. 25, although the spatial picture is unnecessary here. The Raman-beam amplitude changes linearly with frequency, which shifts the resonances linearly with frequency. This changes the separation within the two interferometer pairs by the same amount

4.8.3 Detuning from the excited state.

To scan the difference frequency between the Raman beams, we adjust the frequency of only one of the Raman lasers. Therefore, in the rest frame of the atom, the detuning of the Raman beams from the excited state also changes, which raises the possibility that there will be a systematic error in the recoil measurement based on an ac Stark shift which depends on the difference frequency. For detunings much larger than or much smaller than the ground state hyperfine splitting, a change in detuning changes the ac Stark shift of the two levels in the same way. For the detuning in this experiment, however, each Raman beam affects both levels to some degree, so the two levels are affected differently when the detuning is changed.

The difference in the derivatives with respect to Δ of the ac Stark shifts of the two hyperfine levels is

$$\frac{d\delta^{AC}}{d\Delta} \propto \frac{(I_1 - I_2)}{\Delta^2} - \frac{I_1}{(H+\Delta)^2} + \frac{I_2}{(H-\Delta)^2}. \tag{56}$$

Therefore, when the detuning is smaller than the hyperfine splitting, the phase shift and hence the fractional error in the recoil measurement should decrease as the absolute value of Δ increases. Substituting (38) into (56) and keeping only terms to first order in Δ/H,

$$\frac{d\delta^{AC}}{d\Delta} \approx 2\Omega^{AC}/H,$$

independent of Δ for $\Delta \ll H$.

At the final π/2 pulse pair, the difference between the ac Stark shifts of the levels is different for the two interferometers, and is given by the expression

$$\Delta\delta^{AC} = (N+1)\frac{\hbar k_{eff}^2}{m}\left(\frac{2\Omega^{AC}}{H}\right). \tag{57}$$

With $N = 10$, $\Omega^{AC} = 10$ kHz, and for a detuning much smaller than H, the resonance is shifted by 0.4 Hz. The interferometer phase error caused by $\Delta\delta^{AC}$ enters through φ_{off}, and can be approximated from (35) by

$$\Delta\varphi_{off} \approx \frac{\Delta\delta^{AC}}{2\Omega_{eff}} \tag{58}$$

for a single π/2 pulse. Adding the errors for the final two π/2 pulses, with $\Omega_{eff} = 4$ kHz, gives a fractional error in the recoil measurement of 2×10^{-9}. This is beyond the current precision of our measurement. If it were to become a problem in the future, the systematic error could be easily calculated and corrected for. More reliably, the frequency to which the master laser in the phase lock is referenced could be adjusted to exactly compensate for the shift in the slave laser.

A similar shift can occur if the diode lasers which generate the Raman beams have sidebands near the resonance. Occasionally multi-mode behavior is observed, but when the laser current is adjusted so that the phase lock has minimal noise, the total power outside of the

carrier is $\approx 0.2\%$. Scaling from the numbers in the previous paragraph, only if this sideband were as close to one of the excited state resonances as 10 MHz would it cause as large a systematic shift as the carrier. It is easy to filter out all fequencies within a few hundred MHz of the resonance using a Cs cell. We periodically take data with a filter in place and find no change in our results.

Shifting the Raman frequencies also changes the photon momentum, but the error this causes is on the order of a part in 10^9. It is straightforward to take this into account should it become necessary.

4.9 Summary

Table 2 summarizes the way in which the errors we have discussed vary with various parameters and reversals, for those errors which scale in a simple way. The high N limit is assumed, and the time between the middle $\pi/2$ pulses, T', is assumed to be negligible. Because of their varied

behavior, these errors should be distinguishable from each other. Errors due to speckle interference shifts appear to be more important than those listed in the table, but they do not lend themselves to such simple characterization.

Most of the entries in Table 2 have not been verified experimentally, largely because most are not significant at the level of our current precision. Those that have been empirically studied are denoted with an asterisk.

4.10 Conversion to $\hbar/m_{\mathrm{e}}$

The constants necessary for the conversion of our measured frequency to $\hbar/m_{\mathrm{e}}$ are listed in Table 3. Our present accuracy in determining $\hbar/m_{\mathrm{e}}$ is limited by the accuracy of our measurement, but our current precision is only about a factor of three above the next limiting factors, the wavelength of the Cs primary transition and $m_{\mathrm{Cs}}/m_{\mathrm{e}}$. The possible improvements to those measurements are therefore relevant to the future of this one.

Table 2. The approximate dependence of the fractional error in the recoil measurement as a function of various parameters in the experiment. The high N limit is assumed. When the parameter in the given column is changed, all timing and frequency parameters are assumed to be adjusted to maintain on-resonant $\pi/2$ pulses. For instance, when Δ is changed, the pulse time must be adjusted accordingly. The asterisks denote dependences which have been empirically verified. The following abbreviations are used: ind. = the shift is independent of this parameter; comp. = the dependence is complicated, so see text; 'flip' refers to reversal of the direction of all the pulses and 'sign' refers to whether the measured recoil increases or decreases for negative Δ

Mechanism	T	N	Δ	Δ parity	flip	N parity	sign
Spherical wavefronts, horizontal beams	T^3	ind.	ind.	even	even	even	−
Spherical wavefronts, vertical beams	T	ind.	ind.	even	even	even	−
Defocused Raman beams via φ_{off}	ind.	ind.	comp.	odd	odd	odd	either
Linear B field gradient*	T	ind.	ind.	even	odd	odd	either
Quadratic B field gradient	comp. $(\sim T^2)$	comp. $(\sim N)$	ind.	even	even	even	either
Defocused Raman beams via φ_{acs}	ind.	N	comp.	odd	even	even	+
Beam misalignment*	ind.	ind.	ind.	even	even	even	−
Optical standing waves*	T^{-1}	comp.	comp. $(\sim \Delta^{-1})$	even	even	even	+
Line pulling from non-interfering paths	T^{-4}	N^{-1}	Δ^4	even		depends on the two δ^{AC}	

Table 3. Values of physical quantities relevant to this measurement. The uncertainty attached directly to the measured value corresponds to the rightmost digits of the value

Physical quantity	Measured value		Units	Relative uncertainty	Ref.
Speed of light, c	299 792 458		m/s	Defined	[32]
Rydberg constant, R_∞	10 973 731.568 30	± 31	m^{-1}	1.8×10^{-11}	[12]
$m_{\mathrm{p}}/m_{\mathrm{e}}$	1 836.152 701	± 37	–	2.0×10^{-8}	[6]
Proton mass, m_{p}	1.007 276 470	± 12	u	1.1×10^{-8}	[32]
Cs mass, m_{Cs}	132.905 442	± 4	u	3.0×10^{-8}	[13]
Cs $6S_{1/2} - 6P_{3/2}$, $F = 4$ to $F' = 5$ frequency	351 722 010.6	± 12	MHz	3.5×10^{-8}	[60]
Fine-structure constant, α^{-1} (quantum Hall effect)	137.035 9979	± 32	–	2.4×10^{-8}	[61]
Fine-structure constant, α^{-1} (electron $g - 2$)	137.035 9914	± 11	–	8.0×10^{-9}	[4]

The square of the Cs wavelength enters the measurement, so it is currently the external factor that will most limit the determination of $\hbar/m_e$ from the Cs photon recoil. It also has the best chance for substantial improvement. Absolute optical frequency determination has been accomplished for other wavelengths with an accuracy of ≈ 0.1 ppb. The previous measurement of the Cs wavelength was performed using a wavemeter [60], and such measurements may yield still higher accuracy [62]. An approach which may be more successful involves counting precisely determined mode spacings in a Fabry-Perot interferometer to measure the absolute frequency difference of the unknown beam and an optical reference [63]. Optical frequency differences can also be measured using chains of phase locked lasers [64]. A viable optical reference for this frequency is the quadrupled methane laser line at 848 nm [65].

The best prospect for improvement in knowledge of m_p/m_e is improvement in the current best measurement technique, which compares the oscillation frequencies of a proton and an electron in the same Penning trap [6]. The authors are optimistic that they will be able to improve the current 20 ppb uncertainty by an order of magnitude [26]. At this level of precision m_p/m_e is unlikely to be the limiting factor in comparing an $\hbar/m$ measurement to other determinations of the fine-structure constant.

Mass ratios have been determined with accuracies better than 1 ppb, by comparing the oscillation frequencies of two ions trapped in succession in the same Penning trap [66, 67]. A technique that allows the comparison of particles of different masses has also recently been presented [68]. Adaptation of these or similar apparatuses to measuring the masses of alkali atoms would improve existing mass values by more than an order of magnitude.

For zero detuning from the $F = 4$ to $F' = 5$ resonance, the conversion from the recoil shift to $\hbar/m_e$ is

$$\frac{\hbar}{m_e} = \omega_{\text{meas}} \left(\frac{m_p}{m_e}\right) \left(\frac{m_{\text{Cs}}}{m_p}\right) \frac{c^2}{2\,(N+1)(\omega_1 + \omega_2)^2}$$

$$= \nu_{\text{meas}} \frac{3.501\,579\,39 \times 10^{-9}\,m^2}{(N+1)}, \tag{59}$$

where $\omega_{\text{meas}} = 2\pi\nu_{\text{meas}}$ is the measured recoil value, adjusted to zero detuning. Using the value of α from the $(g-2)_e$ experiment and (1), the accepted value of $\hbar/m_e$ is $1.157\,676\,499 \times 10^{-4}$ m^{2}s^{-1}. Our experimental value for $\hbar/m_e$ from (59) is $1.157\,675\,55 \pm 12 \times 10^{-4}$ m^{2}s^{-1}, where the quoted error only includes statistical error, since no systematic error bars can be assigned until we quantify all of the systematic errors. This is smaller than the accepted value by a fraction of 8.5×10^{-7}. Inverting (59), the accepted frequency, ν_{acc}, that corresponds to ν_{meas}, is determined to be 33.061 522 2 kHz for $\Delta = 0$. For excited state detuning $\Delta = -2.186$ GHz and $N = 3$, which are the conditions to which we adjust our data, the accepted value for the frequency we measure is $132.244\,565 \pm 10$ kHz.

5 Future improvements and prospects

5.1 Lighter atoms

The recoil shift can be made much larger using lighter atoms than Cs. A change to Li, for instance, brings with it a 20-fold increase in the size of the recoil shift due to the lighter mass, with another factor of 1.5 increase due to the higher energy resonant photon. Na yields a 12-fold increase in the size of the single photon recoil shift, and a similar experiment using H would give a remarkable 940-fold increase in the recoil shift. Since the Ramsey fringe spacing in the atomic interferometer depends only on the interaction time, T, which is determined by the height of the atomic fountain, a larger recoil separation between the two sets of fringes translates directly into better resolution.

However, Cs has several advantages from a practical perspective. The minimum temperature due to polarization gradient cooling corresponds to a few photon recoils, so the small recoil has the advantage of providing large signals in the atomic fountain even after many hundreds of ms, without the need to provide extra cooling or collimation. Also, Cs has a very large excited state hyperfine separation relative to the lighter alkalis, which brings with it simpler optical pumping and fluorescent detection. For instance, it is not clear that one can effectively clear away atoms from the lower ground state hyperfine levels of the lighter alkalis without losing an unacceptable fraction to the upper hyperfine level.

Lighter atoms do not yield relief from most potential systematic errors, which depend predominantly on the spatial separation of interferometer pairs. In fact, achieving a large recoil using many small photons instead of few large ones is preferable for some systematic errors, because one need only worry about gradients on the scale of the separation of the interferometers and not on the scale of the separation within each interferometer. The spatial separation between interferometers in the current recoil measurement is already a few mm, and anticipated improvements using Cs should extend this to near 25 cm. There is quite a lot of room to study systematics on this scale before a change in atoms extends the experiment to a less tractable laboratory distance scale. While the ultimate future of the measurement may in fact lie with lighter atoms, it is also possible that Cs will take the measurement to its final accuracy.

5.2 Vertical Raman beams

Reconfiguring the Raman beams so that they propagate vertically, along the path of the atoms, will have several advantages. As we have discussed, systematic errors due to wavefront curvature and magnetic fields can be more easily studied and minimized using vertical beams. In addition, it is desirable to significantly decrease the size of the bias magnetic field, so that the size of errors based on the quadratic Zeeman shift will decrease at least linearly. To lower the bias field requires that it be more homogeneous, which can probably only be accomplished

with magnetic shielding and a solenoid, as is done in atomic clocks. It is clearly easier to surround a perfectly vertical launch with such a solenoid than it is to surround the 5° launch we now employ. The vertical launch also uses gravity to avoid the sticky problem of accelerating the atoms through zero velocity, and all the unwanted Raman processes that can occur as a result.

A longer available interaction time will improve things in several ways, the most obvious being the increase in Ramsey time, which linearly increases the resolution. In addition, there will be more time available for adding π pulses, which also linearly increases the resolution. Furthermore, it seems likely that the signal loss per π pulse can be reduced with vertical beams because it will be easier to restrict the transverse velocity spread. The signal atoms will remain where the Raman beams have the most uniform intensity, which is not the case when the atoms move transversely to the beams.

Vertical Raman beams will bring with them some inconvenience. Gravitational acceleration must be accounted for between each pulse, but because the same adjustment will be done to both interferometers there should be no systematic error associated with this change. Vertical vibration isolation is also much more difficult. However, an active feedback system can be employed to achieve the desired stability [69].

5.3 Effective N-photon transitions

The linear increase in resolution with increased N is critical to this experiment. If it were possible to increase the resolution with N^2, the improvement would be amazing. A straightforward way to achieve an N^2 dependence in the interferometer resolution has been discussed elsewhere [70, 71]. Such an increase in resolution comes at the expense of much of the symmetry which minimizes potential systematic errors in the current interferometer configuration. Still, it seems likely that an N^2 sensitivity will at the very least aid this experiment in the study of systematic errors.

Increasing resolution by increasing the order of the Raman transitions is not possible. For a four or more photon Raman transition, the off-resonant spontaneous emission rate becomes larger than the effective Rabi frequency, which will lead to an unacceptable loss of coherence in the interferometer.

5.4 Other technical improvements

Other technical improvements which are contemplated include increasing the available Raman beam power (by using a Ti-Sapphire laser), increasing the number of atoms that contribute to the signal (for instance, by collimation of the atoms in the fountain), and exciting both interferometers simultaneously.

5.4.1 Increased laser power. The experiment can be improved if more power were available for the Raman

beams. With more power, the Rabi width and hence the number of contributing atoms can be increased. The obvious choice is to use either two Ti-Sapphire lasers, or one Ti-Sapphire laser and a high frequency electro-optic modulator. Even with the latter, more modest approach, a factor of 10 or 20 more power can be expected. The improvement from this source may be limited by the potential systematic error discussed in subsection 4.7, where atoms that fail to make a transition at the next to last π pulse are still in resonance at the final $\pi/2$ pair. More laser power would allow the Raman beam waists to be increased without losing signal or the advantages of a large τ/T (π pulse time to Ramsey time ratio). Larger beams ensure greater uniformity across a given ensemble of atoms, so that the population transfer at a π pulse could be more efficient and more π pulses could be applied. The Rayleigh range increases, but this is probably an unnecessary improvement. Finally, more power allows one to access a larger range of detunings from the excited state, which may be advantageous for studying and perhaps avoiding systematic errors.

5.4.2 Providing more signal atoms. With more slow atoms the velocity width of the pre-selected atoms could be reduced, improving the chances of all the pre-selected atoms following a long series of π pulses. More atoms would increase the flexibility in studying the effect of wavefront curvature, because it would allow more range in decreasing the transverse velocity width of the observed ensemble. Although the experiment is not now shot noise limited, it is not far from the limit. Especially when considerably more π pulses are applied, in the future more atoms may directly reduce the noise. To increase the number of atoms that contribute to the signal, we can either slow more of them, or use those that have been slowed more efficiently, by making them colder.

The optimal slowing technique has not been resolved if one prefers to avoid large inhomogeneous magnetic fields. What is fairly clear, however, is that approximately two more orders of magnitude of atomic flux can be obtained in a vapor cell by slowing the low velocity part of the Boltzman distribution directly into a MOT [72]. To date, this slowing technique has had the serious disadvantage that there are many background atoms which reduce the sensitivity of the detection. A large background unrelated to the fountain atoms would be particularly bad for the recoil measurement, in which a substantial number of signal atoms will be lost during a long sequence of π pulses. The vapor background can be beaten by launching the fountain atoms into a lower vapor pressure, differentially-pumped cell.

The temperature of the fountain atoms in this experiment is near the limit obtainable by polarization gradient cooling. Cooling of Na atoms below a single photon recoil has recently been demonstrated in 1D, using a technique which can be applied to any alkali atom [53, 73, 74]. One dimensional cooling to 1/10 of a photon recoil temperature has been demonstrated, which would increase the number of atoms near the velocity peak by

about a factor of 50, assuming the transverse heating is not substantial. Zeeman pumping after such exquisite cooling would be out of the question, so if the atoms are cooled in an equal distribution of sublevels the improvement in the number of useful $m_F = 0$ atoms would be smaller by at least the factor of 3 to 4 improvement that Zeeman pumping currently yields. Cooling in the other two dimensions would further boost the signal by keeping more atoms near the Raman beam center.

Perhaps a more practical way to improve the number of signal atoms is to conservatively trade off momentum spread for position spread. The atoms are initially confined in the trap to a region that is smaller than necessary for the experiment, so the atomic cloud could be allowed to expand during the launch in a hexapole magnetic field, which is a harmonic potential for the atoms [75]. When the atoms have reached the maximum amplitude in the harmonic well it would be abruptly shut off, leaving them collimated to the extent allowed by Liouville's theorem, $\Delta x_f \Delta p_f \geq \Delta x_i \Delta p_i$ [76]. A magnetic lens with a 3D quadrupole symmetry has been previously demonstrated for slow Cs atoms in a fountain [77]. and should be fairly straightforward to implement. This modification could yield improvements of more than an order of magnitude in the atomic density at the detection time.

5.4.3 Exciting both interferometers at once.
If it is possible to separately image atoms from the two interferometers in a pair, the pulse sequences for the two interferometers could be applied simultaneously. A benefit of this approach is that phase noise from mirror vibrations would completely cease to be a problem, as long as it is too small to damage the fringe contrast. (Mirror vibrations are not currently significant.) Any drifting uniform fields would also not contribute noise or systematic error. Furthermore, data collection would be twice as efficient.

Among the disadvantages of this approach are that the ac Stark shifts and off-resonant scatter would be larger, but only by about a factor of two. Also, other multi-photon processes related to the extra light could occur, and it may be difficult to keep track of all of them. The most significant disadvantage is that the clearing beams could no longer be used. Part of the function of the clearing beams is to remove the amplitudes in the opposite interferometer, which would no longer be necessary. The remaining function is to remove atoms that are lost during the long π pulse sequence. For large N there will be many more of these than signal atoms. However, if T were sufficiently long as to allow these atoms to also be spatially resolved, having no clearing would cease to be a disadvantage.

5.4.4 Other methods for coherent transfer.
In our current experiment, approximately 0.85 of each atom was coherently transferred with each π pulse, and we anticipate that the efficiency of transfer will increase to over 0.90 when we go to a vertical geometry and use higher powered lasers. Nevertheless, improved methods of coherently transferring populations or beamsplitters are always desirable. Also, for some interferometer applica-

tions, large momentum changes associated with a single population transfer may be more desirable.

There are two basic requirements for substitute π and $\pi/2$ pulses in this photon recoil measurement. (i) The transitions must be between magnetic field insensitive states because the accumulated phase errors due to magnetic field inhomogeneities must be less than the expected resolution of the experiment. In this experiment, a magnetic field difference ΔB over the trajectory of the atoms would cause a shift of adjacent magnetic sublevels by $(1.4 \text{ MHz/G}) \Delta B/4$. Hence, our measured resolution of 50 mHz demands that $\Delta B < 10^{-7}$ G. (ii) The transfer must be between two well defined states. If there is a coherent mixture of final states, a precise measurement of the recoil requires that the fraction of each atom in the allowed final states must be known precisely.

The magneto-optic beamsplitter [78] can impart a large momentum transfer to the atoms, but their scheme works with magnetic field sensitive states and also transfers populations into a superposition of states with different momenta.

One method of coherent transfer that may satisfy our requirements is based on population transfer via adiabatic following [79–82]. In this scheme, the transfer of population between ground states $|1\rangle$ and $|3\rangle$ through excited state $|2\rangle$ can be done adiabatically with time delayed pulses of light at ω_1 tuned to the $|1\rangle \rightarrow |2\rangle$ transition and ω_2 tuned to the $|3\rangle \rightarrow |2\rangle$ transition, as shown in Fig. 44a. For given intensities at ω_1 and ω_2, there is a superposition state that is "dark", i.e., not connected to the excited state $|2\rangle$. For example, for $I_1 = 0$, the dark state is $|1\rangle$, and for $I_1 = I_2$, the dark state is $(|1\rangle - |3\rangle)/\sqrt{2}$ if the matrix elements between the ground states and excited state are equal. An atom initially in $|1\rangle$ can be transferred adiabatically to $|2\rangle$ by first turning on I_2 with $I_1 = 0$ and then increasing I_1 as shown in Fig. 44b. Adiabatic transfer has the advantage that an atom in a dark state does
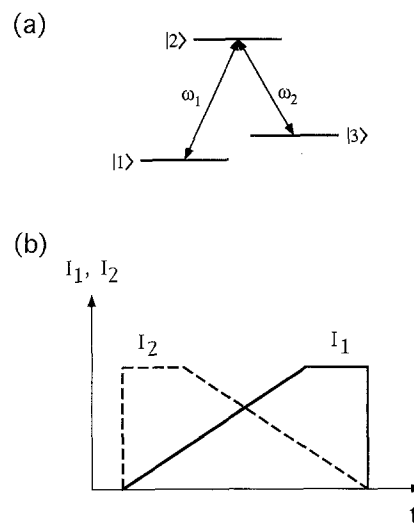
(a)

(b)

Fig. 44a, b. Coherent population transfer by adiabatic following. **a** The level structure and coupling light fields. **b** A pulse sequence such as this can keep the atoms in the dark state during the population transfer

not experience an ac Stark shift and the transfer is insensitive to the exact shape and intensity of the pulse.

The NIST group has demonstrated approximately 40% coherent population transfer between the $m_F = -4$ to $m_F = +4$ ground states of cesium if the 6 $P_{3/2}$, $F' = 5$ excited state is used as the excited state [83]. The imperfect transfer was due primarily to the existence of the nearby $F' = 4$ excited state, which allowed both off-resonant excitation and non-zero ac Stark shifts.

Adiabatic transfer between the $F = 4$, $m_F = 0$ and $F = 3$, $m_F = 0$ states is also possible. If the 6 $P_{1/2}$ excited state of cesium is used, we have calculated that as much as 98% of the population can be adiabatically transferred using a suitable pulse shape and realistic experimental parameters. It appears that this method of transferring population is better than the π pulse method for minimizing the error from the ac Stark shift induced by the pulse. When there is only one excited state, the ac Stark-shift induced by the light beams is zero [84]. The ac Stark shift due to the presence of the other excited state was calculated by time integrating the Schrödinger equation through the pulse sequence, and calculations show that the phase shift introduced by the adiabatic transfer is on the order of 0.02 rad per pulse, roughly 100 times less than the phase shift of one of the hyperfine levels by a Raman pulse. Consequently, any spatial inhomogeneities in intensity should then cause phase shifts for adiabatic following of 1% those for Raman transfer. We note, however, that the ac Stark shift induced by Raman transfer can be canceled with judicious choice of detuning and relative intensities of the two Raman beams while an effective cancellation of the ac Stark shift caused by adiabatic transfer is more problematic.

5.5 Conclusions

We have described an atom interferometer experiment where a fundamental constant has been measured with a relative precision on the order of 0.1 ppm. The current measurement agrees with the accepted value for $\hbar/m_{Cs}$ at the 1 ppm level. Many of the systematic effects have been identified and studied, but some systematic variations persist, and the errors due to wavefront curvature and intensity fluctuations from laser speckle have not yet been quantified, so we can not yet assign a systematic error to this measurement.

Through a number of improvements discussed in this paper, we feel that the precision can be increased by approximately two orders of magnitude in our next generation experiment. We also feel that the suggested changes will allow us to make an absolute measurement of $\hbar/m_{Cs}$ at the few ppb level.

References

1. J.L. Hall, C.J. Borde, K. Uehara: Phys. Rev. Lett. **37**, 1339 (1976)
2. D.S. Weiss: A precision measurement of the photon recoil of an atom using atomic interferometry. Ph.D. Thesis, Stanford University (1993)
3. E. Kruger, W. Nistler, W. Weirauch: Nucl. Instrum. Methods Phys. Res. **A284**, 143 (1989)
4. T. Kinoshita: IEEE Trans. IM-**38**, 172 (1989)
5. B.N. Taylor, E.R. Williams: Private communication
6. R.S.J. Van Dyck, F.L. Moore, D.L. Farnham, P.B. Schwinberg: Bull. Am. Phys. Soc. **31**, 244 (1986)
7. F.G. Mariam, W. Beer, P.R. Bolton, P.O. Egan, C.J. Gardner, V.W. Hughes, D.C. Lu, P.A. Souder, H. Orth, J. Vetter U. Moser, G. zu Putlitz: Phys. Rev. Lett. **49**, 993 (1982)
8. G.T. Bodwin, D.R. Yennie, M.A. Gregorio: Rev. Mod. Phys. **57**, 723 (1985)
9. M.E. Cage, R.F. Dziuba, C.T. Van Degrift, D. Yu: IEEE Trans. IM-**38**, 263 (1989)
10. J.Q. Shields, R.F. Dziuba, H.P. Layer: IEEE Trans. IM-**38**, 249 (1989)
11. E.R. Williams, G.R.J. Jones, Y. Sheng, L. Ruimin, H. Sasaki, P.T. Olsen, W.D. Phillips, H.P. Layer: IEEE Trans. IM-**38**, 233 (1989)
12. F. Nez, M.D. Plimmer, S. Bourzeix, L. Julien, F. Biraben, R. Felder, O. Acef, J.J. Zondy, P. Laurent, A. Clairon: Phys. Rev. Lett. **69**, 2326 (1992)
13. H. Stolzenberg, St. Becker, G. Bollen, F. Kern, H.-J. Kluge, J. Otto, G. Savard, L. Schweikhard, G. Audi, R.B. Moore: Phys. Rev. Lett. **65**, 3104 (1990)
14. N.F. Ramsey: Phys. Rev. **78**, 695 (1950)
15. C.J. Bordé, C. Solomon, S. Avrillier, A. Van Lerberghe, C. Bréant, D. Bassi, G. Scoles: Phys. Rev. A **30**, 1836 (1984)
16. F. Riehle, J. Ishikawa, J. Helmcke: Phys. Rev. Lett. **61**, 2092 (1988)
17. G. Hennig, J.H. Muller, K. Sengstock, U. Sterr, D. Bettermann, W. Ertmer: In *Laser Spectroscopy X*, ed. by M. Ducloy, E. Giacobino, G. Camy (World Scientific, Singapore 1992) pp. 39–44
18. M. Kasevich, D.S. Weiss, E. Riis, K. Moler, S. Kasapi, S. Chu: Phys. Rev. Lett. **66**, 2297 (1991)
19. M.A. Kasevich, E. Riis, S. Chu, R.G. DeVoe: Phys. Rev. Lett. **63**, 612 (1989)
20. M. Kasevich, S. Chu: Appl. Phys. B **54**, 321 (1992)
21. D.S. Weiss, E. Riis, M.A. Kasevich, K.A. Moler, S. Chu: In *Light Induced Kinetic Effects on Atoms, Ions and Molecules*, ed. by I. Moi, S. Gozzini, C. Gabbanini, E. Arimondo, F. Strumia (ETS Editrice, Pisa 1991) pp. 35–44
22. J.F. Clauser: Physica B **151**, 262 (1988)
23. J. Helmcke, D. Zevgolis, B.U. Yen: Appl. Phys. B **28**, 83 (1982)
24. J.W.G. Wignall: Phys. Rev. Lett. **68**, 5 (1992)
25. B.W. Petley: IEEE Trans. IM-**38**, 175 (1989)
26. B.N. Taylor: IEEE Trans. IM-**40**, 86 (1989)
27. R.D. Deslattes: In *The Art of Measurement*, ed. by B. Kramer (VCH, Weinheim 1988) pp. 193–207
28. P. Seyfried: PTB Mitt. **99**, 336 (1989)
29. T. Andreae, W. König, R. Wynands, D. Leibfried, F. Schmidt-Kaler, C. Zimmermann, D. Meschede, T.W. Hänsch: Phys. Rev. Lett. **69**, 1923 (1992)
30. B.W. Petley: Metrol. **29**, 95 (1992)
31. A. Hartland, K. Jones, J.M. Williams, B.L. Gallagher, T. Galloway: Phys. Rev. Lett. **66**, 969 (1991)
32. E.R. Cohen, B.N. Taylor: Rev. Mod. Phys. **59**, 1121 (1987)
33. B.W. Petley: *The Fundamental Physical Constants and the Frontiers of Measurement* (Hilger, Boston 1985)
34. E.A. Cornell, K.R. Boyce, D.L.K. Fygenson, D.E. Pritchard: Phys. Rev. A **45**, 3049 (1992)
35. A. Hartland: Metrol. **29**, 175 (1992)
36. K. Moler, D.S. Weiss, M. Kasevich, S. Chu: Phys. Rev. A **45**, 342 (1992)
37. N.F. Ramsey: *Molecular Beams* (Oxford Univ. Press, Oxford 1956)
38. L. Allen, J.H. Eberly: *Optical Resonance and Two-Level Atoms* (Dover, New York 1975)

39. Y.V. Baklanov, B.Y. Dubetsky, V.P. Chebotayev: Appl. Phys. **9**, 171 (1976)
40. J.C. Bergquist, S.A. Lee, J.L. Hall: Phys. Rev. Lett. **38**, 159 (1977)
41. C.J. Bordé: Phys. Lett. A **140**, 10 (1989)
42. M. Kasevich, S. Chu: Phys. Rev. Lett. **67**, 181 (1991)
43. C.J. Bordé: In *Laser Spectroscopy X*, ed. by M. Ducloy, E. Giacobino, G. Camy (World Scientific, Singapore, 1992) pp. 239–245
44. R.P. Feynman, A.R. Hibbs: *Quantum Mechanics and Path Integrals* (McGraw-Hill, New York 1965)
45. F. Riehle, T. Kisters, A. White, J. Helmecke, C.J. Bordé: Phys. Rev. Lett. **67**, 177 (1991)
46. D.S. Weiss, B.C. Young, S. Chu: Phys. Rev. Lett. **70**, 2706 (1993)
47. W. Ertmer, R. Blatt, J.L. Hall, M. Zhu: Phys. Rev. Lett. **54**, 996 (1985)
48. J.L. Hall, L. Hollberg, T. Baer, H.G. Robinson: Appl. Phys. Lett. **39**, 680 (1981)
49. C. Wieman, L. Hollberg: Rev. Sci. Instrum. **62**, 1 (1991)
50. E.L. Raab, M. Prentiss, A. Cable, S. Chu, D.E. Pritchard: Phys. Rev. Lett. **59**, 2631 (1987)
51. A. Clairon, P. Laurent, A. Nadir, M. Drewson, D. Grison, B. Lounis, C. Salomon: In *Proc. 6th Eur. Frequency and Time Forum* (ESA, Noordwijk 1992) pp. 27–33
52. S. Swartz, J.L. Hall, K.E. Gibble, D.S. Weiss: to be published
53. M.A. Kasevich, S. Chu: Phys. Rev. Lett. **69**, 1741 (1992)
54. C. Monroe, H. Robinson, C. Wieman: Opt. Lett. **16**, 50 (1991)
55. P.R. Bevington: *Data Reduction and Error Analysis for the Physical Sciences* (McGraw-Hill, New York 1969)
56. K.E. Gibble: Private communication
57. C. Salomon, J. Dalibard, A. Aspect, H. Metcalf, C. Cohen-Tannoudji: Phys. Rev. Lett. **59**, 1659 (1987)
58. F. Harris: IEEE Proc. **66**, 51 (1978)
59. M.A. Kasevich: Atominterferometry in an atomic fountain. Ph. D. Thesis, Stanford University (1992)
60. G. Avila, P. Gain, E. de Clercq, P. Cerez: Metrol. **22**, 111 (1986)
61. M.E. Cage, D.F. Dziuba, R.E. Elmquist, B.F. Field, G.R. Jones, Jr., P.T. Olsen, W.D. Phillips, J.Q. Shields, R.L. Steiner, B.U. Taylor, E.R. Williams: IEEE Trans. IM-**38**, 284 (1989)
62. J. Cachenaut, C. Man, A. Brillet, F. Stoekel, A. Jourdan, F. Hartmann: Rev. Phys. Appl. **14**, 685 (1983)
63. R.G. Devoe, C. Fabre, K. Jungmann, J. Hoffnagle, R.G. Brewer: Phys. Rev. A **37**, 1802 (1988)
64. H.R. Telle, D. Meschede, T.W. Hänsch: Opt. Lett. **15**, 532 (1990)
65. T.W. Hänsch: Private communication
66. D. Hagena, G. Werth: Europhys. Lett. **15**, 491 (1991)
67. E.A. Cornell, R.M. Weisskoff, K.R. Boyce, J. Flanangan R.W., G.P. Lafyatis, D.E. Pritchard: Phys. Rev. Lett. **63**, 1674 (1989)
68. V. Natarajan, K.R. Boyce, F. DiFilipo, D.E. Pritchard: Phys. Rev. Lett. **71**, 1998 (1993)
69. D.S. Weiss, B.C. Young, S. Chu: In *Laser Spectroscopy XI* (World Scientific, Singapore 1994) pp. 23–28
70. M. Kasevich: Private communication
71. C.J. Bordé, M. Weitz, T.W. Hänsch: In *Laser Spectroscopy XI* (World Scientific, Singapore 1994) pp. 76–78
72. K.E. Gibble, S. Kasapi, S. Chu: Opt. Lett. **17**, 526 (1992)
73. A. Aspect, E. Arimondo, R. Kaiser, N. Vansteenkiste, C. Cohen-Tannoudji: J. Opt. Soc. Am. B **6**, 2112 (1989)
74. N. Davidson, H.J. Lee, M. Kasevich, S. Chu: Phys. Rev. Lett. **72**, 3158 (1994)
75. E. Riis, D.S. Weiss, K.A. Moler, S. Chu: Phys. Rev. Lett. **64**, 1658 (1990)
76. S. Chu, J.E. Bjorkholm, A. Ashkin, J.P. Gordon, L.W. Hollberg: Opt. Lett. **11**, 73 (1986)
77. E.A. Cornell, C. Monroe, C.E. Wieman: Phys. Rev. Lett. **67**, 2439 (1991)
78. T. Pfau, C.S. Adams, J. Mlynek: Europhys. Lett. **21**, 439 (1993)
79. J. Oreg, F.T. Hioe, J.H. Eberly: Phys. Rev. A **29**, 690 (1984)
80. U. Gaubatz, P. Rudecki, M. Becker, S. Schiemann, M. Kulz, K. Bergmann: Chem. Phys. Lett. **149**, 463 (1988)
81. J.R. Kuklinski, U. Gaubatz, F.T. Hioe, K. Bergmann: Phys. Rev. A **40**, 6741 (1989)
82. P. Marte, P. Zoller, J.L. Hall: Phys. Rev. A **44**, 4118 (1991)
83. L. Goldner, C. Gerz, R. Spreeuw, S. Rolston, C. Westbrook, W. Phillips, P. Marte, P. Zoller: Phys. Rev. Lett. **72**, 997 (1994)
84. M. Weitz, B. Young, S. Chu: Phys. Rev. A (in press)